Assessment of impacts of upstream developments and climate change on Carp River watershed

Baba-Serges Zango

A Thesis

Presented to the University of Ottawa in Partial Fulfillment of the Requirements

for

Master of Applied Science in Civil Engineering

Department of Civil Engineering

University of Ottawa

Acknowledgments

I want to express my sincere gratitude to my supervisors Dr. Ousmane Seidou and Dr. Majid Sartaj, for giving me the opportunity to do my Master's work on this project. I am also thankful for their assistance. Their guidance, support, and comments have been tremendous.

I am deeply grateful for the financial support offered by the MVCA through the MITACS Accelerate program during this work.

I would also like to sincerely thank Kelly Stiles and Nader Nakhaei from the MVCA for their enormous contribution to the completion of this project and their availability during all the project stages.

I have appreciated working with you. To all people at MVCA, directly or indirectly, who have contributed in providing me with all resources I needed during this project, Thank you so much!

Finally, I would like to thank especially my beloved parents from my home country. Your encouragement and support have been very indispensable and motivating.

Abstract

A SWAT hydrological model is developed to evaluate the individual and combined impacts of urbanization and climate change on water quantity (discharge) and quality (N and P) of the watershed of Carp River in Ontario, Canada. Seven numerical experiments (scenarios) were developed to represent the different configurations of the watershed in terms of land use (either current or projected) and climate regime (current or future, observed or simulated). The reference period is 1990-2018, and the future period is 2021-2050. The 2017 land use was used to represent the reference period. The future land use is the projected 2050 land use obtained from the City of Ottawa. The future climate was obtained by downscaling the outputs of nine (9) Regional Climate Models (RCMs) under two Representative Concentration Pathways (RCPs): RCP4.5 and RCP 8.5. The developed scenarios are the following:

- S0o (baseline scenario) corresponding to the current land use map and the observed climate regime on the reference period
- S0m is similar to S0o except that RCM outputs are used instead of the observed climate on the reference period
- S1 corresponds to the future land use and historical climate regime on the reference period.
- S0M45/S0M85 corresponds to the current land use and the future climate regime under RCP4.5 (S0M45) and RCP8.5 (S0M85)
- S1M45/S1M85 corresponds to the future land use map and future climate regime under the two RCPs.

The changes or impacts on quantity and quality in each scenario were estimated by comparing the results with the baseline scenarios S0o/m (reference) at two levels: globally (at the main outlet) and locally (at the outlet of an upstream sub-watershed). For a consistency purpose, S0o is used when assessing land-use change scenario while S0m was the reference in climate change and combined effects scenario. This allowed the comparison to be consistent with the same climate data frame. The results showed that climate change is likely to be the most dominant factor affecting discharge and nitrogen, while urbanization will control the quantity of phosphorus. Unsurprisingly, the combined effect had a more significant impact on water quantity and quality. However, the impact is not additive, and the relationship is not linear. Compared with S0, the annual average discharge increased by 1.57%, 5.49%, 7.52%, 6.75%, and 9.34% in S1, S0M45, S0M85, S1M45, and S1M85, respectively. In comparison, the change for annual N load was estimated at -1.88%, 29.62%, 2.03%, 24.84%, and -1.20% respectively. Change in annual average P was respectively 26.49%, 1.07%, -4.49%, 23.81% and 19.15%. Local impact assessment indicates the impact in upstream sub-watersheds may differ from the main outlet's impact in terms of magnitude and direction of change. Therefore, only considering global change may lead to a wrong interpretation of the impacts over the watershed. It is, therefore, necessary to evaluate the impacts at the local level as well.

Table of Contents

Table of Figures

List of Tables

1. Introduction

1.1. Background

Pressure on natural resources in general, and water in particular, have reached unprecedented levels during the last decades because of climate change, industrialization and the dramatic growth of population (Heo et al., 2015). The United Nations estimated that the world population would increase by 2 billion in the next 30 years, from 7.7 billion in 2020 to 9.7 billion in 2050 (United Nations, 2019). This demographic change will be associated with higher living standards; land and water use regulations, and have become a critical issue affecting water supplies, indispensable for domestic and economical use as well as environment. Communities become more vulnerable to inappropriate water resources supply in quantity and quality (Abbaspour et al., 2015).

According to Environment and Natural Resources (2013), threats to water resources are widespread in Canada. Several major catastrophic floods have hit the country in the past. A notorious one is the Hurricane Hazel in Toronto (Ontario), which occurred in October 1954 and caused an estimated $25M (in 1954 dollars) in damages; Another major flood occurred in the Fraser River area (British Columbia) in June 1948, causing damages estimated at around $20 millions (in 1948 dollars). More recently, the so-called 'Saguenay deluge' in Saguenay (Quebec) in July 1996 cost more than $1.5 billions. Closer to home, unprecedented floods occurred in Ottawa (Ontario) - April 2019 and Gatineau – March 2017. Environment and Natural Resources (2013) also identified rivers and lakes where water quality issues, mostly eutrophication, are likely to occur: St. Lawrence River and Lake Erie in North America. However, all these extreme events cannot only be attributed to population growth and land use changes (urbanization and deforestation). Climate change is partly responsible for the change in hydrological regimes.

Environment and Climate Change Canada (Bush & Lemmen, 2019) estimated an increase of mean temperature in Canada at 1.7 ºC between 1948 and 2016 causing the sea level to rise, especially in Northern Canada with the melting of the ocean ice, and more extreme events. The temperature increase is also predicted to reach more than 6 ºC by the late of 21st century in a high emission scenario (Bush & Lemmen, 2019), meaning natural disaster activities may occur more frequently. The combined effects of climate change and land use changes in tandem on water quantity and/or quality have been documented in the literature (El-Khoury et al., 2015, Hung et al., 2020; Penjor et al., 2020; Kundu et al., 2017; Tu, 2009; Choukri et al., 2020; Wang et al., 2020; Guo et al., 2020; Tirupathi and Shashidhar, 2020; Čerkasova et al., 2018; Karlsson et al., 2016; Dunn et al., 2012; etc.). These studies differ in the location of the study area, the hydrological model, the type of water quantity and quality variables assessed, and the way climate change and land use scenarios are generated. Each of these studies involved numerical experiments where a calibrated hydrological model was forced with climatic inputs representing one or several global warming scenarios and using current and/or projected land use maps. Although these studies confirmed the impact of urbanization and climate change on streamflow, the evaluation was only limited to the impacts at the main outlet (global level).

1.2. Problem statement

The Mississippi Valley Conservation Authority (MVCA) anticipates significant Residential/commercial/ industrial development in the coming years in the Carp River watershed and is concerned that these developments will negatively impact both quality and quantity of waterbodies. The climate in Ottawa has also been unpredictable in the Ottawa region lately, with exceptional floods and increased tornado activities in the past three years (two in March 2017 and

April 2019). Climate change will likely induce significant changes in the hydrology of the watershed, which will, in turn, affect ecosystem health through changes in water quantity and quality.

1.3. Research objective

The main objective of this research is to evaluate and quantify the impacts of urbanization, climate change, and combined effects on water quantity and quality, especially nitrogen (N) and phosphorus (P) in the Carp River water.

1.4. Specific objectives

To conduct this study, a hydrological model will be developed and used as a predicting tool for the assessment of impacts. Therefore, the specific objectives are listed in that order:

- Acquire and process geographic, hydro-meteorological, and water quality data from official institutions or international databases
- Develop a Soil and Water Assessment Tool (SWAT) model of the watershed and calibrate it for water quantity and quality
- Analyze future scenarios of land use and climate changes within the watershed and integrate them into the model - Assess the impacts of climate change and urbanization on water quality and quantity
- Provide recommendations based on the results

1.5. Structure of the thesis

Following this introduction, this thesis includes five chapters, followed by references and appendices. Chapter 2 presents a literature review focusing on hydrological modeling, urbanization, and climate change impacts on water quantity and quality. Chapter 3 covers the materials and methods, including the study area considered for this research, the input data used to develop and calibrate the model, the procedure of developing the model, and the description of future scenarios selected to study the impacts. Results and outputs of these simulations are then presented and discussed in chapter 4. Chapter 5 is a conclusion with the main findings of this study and few recommendations based on these findings.

2. Literature review

2.1. Hydrological modeling

2.1.1. Description

Hydrological models were developed to simulate the hydrological processes and water exchange within a catchment or over a land surface on a continental scale (Marshall, 2014) and the impact of natural variability and anthropogenic factors on the hydrologic system (Yu, 2015). Thus, they can be used to manage and plan a sustainable use of water resources. Modeling hydrologic response to different natural and human-induced changes helps to understand the physical processes in the hydrologic system, including flow and solute transport in the surface and subsurface and the interaction between the atmosphere and land surface. Hydrological models are classified into two groups: Lumped conceptual models and physically-based distributed models. Each of both has its strengths and its weaknesses. Lumped conceptual models are generally applied

in a single point or a region to simulate various hydrological processes, while distributed models simulate the spatio-temporal variation in hydrological processes under climate changes such as global warming (Yu, 2015). Oeurnga et al. (2011) claim that distributed models are preferable since their representation of spatial variability of catchment characteristics is realistic. However, they require large input datasets and set up time requirements (Lewis et al., 2018).

Several hydrological modeling studies have been conducted in various watersheds for different purposes using distributed models (e.g., O'Connell, 1991; Abbott et al., 1986; Huo et al., 2020; Hong et al., 2019; Rokaya et al., 2020; Lewis et al., 2018; Ishida et al., 2018; Skala et al., 2020) witnessing its popularity.

2.1.2. Limitations

A significant limitation in using hydrological models is the uncertainty issues in the prediction. Abbaspour (2012) draws attention to this limitation and identifies three different sources of uncertainty: (1) conceptual model (or structural) uncertainty, (2) input uncertainty, and (3) parameter uncertainty. The conceptual model uncertainty could be one of the following situations: a) Model uncertainties due to simplifications in the conceptual model, b) Model uncertainties due to processes occurring in the watershed but not included in the model, c) Model uncertainties due to processes that are included in the model, but their occurrences in the watershed are unknown to the modeller, and d) Model uncertainties due to processes unknown to the modeller and not included in the model either. Input uncertainty results from errors in input data such as rainfall, and more importantly, the extension of point data to large areas in distributed models (more details are provided in SWAT-CUP User Manual (Abbaspour, 2007).

According to Wu and Chen (2015), parameter uncertainty is inevitable, but it can easily be controlled by selecting a suitable calibration method.

Distributed catchment models need to be carefully calibrated and validated using accurate observed data to reproduce and predict the reality as close as possible. However, the calibration of hydrological models is challenging due to uncertainties in hydrological modeling (Yang et al., 2008). Thus, to help to face this issue, hydrological models such as SWAT (Arnold et al., 1998) have been associated with an automatic calibration program.

SWAT is one of the most complete and frequently used models (Arnold et al., 1998; Neitsch et al., 2005), and it is widely used to assess hydrology in small and large catchments around the world (Khoiab and Thomb, 2015). Few studies were focused on a comprehensive review of SWAT model applications, calibration, and validation processes (Gassman et al., 2007; Moriasi et al., 2007; Arnold et al. 2012). Others were conducted using SWAT model in various locations worldwide: in Asia (Jajarmizadeh et al., 2017; Huo et al., 2013; Du J. et al., 2012, Yang et al., 2008), in America (El-Khoury et al., 2015; Arnold et al., 2012; Havrylenko et al., 2016; Jha and Gassman, 2014; Mbonimpa et al., 2012), in Europe (Abbaspour, 2007) and in Africa (Mengistu et al., 2019, Choukri et al., 2020, AlemayehuMuluneh, 2020).

2.1.3. Surface runoff modeling

In water science, the term “surface runoff” describes the accumulation of the water on the ground surface and its movement towards streams such as lakes and rivers. This accumulation occurs whenever the rate of rain with intensity falling onto the ground surface exceeds the rate of infiltration (Gumbo et al., 2002). Thus, runoff results of a difference between inflow rate (rainfall, snow) rate and outflow (infiltration, percolation, evapotranspiration) rate. Therefore, surface

runoff depends on several hydrological parameters. One of them is the Curve Number (CN), which characterizes a watershed's response to a rainfall event based on the hydrologic soil group (soils' permeability), type of land use (e.g., urban, agricultural, forest, etc.), and antecedent moisture condition of the soil.

In SWAT, the SCS curve number method is used to estimate the accumulated runoff for each sub-basin. The amount of runoff under different watershed characteristics is defined as (Neitsch et al., 2009):

$$\boldsymbol{Q_{surf} = \frac{(\mathbf{P} - I_a)^2}{(\mathbf{P} - I_a + \mathbf{S})}} \qquad \boldsymbol{eq.1}$$

Where:

P = Rainfall (mm)

$\boldsymbol{I_a}$ = Initial abstractions prior to runoff (surface storage, interception, and infiltration)

$\boldsymbol{Q_{surf}}$ = Accumulated runoff (mm)

The initial abstractions are generally approximated to 0.2S, with S being the retention parameter (mm) representing the maximum amount of water that can be abstracted by watershed. S is expressed in terms of a CN, a dimensionless watershed parameter ranging from 0 to 100. A CN of 100 represents a limiting condition of a perfectly impermeable watershed with zero retention, and thus all the rainfall becoming runoff. A CN of zero conceptually represents the other extreme, with the watershed abstracting all rainfall with no runoff regardless of the rainfall amount (Gumbo et al., 2002). The retention parameter varies spatially due to changes in soil, land use, management, and slope. It is defined as (Neitsch et al., 2009):

$$S = 25.4\left(\frac{1000}{CN} - 10\right) \qquad eq.2$$

Where **CN** = the curve number for the decay.

In general, the watersheds will consist of several sub-areas of different topographical patterns, soil types, and land cover. In this case, a composite curve number is determined by weighting the CNs for the different sub-areas based on the proportion of the land area associated with each sub-areas.

Finally, equation 1 becomes:

$$Q_{surf} = \frac{(\mathbf{P} - \mathbf{0.2})^2}{(\mathbf{P} - \mathbf{0.8S})} \qquad eq.3$$

These equations are used in SWAT models to convert the rainfall input data, with many other inputs, in order to determine corresponding runoff quantities flowing out of each sub-basin and the entire watershed. A graphical representation of the relationship between rainfall and runoff is presented in Figure 1.

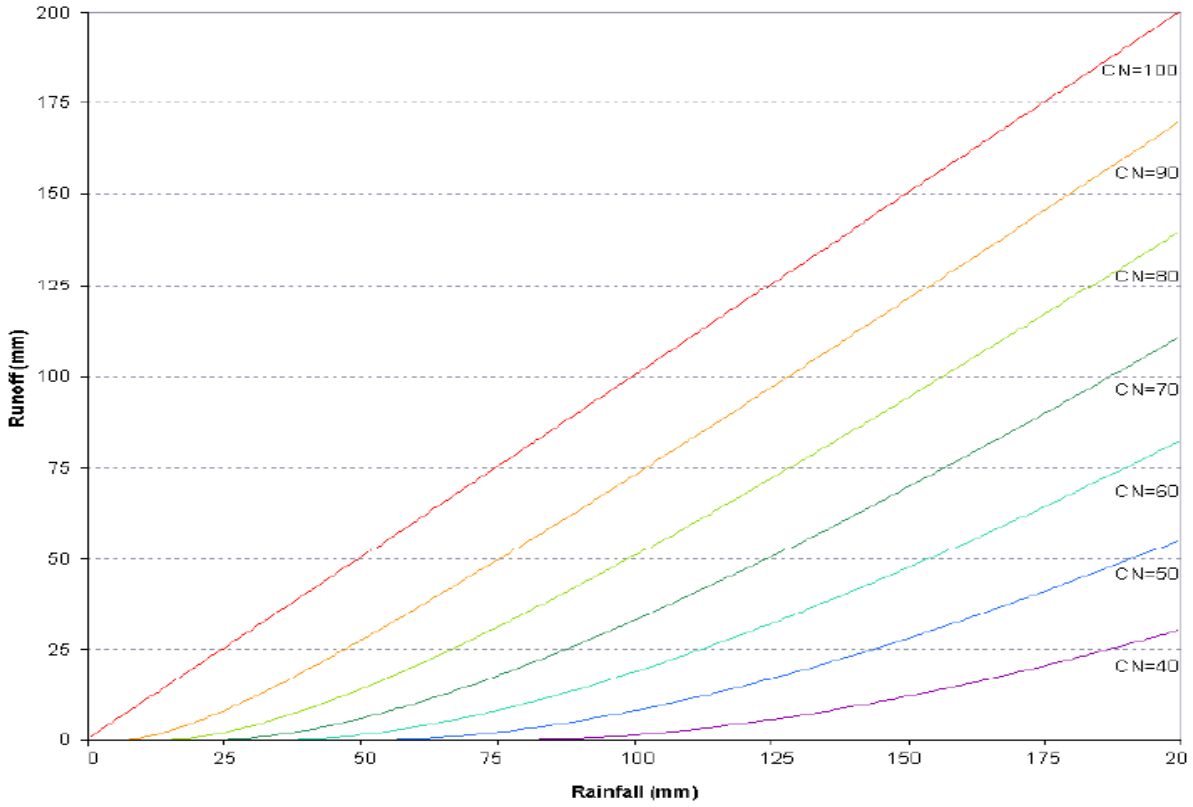

Figure 1 - Relationship of runoff and rainfall in SCS curve number method (Neitsch et al., 2009)

Rainfall-Runoff models are very useful in predicting runoff for future rainfall events. They provide authorities and hydrology/hydraulic experts with the required information for good planning and decision-making related to the community's economic activities and the design of adequate hydraulic structures.

2.1.4. Nutrients modeling

The transport of nutrients into water bodies, especially nitrogen and phosphorus, is a major problem to the quality of the ecosystem (e.g., eutrophication). This is mainly due to different human activities experienced in the basin, such as increased human settlement in the drainage basin, clearing forest for farming, development of urban societies, and consequential disposal of

industrial and agricultural wastes (Kitaka, 2000). Nutrients pollution results from two types of sources: (1) non-point sources (or diffuse) with nutrients washed-off land areas and transported by surface runoff; (2) point sources with effluent discharge from industrial and domestic points.

The quantity of nitrogen and phosphorus loss from non-point sources can be determined by evaluating different components of surface runoff and their spatial and temporal variations in the catchment. When the rainfall intensity is greater than the rate at which it can infiltrate the soil, the water quality constituents will be transported towards streams, and surface water bodies due to runoff occurred by high rainfall intensity (Tiruneh, 2004). The fate and transport of nutrients in a watershed depend on the compounds' transformations in the soil environment (Neitsch et al., 2009). The nutrients present in the soil profile are removed by various processes such as plant uptake and erosion. In the specific case of nitrogen, leaching, volatilization, and denitrification play a significant role. SWAT models the complete nutrient cycle for nitrogen and phosphorus as well as the degradation of any pesticides applied in a Hydrologic Response Unit (HRU, described in section 3.3.1); and the transformation and movement of nitrogen and phosphorus within an HRU are simulated based on the cycles shown in Figure 2 and Figure 3.

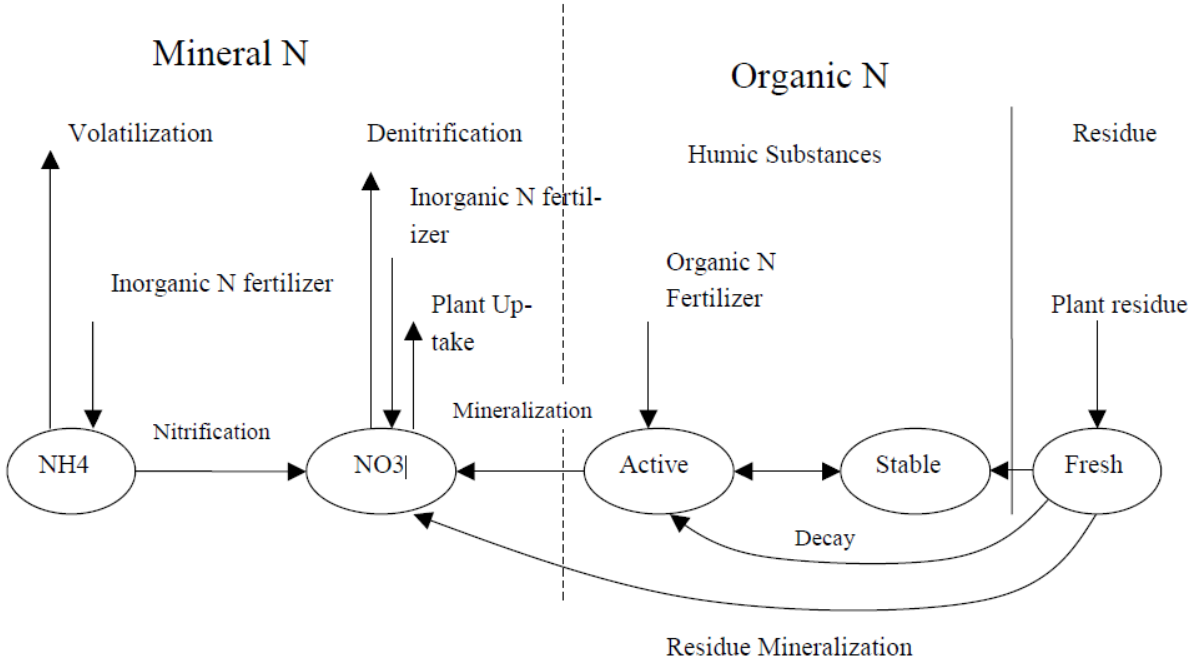

Figure 2 - SWAT soil nitrogen and processes that move nitrogen in and out of pools (Neitsch et al., 2009)

There are three major forms of nitrogen as described in Figure 2: organic nitrogen associated with humus, mineral forms of nitrogen held by soil colloids, and mineral forms of nitrogen in solution (Neitsch et al., 2009). The main primary sources of nitrogen for soil nutrient are fertilizer added for cultivation, manure or residue application, fixation by symbiotic or non-symbiotic bacteria, and rain.

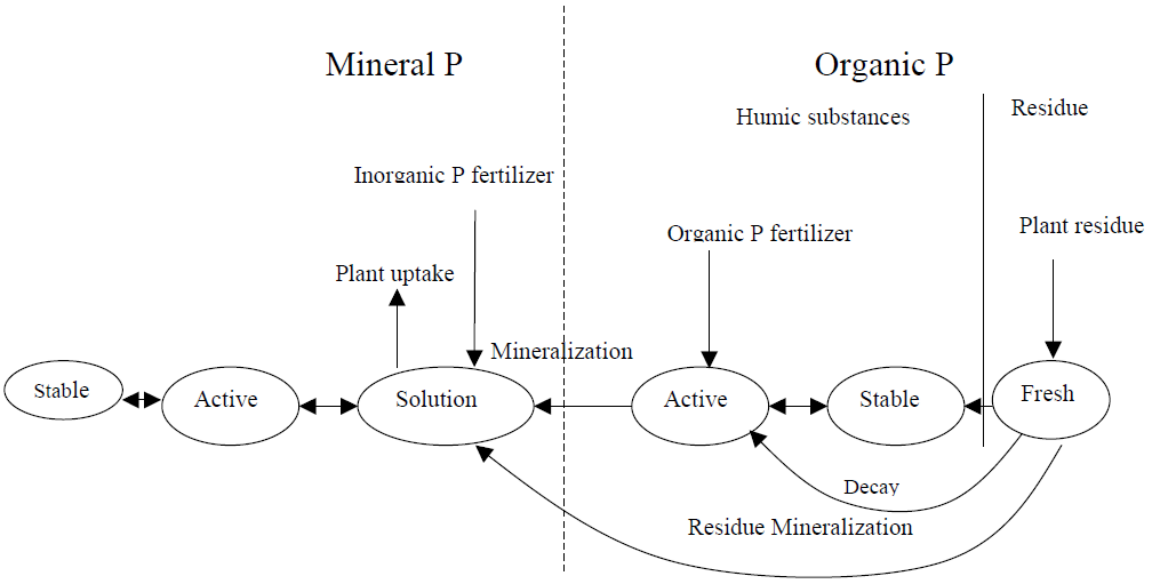

Figure 3 - SWAT soil phosphorus and processes that move phosphorus in and out of pools (Neitsch et al., 2009)

The three major forms of phosphorus in mineral soils that might be added to the soil by fertilizers, manure, or residue application are organic phosphorus associated with humus, insoluble forms of mineral phosphorus, and plant-available phosphorus in soil solution (Neitsch et al., 2009). Thus, six different pools of phosphorus in the soil are monitored, in which three pools are inorganic forms of phosphorus while the other three pools are organic forms of phosphorus (Figure 3).

SWAT calculates nutrient levels on a mass basis while it allows the input data as concentrations. The equation used for the conversion includes the bulk density and the depth of the layer (Neitsch et al., 2009):

$$\frac{conc_{N,P} \times \rho_b \times Z_{ly}}{100} = \frac{kg\ N}{ha} \qquad eq.4$$

Where

$\boldsymbol{conc_{N,P}}$ = Concentration of the nutrient (N or P) in a layer (mg/kg or ppm)

$\boldsymbol{\rho_b}$ = Bulk density of the layer (Mg/m^3)

$\boldsymbol{Z_{ly}}$ = Depth of the layer (mm)

2.2. Climate change

2.2.1. Description

The earth's climate varies naturally on all time scales. However, its long-term and average temperatures are regulated by the balance between incoming and outgoing energy, which determines the earth's energy balance. Therefore, any factor that causes a sustained change to the amount of incoming energy or the amount of outgoing energy can lead to climate change. Thus, climate change is a long-term shift in weather conditions identified by changes in temperature, precipitation, wind, and other indicators (Environment and natural resources Canada, 2019). It is characterized by: (1) change in the average conditions (increase or decrease) and (2) change in the variability of weather parameters (extreme events over time). Among the few reasons behind this change, including volcanic activity, solar output, earth's orbit around the sun, and human activities (burning of fossil fuels and conversion of land for forestry and agriculture), it is the human activities that are considered as the most important cause. On one hand, with the industrial revolution, the emission of substances in the atmosphere has drastically increased. Substances like carbon dioxide, methane, and nitrous oxide, called greenhouse gases (GHG), can stay in the air for a long time, causing global warming. The particularity of GHG is that they trap the heat in the atmosphere, causing an increase in temperature. On the other hand, the rapid increase of the world's population and the high risks related to food security force most countries to modify and

adapt their production policies, including transforming vast area of forests into farmland and intensive production methods. This conversion of forests into farmlands reduces the capacity of the earth to absorb the emissions of carbon dioxide, and consequently, a higher quantity of this gas is present in the atmosphere contributing to global warming. In addition, a non-negligible amount of methane (GHG) released by the animals in farms, especially cows, also contributes to global warming.

2.2.2. Climate change scenarios

Based on the factors described in the previous section, researchers have developed climate change scenarios. In climate change studies, scenarios describe plausible trajectories of different aspects of the future that are constructed to investigate the potential consequences of anthropogenic climate change. The goal of working with scenarios is not to predict the future but to better understand uncertainties and evaluate different potential events in the future to consider how robust different decisions or options may be under a wide range of possible futures (IPCC, 2014). Scenarios also provide a standard framework for all climate research works to be complementary and comparable by ensuring that initial conditions, historical data, and projections are consistent across the various domains of climate science (Wayne, 2013).

Several factors drive the prediction of how global warming contributes to climate change. Development in technology, changes in energy generation and land use, global and regional economic circumstances, and population growth are non-negligible factors. The key parameter is the amount of future GHG emissions (Wayne, 2013). The Intergovernmental Panel on Climate Change (IPCC) stated in their *Fifth Assessment Report* (AR5) that cumulative emissions of CO_2 largely determine global mean surface warming by the late 21st century and beyond. They also

state that projections of GHG emissions vary over a wide range, depending on both socio-economic development and climate policy. It is shown that scenarios can be found with the year 2100 radiative forcing from as low as 2.5 W/m^2 to between 8 and 9 W/m^2 and higher (Van Vuuren et al., 2011). To limit the number of climate model runs and provide distinguishable climate results, the total set should contain a manageable number of scenarios and consist of an even number of scenarios;. At the same time, they should be sufficiently separated (by about 2 Wm−2) in terms of the radiative forcing pathways (Moss et al. 2008). Based on these considerations, the IPCC identifies four different 21st century pathways (or scenarios) of GHG emissions and atmospheric concentrations, air pollutant emissions and land use, known as the Representative Concentration Pathways (RCPs). Among these scenarios, RCP8.5 one scenario corresponds to with very high GHG emissions; RCP4.5 and RCP6.0 represent intermediate scenarios. RCP2.6 represents stringent mitigation scenario, also referred to as RCP3-PD (IPCC Synthesis Report, 2014). The number refers to forcing for each RCP while PD stands for Peak Decline. They are representative because they are one of several different scenarios with similar radiative forcing and emissions characteristics (IPCC Technical Summary, 2007). RCPs are referred to as pathways to emphasize that their primary purpose is to provide time-dependent projections of atmospheric GHG concentrations (Wayne, 2013). RCP8.5 is developed assuming high population and relatively slow income growth with modest rates of technological change and energy intensity improvements resulting in the long term to high energy demand and GHG emissions without any climate change policies. The GHG emissions and concentrations in this scenario increase considerably over time, leading to a radiative forcing of 8.5 W/m^2 at the end of the century with a CO_2 equivalent concentration of 1350 ppm (Riahi et al., 2011). RCP2.6 represents medium development scenario for population, income, energy use, and land use, leading to a pathway first going to a peak forcing

level of around 3 W/m^2 by mid-century followed by a decline to 2.6 W/m^2 (hence the name RCP3-PD) (Van Vuuren et al., "RCP2.6", 2011); the equivalent concentration of CO_2 corresponds to 450 ppm. Meanwhile, the two intermediate RCPs (4.5 and 6.0) follow a stabilizing rate of change in radiative forcing with CO_2 equivalent concentrations of 650 ppm and 850 ppm, respectively (Arnell et al., 2011). As a reference, scenarios without additional efforts to constrain emissions ('baseline scenario') lead to pathways ranging between RCP6.0 and RCP8.5, and RCP2.6 represents a scenario that aims to keep global warming likely below 2°C above pre-industrial temperatures (IPCC, 2014).

For each category of emissions, RCPs contains a set of starting values and the estimated emissions (including historical, real-world information) based on assumptions about economic activity, energy sources, population growth, and other socio-economic factors. Data covers the 1850 - 2100 period, and RCPs are supplemented with extensions know as Extended Concentration Pathways (ECPs), allowing climate modeling experiments through the year 2300 for long-term research. The final products form a comprehensive data set with high spatial and sectoral resolutions for the period. Land use and emissions of air pollutants and GHG are reported mostly at a 0.5 × 0.5 degree spatial resolution, with air pollutants also provided per sector (for well-mixed gases, a coarser resolution is used) (Van Vuuren et al., "RCPs-Overview," 2011). After being refined at a smaller scale (described in the next section), these standard sets of data are used by modellers as input data to initialize climate models and avoid initialization inconsistencies with other scientific works. Arnell et al. (2011) argued that referencing the RCP and climate change projections has two potential benefits: they would facilitate comparison across research results in the climate modeling (CM), Integrated Assessment Models (IAM), and impacts, adaptation and vulnerability (IAV)

communities, and they also facilitate the use of new climate modeling results in conjunction with IAV research.

2.2.3. Statistical downscaling

Downscaling aims to transform climate information from large scale (global or regional) to a smaller or local scale (catchment). Two approaches are generally used: statistical downscaling and dynamical downscaling. The dynamical method requires running high-resolution climate models on a regional sub-domain, using observational data or lower-resolution climate model output as a boundary condition. These models use physical principles to reproduce local climates but are computationally intensive. Also, the extrapolation beyond observed values is difficult. Statistical downscaling is commonly used because of its simplicity and capability to reproduce a wide range of plausible climate scenarios (Huo and Li, 2013).

The change factor method is considered the most straightforward means of obtaining higher spatial resolution scenarios to apply coarse-scale climate change projections to a high resolution observed climate baseline (Wilby et al., 2004). This approach relies on empirical relationships between large-scale atmospheric variables (i.e., predictors) and local variables (i.e., predictands) such as precipitation and temperature by using observed meteorological data. It assumes that the relationships between predictors and predictands are constant under climate change conditions. The large-scale information from the global model is used to estimate the corresponding regional/local climate characteristics. The estimation is performed using three main methods:

- **Weather typing**: based on traditional synoptic climatology (including analogs and phase space partitioning) that relate a given atmosphere/ocean state to a set of local climate variables
- **Weather generators**: random generators of realistic-looking "weather" sequences/events conditioned in their occurrence/location statistics by the GCM large-scale
- **Regression methods**: a (set of) predictive relationship(s) between the large-scale and the target (local-regional) small scale. Such relationships are generally built up by (lagged/non-lagged multiple regression) analysis of observed large-scale climate conditions and local-regional scale (near-surface) observations

A summary of their strengths and weaknesses is presented in Table 1 (Wilby et al., 2004):

Table 1 - Characteristics of statistical Downscaling methods

Methods	Strengths	Weaknesses
Weather typing	• Yields physically interpretable linkages to surface climate • Versatile (e.g., can be applied to surface climate, air quality, flooding, erosion, etc.) • Compositing for analysis of extreme events	• Requires additional task of weather classification • Circulation-based schemes can be insensitive to future climate forcing • May not capture intra-type variations in surface climate
Weather generators	• Production of large ensembles for uncertainty analysis or long simulations for extremes • Spatial interpolation of model parameters using	• Arbitrary adjustment of parameters for future climate • Unanticipated effects to secondary variables of changing

	landscape • Can generate sub-daily information	precipitation parameters
Regression methods	• Relatively straightforward to apply • Employs full range of available predictor variables • 'Off-the-shelf' solutions and software available	• Poor representation of observed variance • May assume linearity and/or normality of data • Poor representation of extreme events

The major weaknesses of statistical downscaling methods are that the fundamental assumption on which they are based is not verifiable, i.e., the statistical relationships developed for the present-day climate also hold under different forcing conditions of plausible future climate. This weakness also applies to the physical parametrization of the dynamical method (Wilby et al., 2004), and they cannot explicitly describe the physical processes that affect climate (Hessami et al., 2008).

Statistical downscaling may be appropriate for situations of heterogeneous environments with complex physiography or steep environmental gradients (as in island, mountainous, or land/sea contexts). Due to its low computational demand, it is also convenient in the case of important limitations on computational resources and strong relationships to synoptic-scale forcing. However, it may not be appropriate when station data are unavailable for model calibration (Wilby et al., 2004).

2.2.4. Impacts on water quantity and quality

Climate change affects temperature, precipitation, and evaporation patterns in the water cycle (Kundu et al., 2017). It impacts hydrological processes such as infiltration, recharge of

groundwater, runoff generation, etc. (Dosdogru et al., 2020). This results in the potential alteration of the timing and the magnitude of peak flows (Prowse et al., 2006), reductions in water availability (Kingston and Taylor, 2010), impact on sediment yield and transport (Samaras and Koutitas, 2014; Shrestha et al., 2016), water quality (Trang et al., 2017), and reservoir capacity (Shrestha et al., 2016; Ehsani et al., 2017).

Impacts will likely vary substantially within individual regions according to differences in biophysical resources, management, and other factors (Lobell et al., 2008). A study in a rapidly urbanizing watershed in Alabama (USA) demonstrated that: (a) impacts of climate change on monthly flows indicate seasonal variation, (b) and low flows are more sensitive to land use/cover change than climate change (Dosdogru et al., 2020). Similar investigations performed in 2013 on Jianzhuangcuan catchment (Shaanxi, China) reports scenarios, where a 0.6-0.9 °C increase in annual temperature and changes of 12.6-18.9 mm in seasonal precipitation led to an augmentation in stream flow of 12% and 69% for 2020 and 2030 predictions respectively. The highest monthly increases occurred during the February-June period (Huo and Li, 2013). Anjum et al., (2019) conducted a study to assess the potential impacts of projected climate changes on the outflows of a humid subtropical basin in Pakistan under extremum Representative Concentration Pathways (RCPs 4.5 and 8.5) using SWAT model. They concluded that: (a) increase in the annual average flow under both RCPs (ranging from 0.3 to 44.4% compared to the annual average flow in the baseline period), (b) an increase in the low and medium flows, and (c) advancement in the peak flow month (from July to June).

In Canada, few studies have also demonstrated the increase of water flow in the future (e.g., Shrestha et al., 2017; El-Khoury et al., 2015). Shrestha et al. (2017) used future (mid- and late century) climate projection generated by the Canadian Center for Climate Modelling and Analysis

Regional Climate Model (CanRCM4) under RCP 4.5 and 8.5 and predict the climate of the basin to be wetter by 21–34% and warmer by 2–5.4 °C on an annual time scale, increasing the annual average blue and green water flow by 16–54% and 11–34%, respectively. However, the estimated predictions depend on the region, future period, and emission scenario. On the other hand, El-Khoury et al. (2015) reported changes in streamflow will mainly be impacted by climate change. Findings from this research showed that a) climate change will drive up the maximum monthly streamflow and b) land-use changes were found to drive the same water quantity variable in the same direction as climate change. A few years later, Persaud et al. (2020) carried out a more extensive study (surface water and groundwater) on the cross-border Great Lakes Basin (USA, Canada). He used projections derived from Regional Climate Models (RCMs), a synthetic scenario based on IPCC fifth assessment report predictions (AR5), and temporal analogs. The conclusion was a greater likelihood for a significant reduction in mid-century discharge relative to any significant change in groundwater head or net exchange flux between surface and subsurface domains.

Climate change also affects water quality. The investigations of El-Khoury et al. (2015) on the climate change impacts on water quality in a Canadian river basin quantified the percentages of change in nitrogen and phosphorus concentrations in the river over the 2025-2050 period. Annual average variations of -0.1%, -9.4%, -24.1% were predicted for Nitrate, Nitrite, and Organic nitrogen, respectively, under future climate change scenarios. However, an increase of 29.4% and 49.1% was predicted for organic phosphorus and mineral phosphorus. Also, more generally, climate change will drive up maximum monthly nitrate loads and organic phosphorus loads while decreasing organic nitrogen and nitrite loads.

2.3. Urbanization impacts on water quantity and quality

Land-use change is considered as one of the major factors impacting the quantity and quality of water. The replacement of natural cover by roads, residential, commercials, and other types of impermeable land uses blocks the infiltration of water into the ground, causing the increase of surface runoff and floods. Several studies have shown that increasing the extent of an urban area increases peak discharge (Debbage and Shepherd, 2018; Beighley and Moglen, 2002; Barringer et al., 1994, Brun et al., 2000; Cheng. et al., 2002; etc.). However, the extent of the developed area is not the only factor to be considered. Debbage and Shepherd (2018) draw our attention to the overall importance of considering the configuration and positioning of urban development when devising land-use policies to minimize streamflow alteration due to urbanization. Recent research carried out by Blum et al. (2020) concludes that a one percentage point increase in impervious basin cover causes a 3.3% increase in annual flood magnitude on average in the United States. This study was performed using 39 years of data from 280 U.S. stream gages, and a higher increase of 4.6% was observed with 2,109 stream gages. A similar study in the Qinhuai River basin (China) using an integrated hydrological modeling system reveals that a change of impervious ratios from 3% (1988) to 31% (2018) results in a slight increase of the mean annual runoff (Du J. et al., 2012). The daily peak discharge of eight selected floods would increase from 2.3% to 13.9% This increase of more than 11% may have considerable effects over a long period. Du J. et al. (2012) also indicated that small floods were more sensitive than large floods to urbanization. Several years ago, Bhaduri et al. (2001), investigated in the relationship between urban area change and runoff using two models: the L-THIA (Long-Term Hydrologic Impact Assessment) model to initially assess how land-use change affects annual average runoff; and the U.S. Environmental Protection Agency's SWMM (Storm Water Management Model), a well-known and widely used model used

for runoff calculations. L-THIA and SWMM were applied to two watersheds in Chicago (USA), and both models predict a linear relationship between average annual runoff and increasing imperviousness.

Land land-use change also affects water quality. Changes in nitrogen species will mainly be driven by land-use changes (El-Khoury et al., 2015). Like runoff, the deterioration of water quality is related to the impervious area in urbanized zones. The primary factor is the pollutants coming from the de-icing process of roads followed by the snowmelt during the spring season and storm water during summer/fall, which carries pollutants, including nitrogen and phosphorus, from urban surfaces into local waterways. In cold countries like Canada, salt is used for street de-icing in winter and becomes a roadway component removed with snow and the resulting meltwater. Dissolved in the meltwater, the salt ions chloride and sodium can either flow into receiving streams or infiltrate into ground water (South Dakota Department of Water and Natural Resources, 1990). Judd (1970), in his study on First Sister Lake (Michigan), has shown that salt contamination can cause increased density in the lower lake strata, preventing normal mixing.

Point sources such as wastewater treatment plants, discharging considerable amount of nutrients (nitrogen and phosphorus mainly) are also a part of the problem related to the water quality. In America, nutrient pollution caused by excess nitrogen and phosphorus in the air and water is one of the most widespread, costly, and challenging environmental issues (U.S. EPA, 2019). It affects both ground water people use as their drinking water source, and surface water bodies (lakes, rivers, coastal waters, bays, etc.) are indispensable for socio-economical activities. One effect of this pollution in lakes is eutrophication, one of the most severe problems in water resources management worldwide (Taranu et al., 2017; Hayes and Vanni, 2018). In a quantitative view, land use was the dominant factor affecting nitrate load. The relative importance of land use alone was

~50%, according to a recent study on Prince Edward Island in Canada (Liang et al., 2020). However, El-Khoury et al. (2015) found out that climate change, and land land-use change on organic and mineral phosphorus were roughly equal. More specifically, Liu et al. (2015) demonstrated the increase of agricultural land uses within watersheds deteriorates the quality of water.

All these studies confirm and describe the impacts of urbanization on water quantity and quality. This review also demonstrates that importance should be accorded particularly to discharge, nitrogen, and phosphorus in the assessment of impacts and justifies our choice for these last two parameters of water quality for the hydrologic modeling in this work.

2.4. Literature gaps and research justification and novelty

Climate change is undoubtedly a reality, and it affects every region on the earth. With the rising living standards and socio-economical levels to meet the rapid increase of global population demand, the evaluation and planning of the resulting impacts on natural resources become a necessity. In this context, several countries, including Canada, have ratified an agreement in 2015, known as Paris Agreement, to limit their contribution to climate change.

Since 2005, several studies related to the preparation of the Carp River model were conducted:

- Characterization and Flood Level Analysis for Carp River, Feedmill Creek and Poole Creek (CH2MHill, October 2005)
- Post Development Flow Characterisation and Flood Level Analysis for Carp River, Feedmill Creek and Poole Creek (CH2MHill, June 2006)
- Kanata West Master Servicing Study (Stantec, 2006)

- Third-Party Review - Carp River Restoration Plan (Greenland International Consulting Ltd., March 2009)
- Carp River Restoration Plan – Widening Alternatives (Greenland International Consulting Ltd., May 2010)
- Carp River Model Calibration Validation Exercise Final Report (Greenland International Consulting Ltd., July 2011)
- Model Development Program - Carp River Restoration Plan Draft Report (Greenland International Consulting Ltd., February 2014).
- Carp River PCSWMM Model documentation (City of Ottawa, March 2016)

The focus of all these works was on flood level analysis and restoration plan. The most recent study, prepared by the City of Ottawa, consisted of converting several previous hydrological/hydraulic models (XPSWMM/QUALHYMO/HEC-RAS) prepared by Greenland International Consulting Ltd into an integrated PCSWMM platform. After a review of the report of this last study, it emerged the preparation of the model considered the future developments. However, the climate change effect was not taken into consideration. Also, the impact on water quality, especially the nutrients, was not assessed. Beyond that, a limited number of local studies addressing the combined effect of climate change and urbanization were available. Due to the similarity to this study, the one that was of a particular interest assessed the impact of climate change and deforestation on the South Nation watershed (El-Khoury et al., 2015) in opposition to urbanization.

Finally, a comprehensive review of similar studies worldwide (including the impact study on the South Nation watershed) pointed out the limitation of most studies to the watershed-scale impact

assessment. Not enough investigations were conducted to evaluate and compare the impact at the sub-watershed level.

Therefore, based on the listed limitations of previous works, the novelty of this study was primarily and mainly the global/local approach used for an extended impact assessment as well as the consideration of the climate change and urbanization effects together, especially with the developments occurring in the headwaters and not downstream.

This study will provide information on planning and decision-making on water management, in terms of quantity and quality, under future climate and land-use conditions.

3. Materials and methods

3.1. Study area

The Carp River is an essential natural ecosystem located west of the City of Ottawa in the province of Ontario (Canada). It is 42 km long and drains an area of approximately 265 km² with coordinates ranged from 76°13'54.586"W to 75°53'40.344"W (longitude) and 45°13'42.281"N to 45°29'43.270"N (latitude). It has its headwaters in the Glen Cairn area of Kanata and flows north into the Ottawa River at Fitzroy Harbour, the main outlet. The Carp River is one of the sources of the City of Ottawa's drinking water. A hydraulic model of the carp river was previously developed by the City of Ottawa, including major tributaries such as Corkery Creek, Huntley Creek, Feedmill Creek, and Poole Creek (Figure 4). In this work, the watershed has been extended to cover the catchment area of the section of the river going from the outlet to the main outlet located at Fitzroy Harbour (Figure 4). This added area is mainly agricultural land.

The watershed has its highest elevation on the South-East side with an altitude of 203 m, while the lowest point (the outlet at Fitzroy Harbour) has a height of 59 m. In 2017 (the latest update of land use data, OFAT), the dominant land use was agricultural (AGRC), occupying about 52% of the total area (Figure 5.B), followed by wooded wetland (18%). Eight (8) other land uses are present within the basin, shown in Table 2. Globally, natural land-use area represents 90.1% while urban area is only 9.9%. It is important to mention that the land use is assumed unchanged during the period of simulation. This assumption is not realistic for an extended period of study. Still, it will establish a direct relationship between the land use change and water discharge and water quality variables.

Soil characteristics downloaded from a global database (FAO, 1979) show four (4) types of soil within the watershed, with the most dominant representing 51% of the total area (Table 3).

Details related to these data (sources, the resolution) are further discussed in the next section.

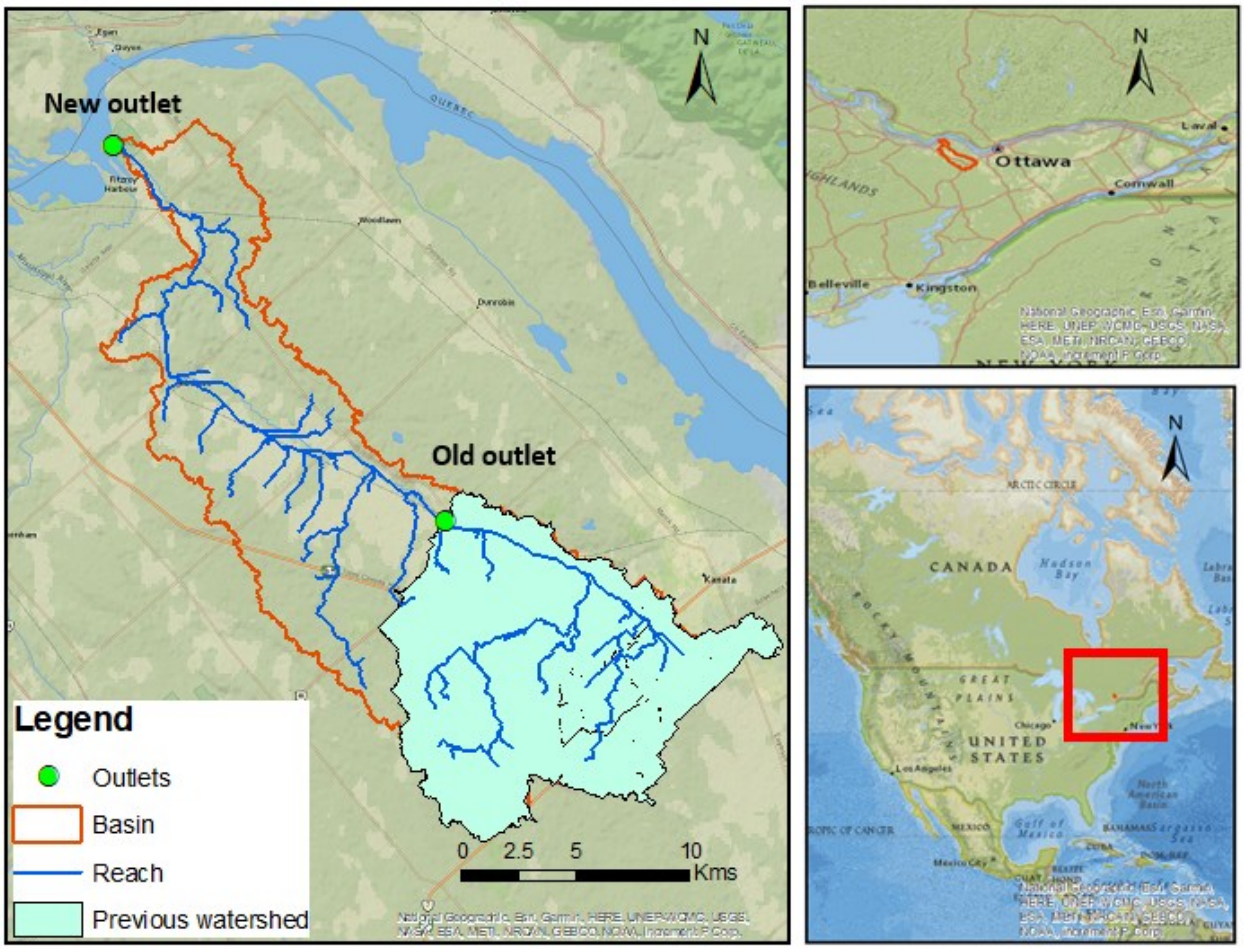

Figure 4 - Location of Carp River watershed

A)

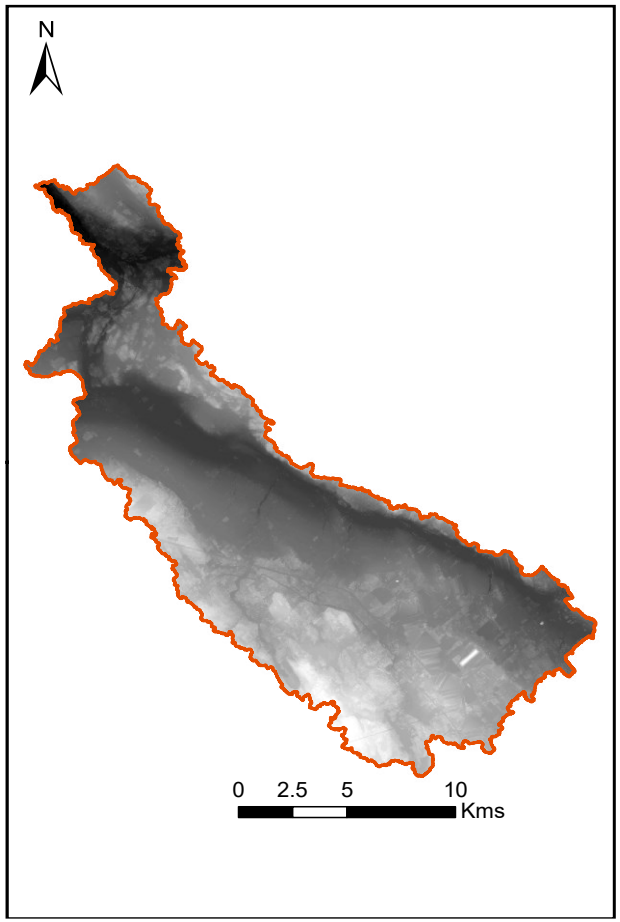

B)

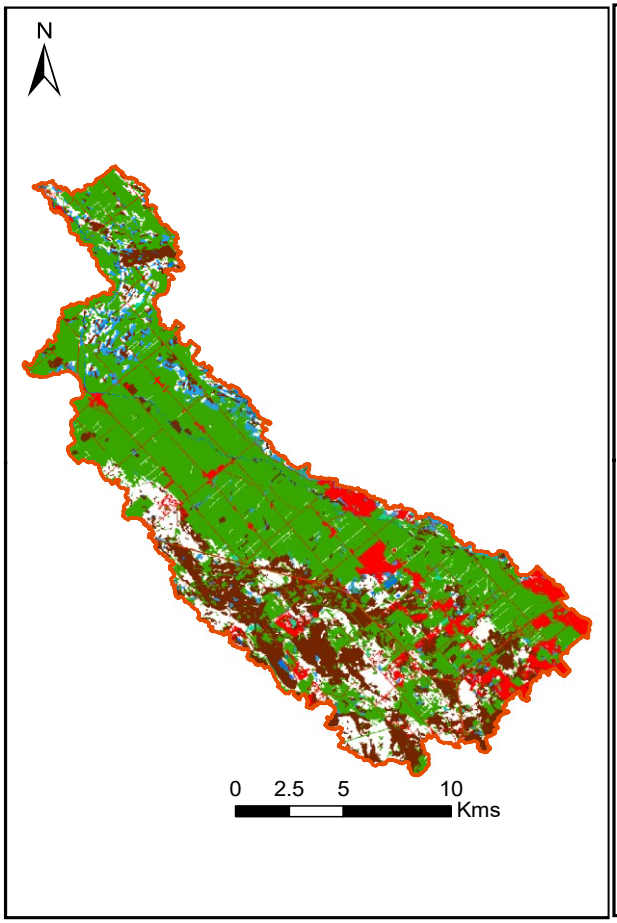

C)

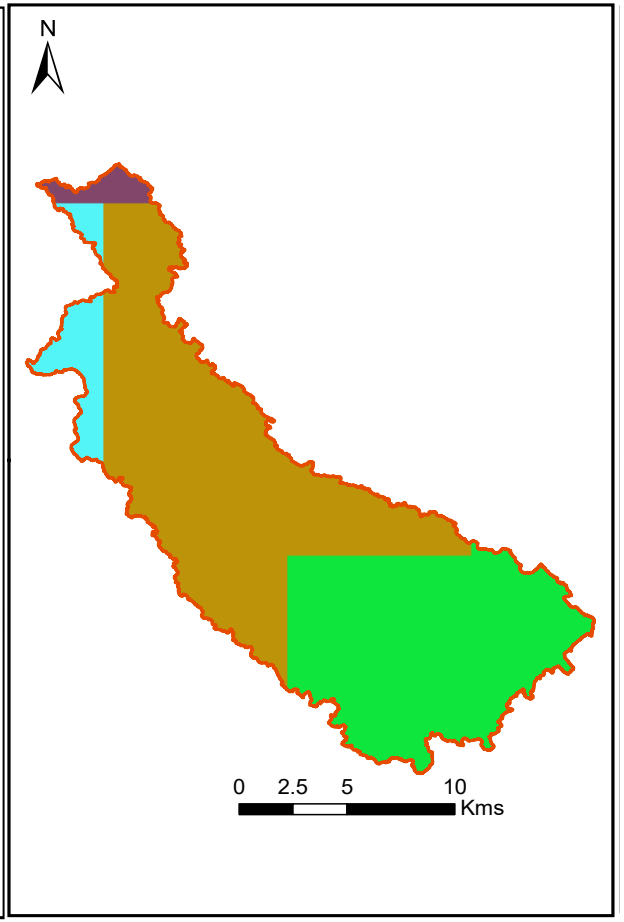

Figure 5- Carp river watershed: A) Topography map. B) Land use map. C) Soil map

Table 2 - Land use characteristics (Provincial database)

LU Type	SWAT Code	Area %
1. Agricultural Land	AGRC	52.34
2. Wooded Wetland	WEWO	18.02
3. Evergreen Needleleaf Forest	FOEN	9.93
4. Urban	URBN	9.90
5. Forest - Deciduous	FRSD	4.16
6. Forest-Mixed	FRST	3.25
7. Barren Or Sparsely Vegetated	BSVG	0.82
8. Water	WATR	0.69
9. Mixed Forest	FOMI	0.55
10. Cropland/ Woodland Mosaic	CRWO	0.34

Note: SWAT Codes based on the Swat database

Table 3- Soil characteristics (Global database)

Soil texture	SWAT Code	Area %
Loam*[1]	Be1-2a-4649	51.29
Loam*[2]	Be1-2a-4648	40.30
Sandy Loam	Po2-1-2b-4971	6.33
Clay	Gm3-3a-3070	2.08

Note: The two types of loam differ in their available water holding capacity: 0.08 mm/mm (*[1]) and 0.175 mm/mm (*[2])

3.2. Input data

The model building requires three (3) sets of input, including geographic data: topographic map (Figure 5.A), land use map (Figure 5.B), soil map (Figure 5.C); weather data: precipitation, temperature, solar radiation, relative humidity and wind speed; and water quantity and quality data (flow, nitrogen, phosphorus). Table 4 provides a summary of all the data sets used.

Table 4- Data and sources used in the setup of the initial SWAT model, calibration, and validation

Type	Description	Scale/Resolution	Source
	Model setup		
Topography	Elevation - LiDAR	1 m	City of Ottawa
Land use	Categories of land occupation (wood, urban, agricultural, etc.)	30 m	Ministry of Natural Resources and Forestry - Ontario
Soil	Soil types and physical properties	10 km	Food and Agricultural Organization (FAO)
Weather	Precipitation, Temperature	Daily	Environment and Climate Change Canada (ECCC)
	Solar radiation, Relative humidity, Wind speed	Daily	Watch-Forcing Data ERA-Interim (WFDEI)
	Calibration / Validation		
Water quantity	Stream Flow recorded at a specific point	Monthly	HYDAT – Environment Canada
Water quality	N, P	Monthly	Ministry of Environment (Ontario)

3.2.1. Geographic data

Geographic data presented as maps should be projected on the same coordinate system before their use. A projected coordinate system is defined as a representation of the earth (or a part) on a flat, two-dimensional surface (Environmental Systems Research Institute (ESRI) - ArcGIS for Desktop, 2016). Unlike the geographic coordinate system, which indicates "*where*" the data is located on the earth's surface, the projected coordinate system indicates "*how*" the map should be drawn (ESRI, 2020). An illustration of this process is when trying to roll out a spherical object (football ball, for example) on a flat surface, a distortion will occur naturally. Similarly, that is what happens when the globe is represented on a flat map.

It is crucial to select an adequate projected coordinate system. For example, based on the UTM grid zone map (Figure 6) available on the Natural Resources Canada website, the projected system used for the watershed of Carp River located in the region of Ottawa is UTM_Zone_18N (EPSG 32618) on a WGS_1984 datum.

Geographic data include topography, land use, and soil information. They are required to delineate and characterize the watershed (slopes, channel lengths, area of sub-watersheds, etc.). Therefore, an accurate topographic map is highly recommended to complete a good watershed delineation and create a stream network close to the existing network. In this study, the topography is obtained from LiDAR (Light Detection And Ranging) data. LiDAR is a remote sensing method used to produce accurate elevation information in the form of raster data. It was completed in 2015 and kindly provided by the Department of Surveys and Mapping of the City of Ottawa. The resolution is 1m x 1m. The latest year of publication was in 2015. Data were initially presented as several continuous tiles in Lidar's original format ".las" and a pre-processing (merging, clipping, and converting) was required to be converted into usable data by the model (.tif).

The land use data was downloaded from the local authority database and had a resolution of 30m x 30m. The map is available on the Ontario Flow Assessment Tool (OFAT) website, powered by the Ministry of Natural Resources and Forestry (2017). OFAT is a provincial database coupled with a GIS environment and presented as a featured tool able to create watersheds, calculate watershed characteristics, execute hydrology models, and report water flow statistics. To use the data in SWAT, the initial types of land use defined in OFAT have been reviewed and reclassified to correspond to the SWAT database. Since the land use map is not provided with all the information needed by the model for each land use, this standardization was required to avoid missing characteristics and have consistent information related to the model's database.

Maps with different resolutions were available in terms of soil map, from local (250 m) to global scale (up to10 km). Among the different databases, the soil map from the Food and Agricultural Organization (FAO), a global database, was already prepared to be used directly in SWAT without any further processing of reclassification. Although the resolution of this database is coarse compared to others, it has been demonstrated increasing the resolution of the soil map particularly does not necessarily improve the simulation (Ye et al., 2010; Mukundan et al., 2010; Geza & McCray, 2008). Therefore, the global database of FAO with a resolution of 10 km x 10 km was used (UNESCO, FAO, 2007). The soil map (Figure 5.C) includes four types of soils and are defined by codes. Soil texture, available water content, hydraulic conductivity, bulk density, and organic carbon content information were available for each soil type. Therefore, FAO soil map is already prepared to be used in SWAT without any specific processing, except for the projection that we have discussed in the previous section.

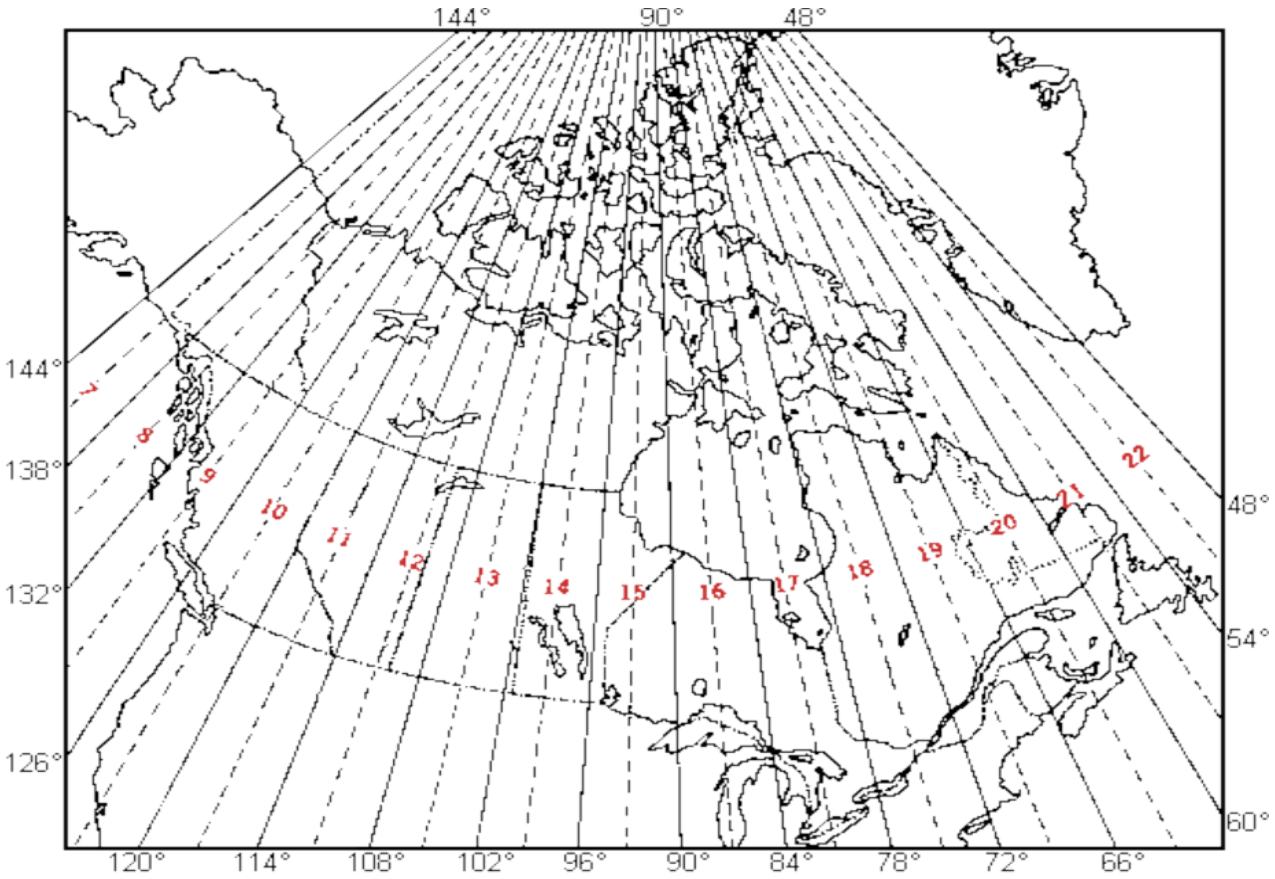

Figure 6- UTM Zones and Central Meridians for Canada (Source: Natural Resources Canada)

3.2.2. Weather data

Weather data consist of precipitation, maximum and minimum temperatures, solar radiation, relative humidity, and wind speed. These data are used by SWAT/ArcGIS as input to simulate physical and hydrological phenomena within the watershed, such as infiltration, evaporation, and runoff as well as interactions between groundwater and surface water.

Once the model has been set up, water quantity and quality data are required to calibrate streamflow and selected water quality parameters.

Two types of weather data were used in the model: observed historical data for precipitation and temperature and reanalysis data for solar radiation, relative humidity, and wind speed. Historical

data represent the actual weather condition recorded in the past at two specific locations outside the watershed (no station with data within were available) near the International Airport of Ottawa (Figure 7), which are the closest stations to the Carp River watershed where sufficient data were available. They were obtained from the national database (Environment and Natural Resources Canada, 2020) and cover the simulation period of 1990-2018. Closer stations were available; however, their data were either out of date or not long enough to run the model efficiently. Average monthly values for precipitation and temperature (maximum and minimum) are illustrated in Figure 8.

The reanalysis data are downloaded from the database of Watch-Forcing Data ERA-Interim (WFDEI – Weedon et al., 2014), lastly updated in May 2016. They were used as an alternative to the lack of data for solar radiation, relative humidity, and wind speed. They are "produced via data assimilation, a process that relies on both observations and model-based forecasts to estimate conditions" (Parker, 2016). Therefore, they cannot be considered as observations or measurements (Bosilovich et al., 2013), but higher quality simulated data. Reanalysis data are simulated on uniform grid points over the world as daily average. As shown in Figure 7, four points are used. They are located at each corner of the watershed and form a rectangular grid of at 0.5^0 x 0.5^0 resolution. The original data files are NetCDF files used as community standard for sharing scientific data according to the UCAR Community Program (2012). They have been pre-processed into time series excel files using MATLAB (v. 2019) software.

The characteristics of weather stations are presented in Table 5.

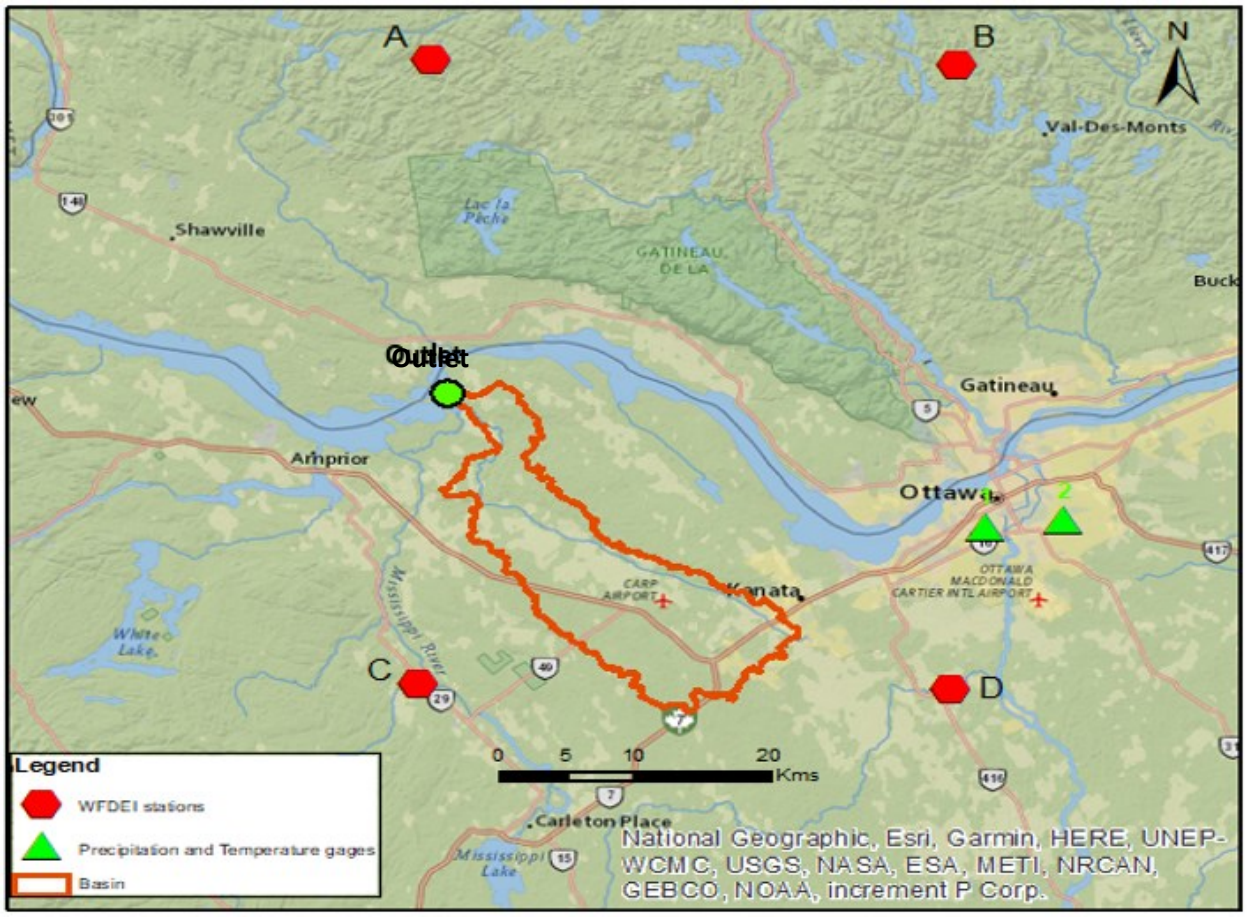

Figure 7- Location of weather stations

Table 5 - Weather stations characteristics

	Station Name (Climate ID)	LONG.	LAT.	Distance to watershed (KMs)
1	Ottawa CDA (6105976)	-75.720	45.380	16.5
2	Ottawa Macdonald-Cartier Int'l (6106000)	-75.645	45.385	22
A	-	-75.250	45.750	30
B	-	-75.750	45.750	42
C	-	-75.250	45.250	11
D	-	-75.750	45.250	11

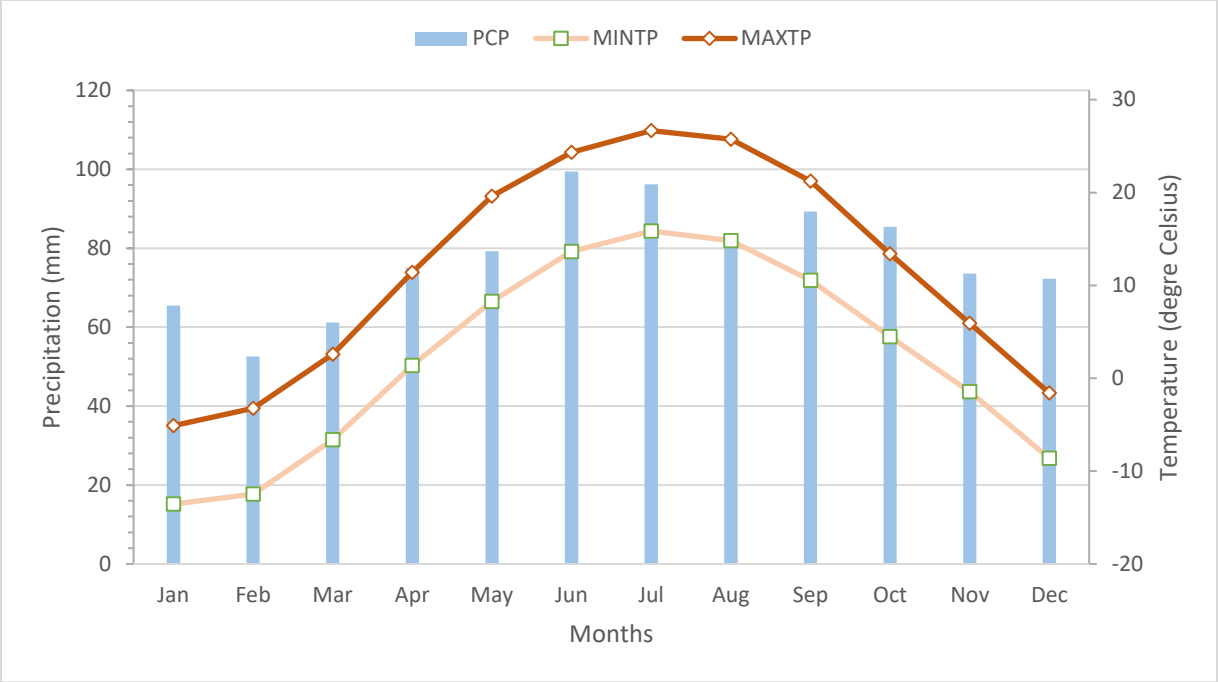

Figure 8 - Monthly average precipitation and temperature

PCP = Precipitation, MINTP = Minimum Temperature, MAXTP = Maximum Temperature

3.2.3. Water quantity and quality data

Monthly flow data are recorded and compiled by the Water Survey of Canada (Environment Canada). The data are free to access and housed on two databases: HYDEX and HYDAT (Environment and Natural Resources, 2018). A single flow station located within the watershed was available covering the period of 1990 to 2015. Since there was no gage available at the main outlet, the calibration for streamflow is performed for the parameters of sub-watersheds upstream draining to the outlet where the available gage is located (Figure 9).

Water quality data were kindly provided by the Mississipi Valley Conservation Authority (MVCA). Samples were collected at monthly time step at several locations and analyzed for water quality parameters. However, only the sampling points located within the watershed and on the river's main channel are considered for the study. Therefore, two stations were considered (Figure

9). Unfortunately, water sampling was not possible during winter (December - March) because of the freezing condition of the water.

Table 6 presents the characteristics of the stations discussed above.

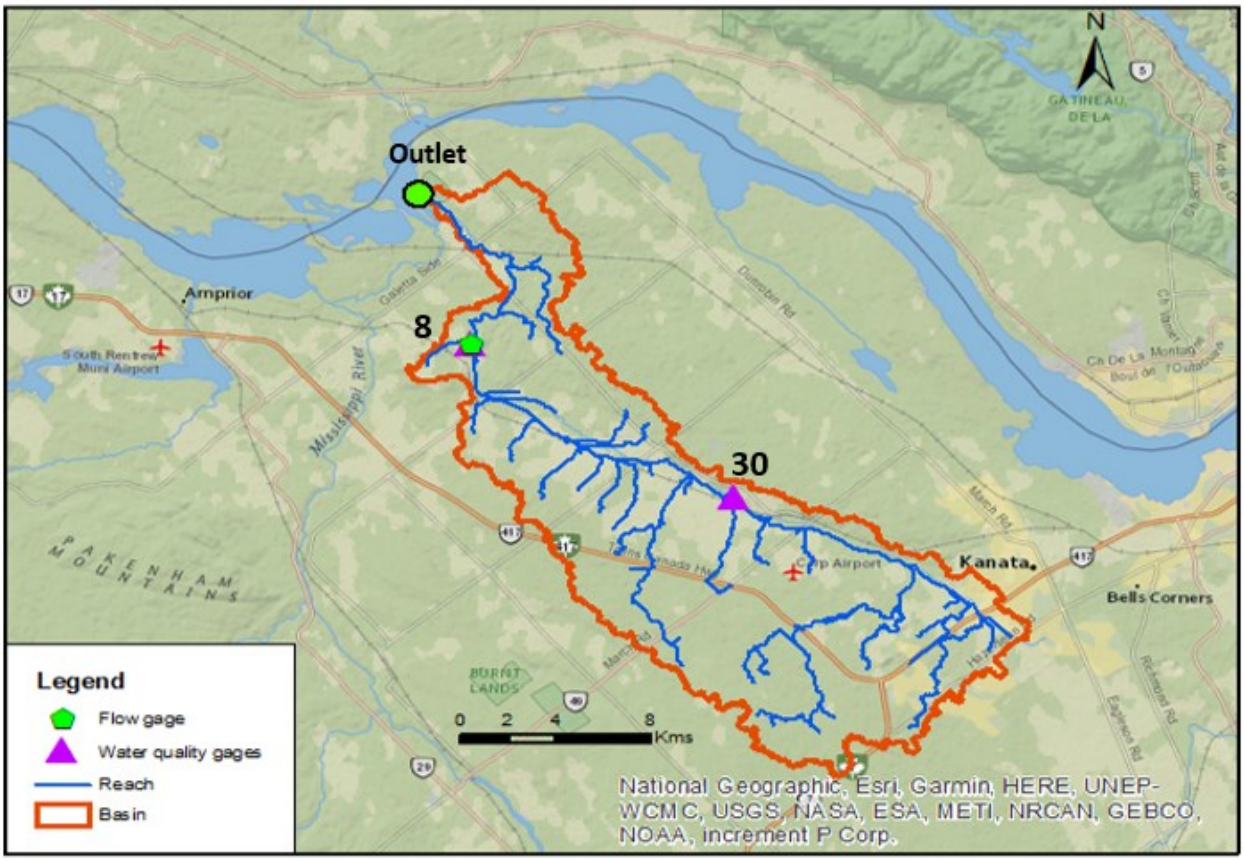

Figure 9- Location of water quantity and quality stations

Table 6- Characteristics of water quantity and quality gages

	Sub-basin No.	Longitude	Latitude	Period
Flow	8	-76.197	45.420	1990-2015
Water quality (N, P)	8	-76.197	45.420	2000-2018
	30	-76.059	45.352	2000-2006

3.3. Methodology

3.3.1. SWAT: Description

SWAT has been used for Carp River watershed delineation. It is a physically-based, semi-distributed and continuous model used to evaluate and predict and predict and predict the impacts of climate change and land use management on water quantity and quality. It is used within a Geographic Information System (GIS) environment, ArcGIS in this case. The model operates on a daily time step and can simulate continuously over a long time. The simulation period in this study starts from 1990 to 2018, representing the period covered by the available weather input data.

The processing mode of SWAT consists of dividing the watershed into several sub-watersheds, which are further subdivided into Hydrologic Response Units (HRUs). HRU is described as a unique combination of topographical, land use management and soil characteristics (Arnold et al., 2012). For the Carp River watershed, a total of 55 sub-watersheds (Figure 10) were delineated with 131 HRUs. Attributes of these sub-watersheds include mean slope, mean/max/min elevations (from DEM), area and perimeter.

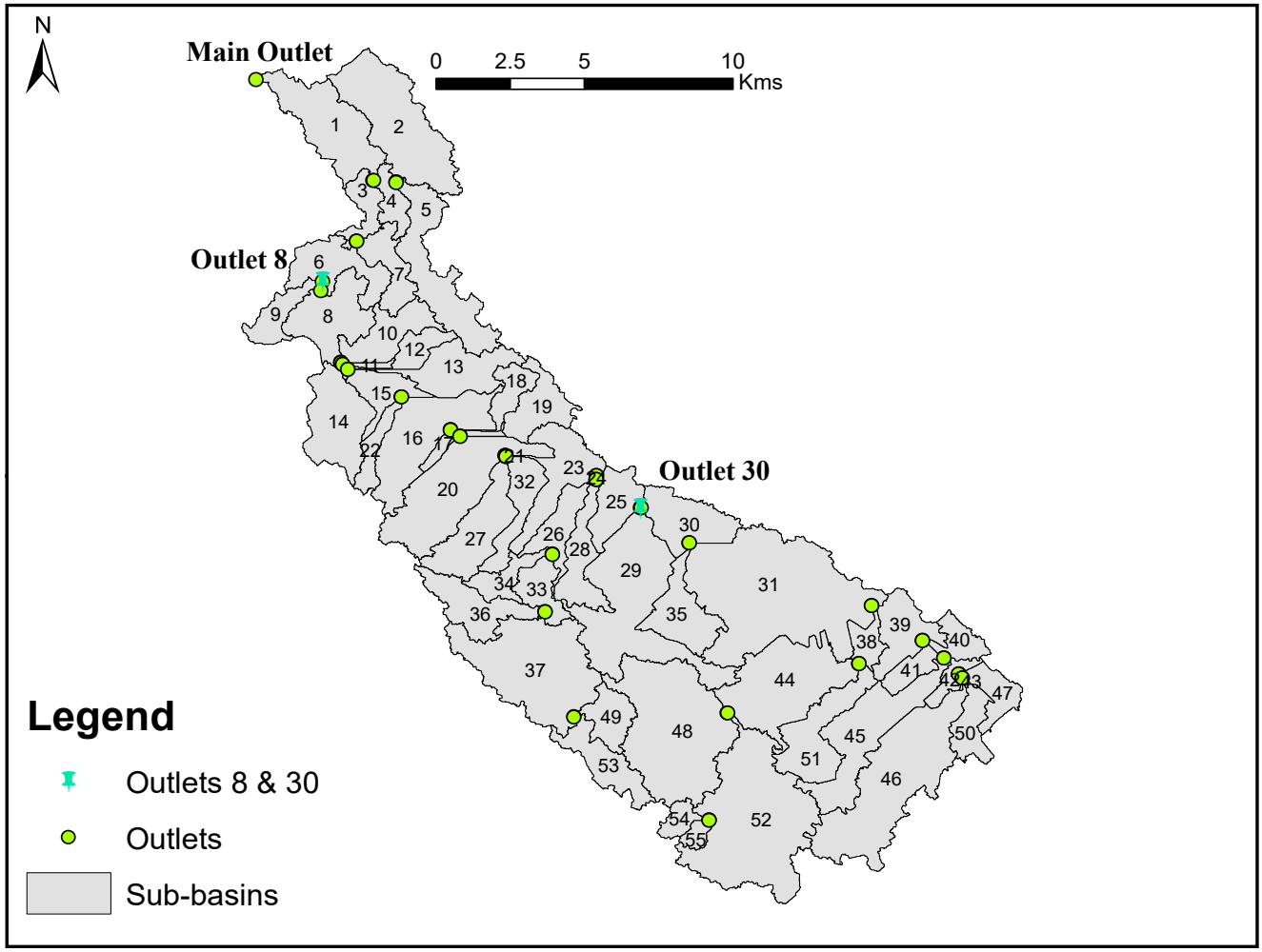

Figure 10- Carp River watershed delineation in ArcGIS

3.3.2. SWAT: Setup

SWAT modelling goes through several steps before having a final "good" model. The first step is the acquisition and preparation of input data. The processing includes several sub-steps:

1. the conversion and the merging of Lidar data (.las files) into a single and usable raster map by SWAT;
2. cropping the map to cover only the study area to reduces the process time of the watershed delineation considerably;

3. the reclassification of land use categories as described in section 3.2.1,
4. the processing of weather data from NetCDF to Excel time-series.

The second step is watershed delineation. Jajarmizadeh et al. (2017) mentioned that this step consists of:

1. digital elevation map set-up,
2. stream network burning,
3. outlet and inlet localized
4. basin outlets selection,
5. definition and calculation of sub-basin parameters.

Jajarmizadeh et al. (2017) also stated that for overlying the digital streams, the threshold-based stream burning was used by considering the minimum size of the sub-basin. A smaller minimum area gives a larger number of reaches. The next step consists of importing land use and soil maps and specifying slope information. Based on the elevation data, different slope classifications are possible due to the spatial distribution of the watershed and better identification of the spatial location of HRUs (Jajarmizadeh et al., 2017). Considering the relatively flat topography of the area, a single slope class was selected (uniform slope class over the watershed). Finally, these three data are overlaid and linked to the SWAT database. The database contains all the characteristics required by the model to define HRUs. Once the definition of HRUs is completed, the weather data are then written into the model as input. All the files must be prepared as .txt files containing information about the location of different gages, the starting date of data, and time series related to each weather variable recorded at each station. Data must start at the same date and cover the same simulation period (1990-2018). The last step is to set up the model. The user can specify the simulation period (must be shorter or equal to the period covered by data), select the printout time

step (daily/monthly – monthly time step was chosen), the variables to be printed out (e.g., water depth/velocity output, water quality output) and the warm-up period. Warm-up period is used to ensure there are no effects from initial conditions in the model. For a simulation of 5 years or less, equilibration and warm-up by SWAT are recommended; meanwhile, it can be optional (Jajarmizadeh et al., 2017). Therefore, the warm-up period could be ignored since the simulation period in this study is more than 5 years. However, a warmup period of 2 years was selected for more accuracy and to avoid more sources of error than the uncertainties previously discussed in section 2.1.2. Finally, the model is run at a daily time step for 29 years.

Table 7 presents the model setup, and a flow chart of the methodology is presented in Figure 11.

Table 7 - Carp River SWAT model setup

Watershed area	263.85 km^2
Number of sub-basins	55
Number of HRUs	131
Simulation period	1990/01/01 - 2018/12/31 (29 years)
Warm up period	2 years
Output time step	Monthly

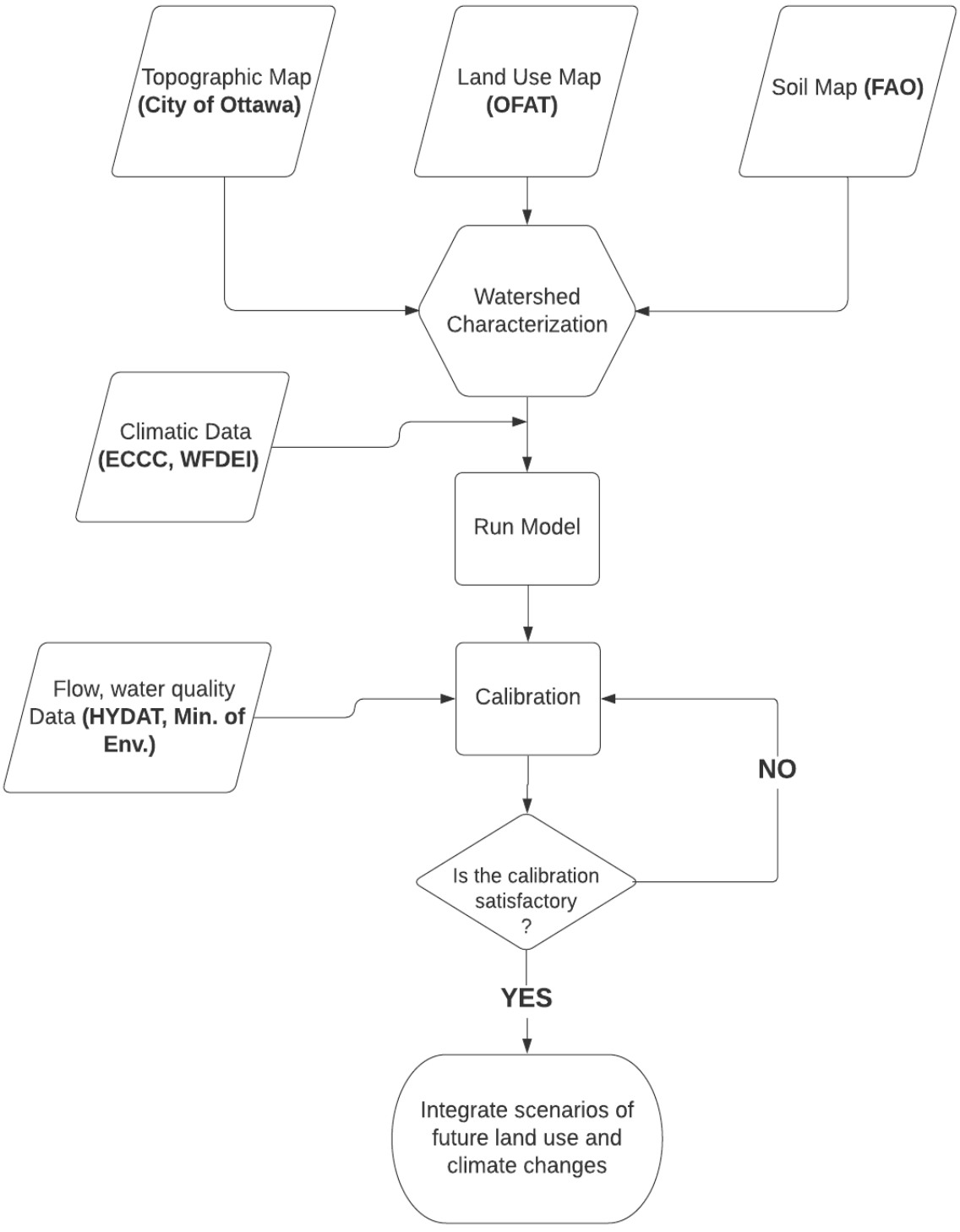

Figure 11- SWAT model methodology flow chart

3.3.3. Calibration and validation of the model

Calibration consists testing the model with known input and output used to estimate or adjust hydrological parameters, while validation is the comparison of model output with independent data without any further adjustment. Two calibration techniques exist manual calibration and automated calibration. In manual calibration, the user may need to manually modify the hydrological parameters once the original model is built, while the automated procedure uses a systematic iterative approach and is more complex. Manual calibration is performed using the *Manual Calibration Helper* option in the SWAT Editor. Besides the ease to learn and convenience, however, there are some drawbacks of this method: (1) parameters to be modified are selected and may not be sufficient for the model (relevant parameters such as OV_N, RCN, N_UPDIS, ERORGN, etc.. are not listed); (2) parameters of specific soil layer cannot be modified (e.g., Sol_K means Sol_K of all soil layers will be updated); (3) the modified value may exceed the absolute value range which is defined in Absolute_SWAT_Values.txt; (4) manually operation is tedious and error-prone. These reasons justify the preference for automated method.

SWAT-Cup (Abbaspour ,2007) is used for the Carp River model calibration/validation. It was performed using the SUFI-2 (Sequential Uncertainty Fitting) algorithm because it is the one that needs the smallest number of runs to achieve good prediction uncertainty ranges with reasonable coverage of data points among the calibration techniques available in SWAT-CUP (Yang et al., 2008). The first step is the determination of the most sensitive parameters of the watershed. In this step, the most sensitive parameters that highly influence the model's performance are determined for adjustment in the next step, while other parameters are removed. SWAT input parameters are process-based and must be held within a realistic uncertainty range, generally from experience or

sensitivity analysis, defined as the process of determining the rate of change in model output concerning changes in model inputs/parameters (Arnold et al., 2012).

The second step is the calibration and aims to better parameterize the model by reducing the uncertainty. The values of the most sensitive parameters (from the previous step) are carefully selected considering their respective realistic range and compared to model predictions (output) for a given set of assumed conditions with observed data for the same conditions. The process is iterative, and the number of iterations needed depends on the complexity of the watershed (e.g., presence of dam) or the number of variables to be calibrated. However, the number of runs in each iteration is generally set to 500.

The last step is the validation of the model. The set of parameters determined from the calibration process are used to run the model once, and the outputs are compared to observed data. The validation provides the user with the performance of capability of the model to simulate the watershed conditions for a different period. The better the performance in the validation process, the more accurate its ability of predicting under different scenarios.

The general calibration procedure recommends the calibration of parameters sequentially, and the order of calibration is based on the relevance of the parameter (Arnold et al., 2012). Other studies (e.g., Santhi et al., 2001; Engel et al., 2007) recommended that streamflow, sediment, and nutrient transport be calibrated sequentially (in that order) because of interdependencies between constituents due to shared transport processes. (Arnold et al., 2012). More parameters such as water temperature, pesticide transported could also be calibrated since the data were available. However, this would impact the calibration performance related to the precedent parameters we are interested in in this study. For this reason and because sediment load data was unavailable, only flow, nitrogen and phosphorus could be calibrated.

The period of 1990 to 2005 was selected for the calibration of discharge. Due to lack of data, shorter and different periods were used for water quality calibration (Total nitrogen and Total phosphorus): 2000 to 2012 and 2000 to 2003 for the two stations available at outlet of sub-basins 8 and 30 respectively (Figure 9). Monthly data for each variable is divided into two periods: one for calibration and the other for validation.

Table 8-Data distribution for calibration and validation

Variable		**Period**	
		Calibration	**Validation**
Discharge*		1990-2005	2007-2015
nitrogen	**Outlet 8**	2000-2012	2013-2018
	Outlet 30	2000-2003	2004-2006
phosphorus	**Outlet 8**	2000-2012	2013-2018
	Outlet 30	2000-2003	2004-2006

***The one-year gap (2006) in discharge data is due to missed data. Therefore, 2005 and 2007 are the ending point and starting points, respectively, for calibration and validation for the discharge variable.

The list of parameters initially used as well as the uncertainty ranges for the sensitivity analysis are presented in Table 9, Table 10, and Table 11. They are chosen based on a careful selection procedure including the comparison and combination of most relevant parameters analyzed in literature (e.g., Abbaspour, 2007; Arnold, 2012; Khoiab and Thomb, 2015; Abbaspour et al., 2015; Mengistu et al., 2019 and Khalid et al., 2016). In total, 22 parameters were used for the process:

10 are related to discharge, 6 for N and the remaining 6 for P. SWAT-CUP also provides absolute values of each parameter, which helped set maximum and minimum values under calibration.

SWAT-CUP allows three types of operations that can be used when modifying the parameters during calibration: (1) Replace or ***v_*** - the existing parameter value is to be replaced by the given value, (2) Absolute or ***a_*** - the existing parameter value is added to a given value and (3) Relative or ***r_***- the existing parameter value is multiplied by (1 + a given value). Replace is generally selected when the parameter to modify has the same value for all sub-watershed (e.g., phosphorus sorption coefficient).

Table 9- Selected parameters for the calibration of discharge.

Parameters	Description	Range
1. r__CN2.mgt	Initial SCS CNII value	-0.2 - 0.5
2. v__ESCO.hru	Soil evaporation compensation factor	0.01 - 1
3. v__GWQMN.gw	Threshold water depth in the shallow aquifer for flow	0 - 2500
4. v__ALPHA_BF.gw	Baseflow alpha factor	0 - 1
5. a__REVAPMN.gw	Threshold depth of water in the shallow aquifer for "revap" to occur (mm)	0 - 500
6. v__SOL_AWC.sol	Available water capacity of the soil layer (volume fraction)	0 - 0.8
7. a__OV_N.hru	Manning's "n" value for overland flow	0.01 - 4
8. v__GW_REVAP.gw	Groundwater ‘revap’ coefficient	0.02 - 0.15
9. a__SLSUBBSN.hru	Average slope length	10 - 130
10. v__SOL_K.sol	Saturated hydraulic conductivity (mm/hr)	0 - 1

Table 10- Selected parameters for the calibration of nitrogen

Parameters	Description	Range
1. a__RCN.bsn	Concentration of nitrogen in rainfall (mg N/L)	0 - 15
2. a__ERORGN.hru	Organic N enrichment ratio	0 - 5
3. a__SHALLST_N.gw	Concentration of nitrate in groundwater contribution to streamflow from sub-basin (mg N/l)	0 - 1000
4. a__N_UPDIS.bsn	nitrogen uptake distribution parameter	0 - 100
5. a__NPERCO.bsn	nitrogen percolation coefficient	0 - 1
6. a__ANION_EXCL.sol	Fraction of porosity (void space) from which anions are excluded	0.01 - 1

Table 11- Selected parameters for the calibration of phosphorus

Parameters	Description	Range
1. a__P_UPDIS.bsn	phosphorus uptake distribution parameter	0 - 100
2. a__PPERCO.bsn	phosphorus percolation coefficient	10 - 17.5
3. a__ERORGP.hru	Organic P enrichment ratio	0 - 5
4. a__GWSOLP.gw	Concentration of soluble phosphorus in groundwater contribution to streamflow from sub-basin (mg P/l)	0 - 1000
5. a__PSP.bsn	phosphorus sorption coefficient	0.01 - 0.7
6. a__PHOSKD.bsn	phosphorus soil partitioning coefficient	100 - 200

It was important to check the initial values of each parameter to ensure they are changing from one run to another. For example, in the uncalibrated model, RCN, ERORGP, ERORGN, GWSOLP were equal to 0. Therefore, the "relative" operation should not be applied as it won't change the value.

The SWAT model was calibrated and validated on a monthly time step for all three variables.

3.3.4. Evaluation of the performance

The performance of the calibration/validation of the model is generally evaluated using statistical and graphical methods. Examples of such methods include time-series plot, Nash-Sutcliffe Efficiency (NSE, Nash and Sutcliffe, 1970), coefficient of determination (R^2), Percentage Bias (PBIAS: Gupta et al., 1999), Kling–Gupta efficiency (KGE: Gupta et al., 2009), etc. Recent works such as Jajarmizadeh et al. (2017), Čerkasova et al. (2018) selected NSE/R^2 and PBIAS, combined with time-series plot to evaluate the model performance. However, NSE is better suited to evaluate model "goodness-of-fit" than the coefficient of determination because R^2 is insensitive to additive and proportional differences between model simulations and observations (Harmel and Smith, 2007). In this study, NSE and PBIAS are used as indicators of model performance. Both criteria are determined based on the following equations:

$$\boldsymbol{NSE = 1 - \frac{\sum_{i=1}^{n}(Q_m - Q_s)_i^2}{\sum_{i=1}^{n}\left(Q_{m,i} - \overline{Q}_m\right)^2}} \qquad \boldsymbol{eq.5}$$

$$\boldsymbol{PBIAS = 100 * \frac{\sum_{i=1}^{n}(Q_m - Q_s)_i}{\sum_{i=1}^{n} Q_{m,i}}} \qquad \boldsymbol{eq.6}$$

Where

Q = Variable (e.g., discharge, nitrogen and phosphorus quantity), the bar stands for average

m = Measured data

s = Simulated data

i = Time,

n = Total number of periods

NSE is ranged from – ∞ to 1, with the optimal value being 1 meaning the plot of observed data fits the simulation (Khoiab and Thomb, 2015) perfectly while values less than 0 indicate that the mean of observed data is a more accurate predictor than the simulated output (M. Jajarmizadeh et al., 2017). The target interval for P-Bias is 0 to +/-25%, with 0 corresponding to the optimum. Positive values indicate the model is underestimating the observations, while negative values indicate an overestimation.

The typical ranges of both criteria for evaluating the "goodness-of-fit" related to the calibration of the flow, total nitrogen, and total phosphorus are provided in Table 12 (Moriasi et al., 2007). The criteria are independent, which means the condition should be met for all the criteria simultaneously (ideally but not always the case).

Table 12- Model performance criteria from Moriasi et al. (2007)

	Satisfactory	**Good**	**Very good**
NSE	0.5 - 0.7	0.7 - 0.8	0.8 – 1.0
PBIAS (%)*	15 – 25	10 – 15	Less than 10%

* Opposite interval indicates the same performance (e.g., PBIAS of -2% is considered very good, but the simulation is overestimating the observations)

The model's performance is expected to be lower for nutrients than discharge due to the greater uncertainties in nutrient data associated with errors in streamflow measurements and sample collection, storage, and analysis (Harmel and Smith, 2007).

3.3.5. Sensitivity analysis

The model calibration aims to optimize the internal parameters to achieve a good fit between simulated output and observed data. This optimization is carried out with the sensitivity analysis allowing the calibration to perform with only a limited number of parameters considered the most sensitive. A parameter sensitivity analysis provides insights on which parameters contribute most to the output variance due to input variability (K. Holvoet et al., 2005). It is computed by altering each parameter, one by one, while all other parameters remain fixed. It is then evaluated using the values of t-stat and p-value determined with a multiple regression analysis using the following equation (Abbaspour et al., 2007):

$$\boldsymbol{g = \alpha + \sum_{i=1}^{m} \beta_i \, b_i} \qquad \boldsymbol{eq.7}$$

Where $\boldsymbol{g}$ is the objective function value used to evaluate the model calibration effectiveness;

$\boldsymbol{b}$ is the parameter;

$\boldsymbol{\alpha}$ is the regression constant;

β corresponds to the technical coefficient attached to the variable b, and m is equal to the number of parameters.

The mean of the variations in the objective function estimates the sensitivity. The t-stat is the regression coefficient of a parameter divided by its standard error. The p-value for each parameter tests the null hypothesis that the regression coefficient is equal to zero. The higher the absolute value of t-stat and the smaller the value of p-value, the more sensitive the parameter is (Abbaspour et al., 2007). A small p-value, typically lower than 0.05, means the sensitivity of the parameter is statically significant (Verhagen et al., 2004), while a value of 0.05 indicates that there is a 95% probability that a parameter change will affect the dependent variable (Abbaspour et al., 2009).

3.4. Scenarios development

3.4.1. Climate change projection

Averaged globally, air temperature has increased by approximately 0.85°C over the 1880 -2012 period (IPCC, 2014), though the warming has not been uniform in time or space. Of particular note is that warming has been greater over high latitudes, including Canada and Eurasia (Environment and Natural resources Canada). As the climate has warmed globally, extreme temperatures have also changed with increases in the frequency of hot days and heatwaves and decreases in cold days (IPCC, 2014). Based on best practices in the global science community, the Government of Canada usually presents the three following RCPs (Government of Canada, 2018) also illustrated in Figure 12:

1. RCP8.5: indicates global average warming levels of 3.2 to 5.4°C by 2090.

2. RCP4.5: includes measures to limit (mitigate) climate change and indicates global average warming levels of 1.7 to 3.2°C by 2090.
3. RCP2.6: requires strong mitigation actions. This scenario indicates global average warming levels of 0.9 to 2.3°C by 2090.

In Canada, between 1948 and 2016, the average temperature increased by 1.7°C, while the north experienced an average increase of 2.3°C (ECCC, 2019a). The increase in average temperatures is expected to continue for all parts of Canada, with northern regions experiencing warming that is more than double the national average (ECCC, 2019a). This indicates the current climate conditions have already passed the RCP 2.6, and therefore, the climate change impact in this study will be assessed based on the other two scenarios: RCP4.5 and RCP8.5. This approach provides the stakeholders with pessimistic and optimistic planning information and allows a safer prediction and evaluation of risks related to these scenarios.

Before developing future climate change scenarios, a meticulous check and comparison between RCPs simulation data and observed weather data are performed. Once the reliability of data is checked, they are downscaled using a statistical approach (described in section 2.2.3). The resulting outputs are presented at the end of this document (Appendix C).

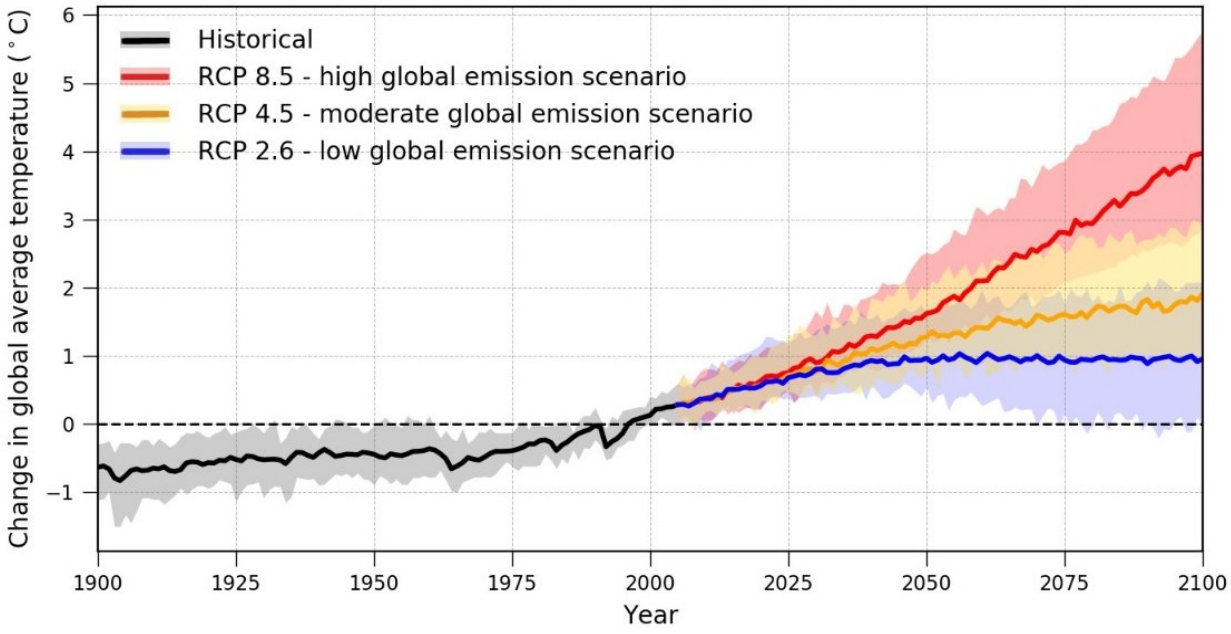

Figure 12 - Change in global average temperature relative to the 1986-2005 reference period (Government of Canada, 2018)

3.4.2. Selection of scenarios

For this study, the near future change during 2021–2050 was considered to inform decision making and policy processes to the practical implications of climate change for near to mid-term planning and management. Therefore, the 1990–2018 period is used as the current baseline data.

Based on the projected change of land use and climate discussed previously, seven (7) scenarios, including the baseline scenarios, are elaborated:

- ✓ **Scenario S0o (Baseline - observations)** – considers historical observed weather data (1990-2018) and land use map of 2017 (used to develop the current model).
- ✓ **Scenario S0m (Baseline - model)** – considers historical simulated weather data (1990-2018) and land use map of 2017.

- ✓ **Scenario S1**: land use map is upgraded to future land use condition, i.e. post-development (2050). The same climate data frame as the baseline is used.
- ✓ **Scenario S0M45**: RCP4.5 downscaled climate data run over the current land use map (2017)
- ✓ **Scenario S0M85**: RCP8.5 downscaled climate data run over the current land use map (2017)
- ✓ **Scenario S1M45**: RCP4.5 downscaled climate data run over the future land use map (2050)
- ✓ **Scenario S1M85**: RCP8.5 downscaled climate data run over future land use map (2050)

All the seven scenarios and their characteristics are summarized in Table 13. S1 represents the impact of urbanization on the current model, while S0M45 and S0M85 will represent the impact of climate change under RCP4.5 and RCP8.5, respectively. The effects of combined urbanization and climate change are assessed with S1M45 and S1M85 under RCP4.5 and RCP8.5. To have a consistent comparison, the climate change impact assessment is performed using the same climate data frame (RCMs), meaning the historical climate data simulated are from the RCMs and not from the observations. The scenario with historical simulations from RCMs was represented as S0m. It presents the same land use conditions and the same climate period; the lowercase "m" stands for "model" to differentiate with S0o scenario. It also differs from the S0M (uppercase "m") scenario, which represents the future climate conditions scenario and is always followed by 45 or 85 (for RCP4.5 or RCP8.5).

Table 13 - Description and characteristics of scenarios

No.	Scenarios	Climate data frame	Land use map	Description
1.	S0o	Historical observations (1990-2018)	2017	Current model (Baseline)
2.	S0m	Historical model (1990-2018)	2017	Baseline scenario for climate change and combined effects scenarios
3.	S1	Historical observations (1990-2018)	2050	Land use change
4.	S0M45	RCP4.5 (2021-2050)	2017	Climate Change under RCP4.5
5.	S0M85	RCP8.5 (2021-2050)	2017	Climate Change under RCP8.5
6.	S1M45	RCP4.5 (2021-2050)	2050	Combined land use change and Climate Change under RCP4.5
7.	S1M85	RCP8.5 (2021-2050)	2050	Combined land use change and Climate Change under RCP8.5

To evaluate the individual and combined impacts of climate and land-use dynamics on discharge, N, and P, the seven modeling experiments were incorporated into the calibrated SWAT model. The simulated output values were compared to the baseline model (current conditions) outputs at

global and local scales using the percentage of change. It is estimated according to the equation below:

$$\boldsymbol{Percent\ change} = \left(\frac{\boldsymbol{Scenario_{S1,S0M,S1M}} - \boldsymbol{Scenario_{S0}}}{\boldsymbol{S_{Baseline}}}\right) \times \mathbf{100} \qquad \boldsymbol{eq.8}$$

A negative percent change implies a reduction of the quantity from the current condition scenario to the corresponding future scenario, while a positive value means the quantity increases.

In terms of local impact, a sub-watershed located upstream (sub-watershed 46 - Figure 10) where a more significant land-use change (25.36% increase of urban area) was observed has been randomly selected. This approach will help investigate the directions of change and the magnitude of the impact of each scenario over the entire study area and at a smaller scale.

3.4.3. Land use change (urbanization) projection

Urbanization is integrated into the model as an increase in the ratio of urban areas and the reduction of the agricultural/forested areas at some pre-defined locations. Therefore, a projected development map for the watershed is required. This map has been elaborated for a mid-to-long-term prevision (next 30 years) and kindly provided by our collaborators from the MVCA. The map shows developments are expected to take place upstream with high density built out: it will consist of commercial sites including parking lots and building footprint, and dense mixed residential such as roads, roofs, driveways, hardened landscape areas. This extreme urbanization scenario may

result in an overestimate of impact (direct runoff and water quality), but it will help illustrate the maximum impact scenario. The urban area has increased by 3.64%, corresponding to 957 ha.

A summary of each land use occupation before development (2017 – Current map) and after development (2050 - Projection) is presented in Table 14, and pre and post-development conditions are shown in Figure 13.

Table 14- Summary of land use change

LU Type	Pre – development (%)	Post – development (%)	Change (%)
1. Agricultural Land	52.34	49.71	(-2.63)
2. Wooded Wetland	18.02	17.48	(-0.54)
3. Evergreen Needle leaf Forest	9.93	9.80	(-0.13)
4. Urban	9.90	13.54	(+3.64)
5. Forest - Deciduous	4.16	3.99	(-0.17)
6. Forest-Mixed	3.25	3.08	(-0.17)
7. Barren Or Sparsely Vegetated	0.82	0.82	(+0)
8. Water	0.69	0.69	(+0)
9. Mixed Forest	0.55	0.53	(-0.02)
10. Cropland/ Woodland Mosaic	0.34	0.34	(+0)

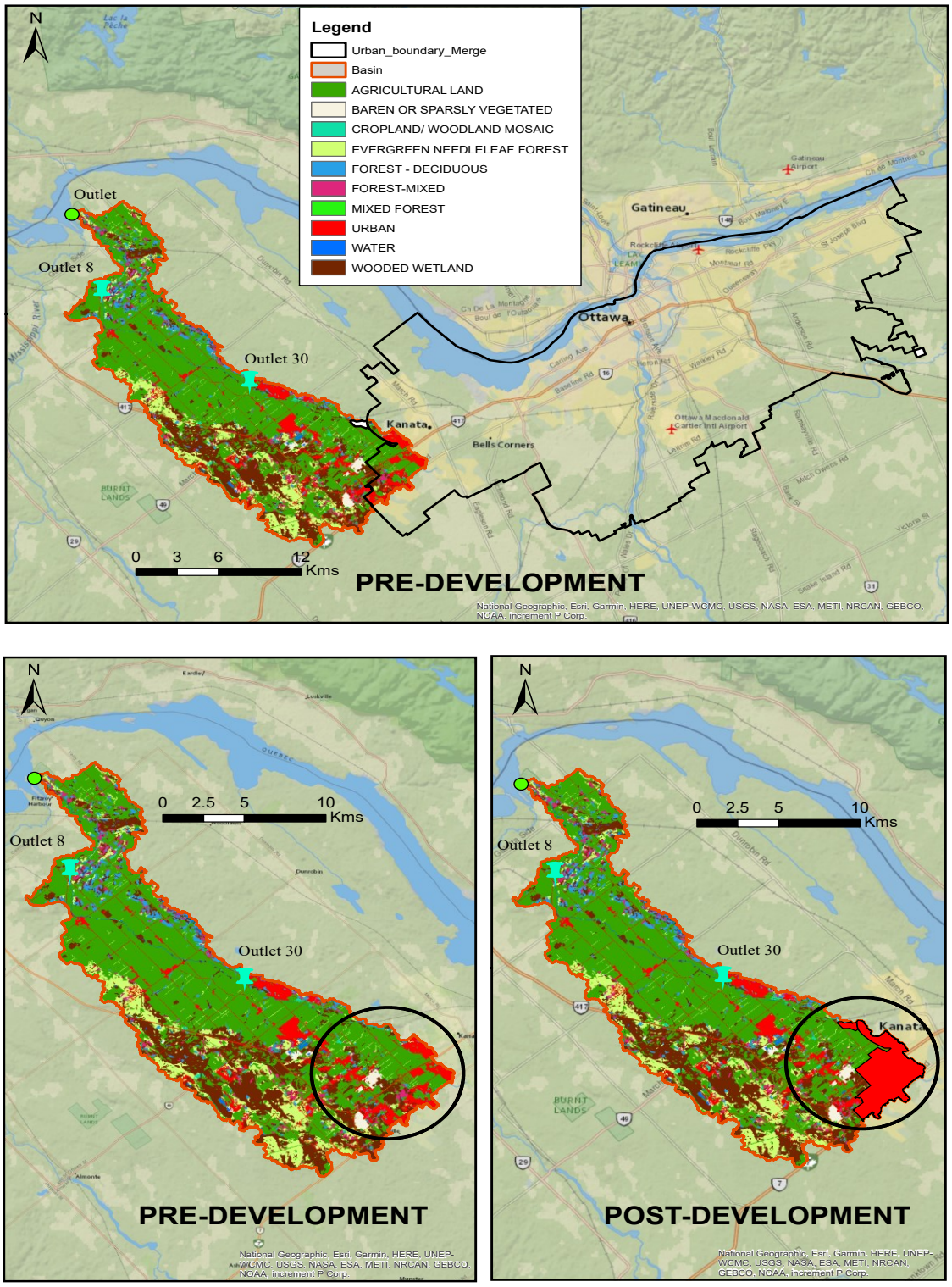

Figure 13- Comparison of pre-development and post-development conditions

4. Results and discussion

4.1. Calibration and validation

Final parameters after the calibration process, known as “fitted values” are shown in Table 15. The results of calibration and validation at the two stations where discharge, nitrogen, and phosphorus recorded data were available are presented in the following figures (Figure 14 and Figure 15 for outlet 8 and outlet 30, respectively):

Table 15 - Calibration final values

Parameters	Fitted ranges	Fitted values
r__CN2.mgt	[0.11713, 0.12033]	0.11873
a__GWQMN.gw	[-1347.63, -1136.19]	-1241.907471
v__GW_REVAP.gw	[0.097516, 0.100094]	0.098805
v__ESCO.hru	[0.997944, 1.010913]	1.004428
v__ALPHA_BF.gw	[0.482128, 0.54378]	0.512954
v__SOL_AWC().sol	[0.974373, 1.001545]	0.987959
a__REVAPMN.gw	[187.1984, 212.1717]	199.685043
v__SOL_K().sol	[0.577949, 0.600627]	0.589288
a__OV_N.hru	[7.371342, 8.932384]	8.151863
a__SLSUBBSN.hru	[135.1207, 137.2007]	136.160721
a__RCN.bsn	[14.5449, 16.35953]	15.452218
a__N_UPDIS.bsn	[-20.5479, -16.0446]	-18.296215
r__SHALLST_N.gw	[-135.764, -86.191]	-110.977379
a__ERORGN.hru	[-0.13804, 0.148926]	0.005445
a__NPERCO.bsn	1.144399, 1.161047]	1.152723
a__ANION_EXCL.sol	0.763784, 0.786918]	0.775351
a__PSP.bsn	[0.570577, 0.594221]	0.582399
a__PHOSKD.bsn	[116.2567, 120.4304]	118.343544
a__P_UPDIS.bsn	[89.41322, 99.38607]	94.399643
a__PPERCO.bsn	[12.34229, 12.44181	12.392052
a__ERORGP.hru	[0.011739, 0.019001]	0.01537
r__GWSOLP.gw	[297.5318, 319.4124	308.472107

OUTLET 8

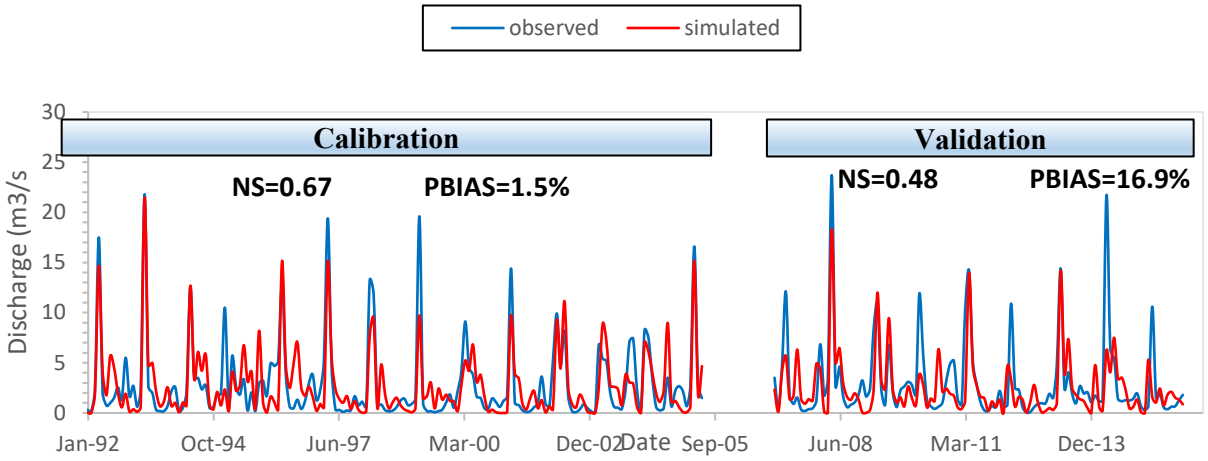

(a)

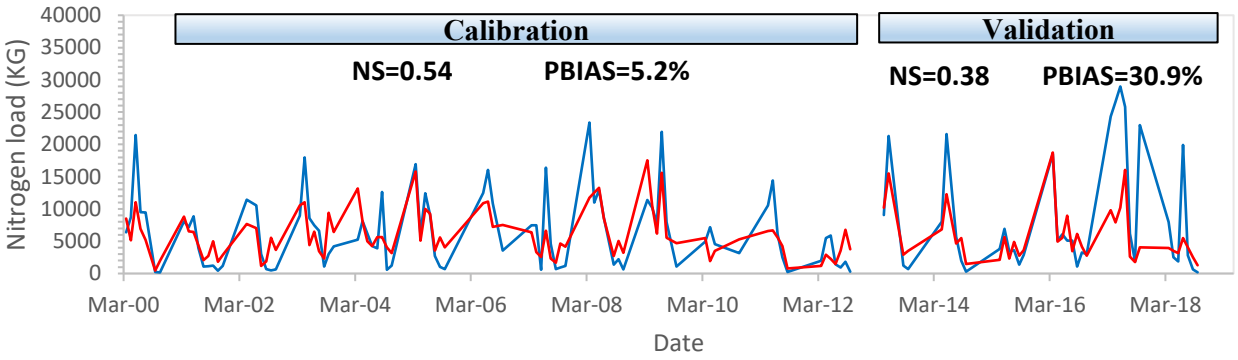

(b)

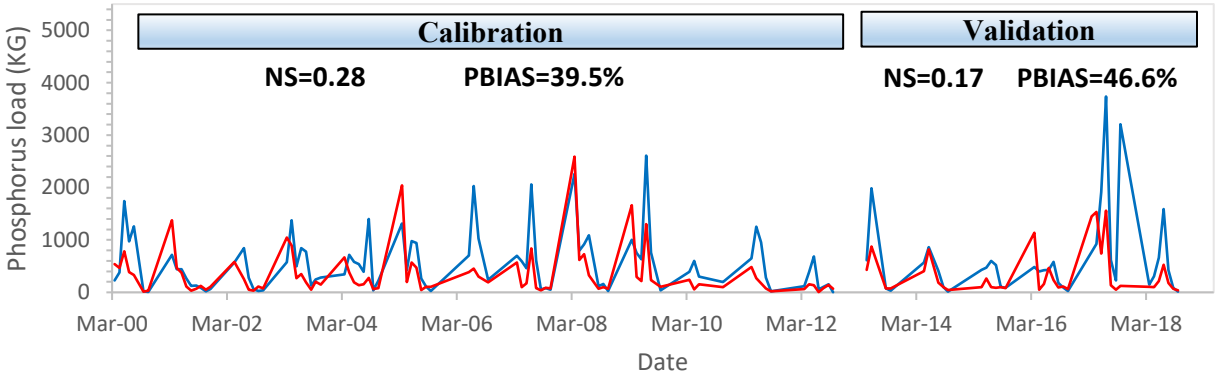

(c)

Figure 14- Calibration & Validation performance for outlet 8: a) Discharge b) nitrogen c) phosphorus

OUTLET 30

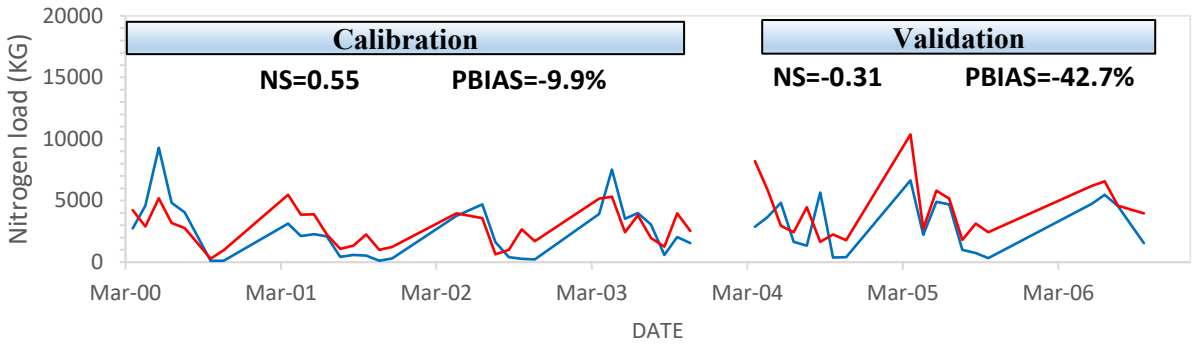

(d)

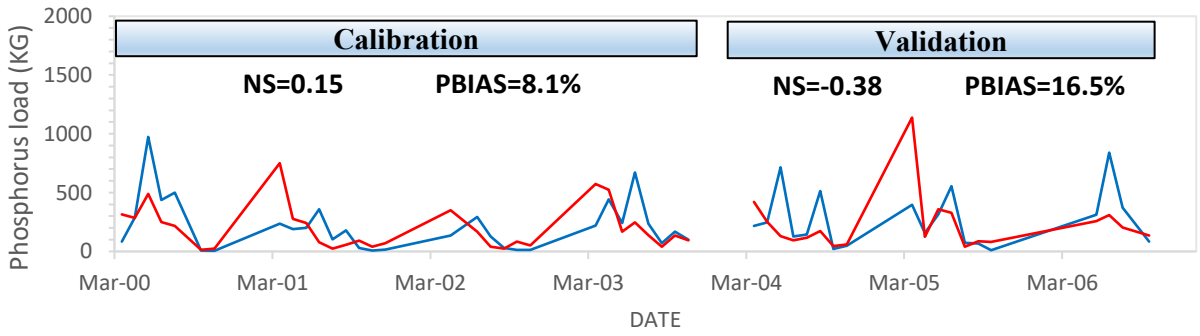

(e)

Figure 15- Calibration & Validation performance for outlet 30: d) nitrogen e) phosphorus

Overall, the model shows a good performance for the discharge at outlet 8 in calibration: NS is in the satisfactory range (0.5<NS=0.67<0.7) while the PBIAS is excellent (close to 0). The comparison of the means and standard-deviations is also satisfactory with 2.84 m^3/s (simulation) vs 2.89 m^3/s (observation) and 3.54m^3/s (simulation) vs 4.04m3/s (observation), respectively. In the validation exercise, relatively satisfactory performance is reached with NS=0.48 and a value of PBIAS of +16.9% (Figure 14.a). However, the graphical comparison shows the model tends to underestimate the observations. This may be in part due to using the NS as an objective function

in the calibration process since it is sensitive to high values due to the squared differences (Moriasi et al., 2007).

As expected for the water quality parameters, lower performance was obtained, especially for phosphorus. The simulation of the nitrogen at both outlets showed acceptable results in the calibration period according to the NS (0.54 for outlet 8 and 0.55 for outlet 30). The PBIAS for both periods are excellent: 5.2% and -9.9%. The sign of these values indicates that the model is underestimating the N load at outlet 8, and overestimating it while at outlet 30. On the other hand, the simulation of phosphorus shows a much lower performance at both outlets. NS for outlet 8 is 0.28 and 0.15 for outlet 30, which is unsatisfactory. However, the PBIAS at outlet 30 shows better results than outlet 8 (8.1% vs 39.5%).

In the validation exercise, all the simulations for water quality parameters showed unsatisfactory performance for both criteria except for phosphorus at outlet 30 where PBIAS was 16.5%. A graphical comparison shows the model simulates better the nitrogen at outlet 8 (Figure 14.b). However, it is not reliable in simulating the peaks. In addition to the reasons previously specified, another reason for the low performance of the model in simulating water quality parameters (N and P) in this study was the limited data available. In comparison, the length of the validation period for discharge was 11 years (2007-2015) while only 6 and 3 years data were used for N and P at outlets 8 and 30, respectively.

It is important to note that although the performances obtained are low in some cases, especially for N and P, these results are in the same range as some published studies. El-Khoury et al. (2015) obtained a value of NS=0.24 and 0.28 in the calibration of Nitrite-nitrogen and Organic phosphorus, respectively; Shrestha et al., (2021) obtained a value of NS=-0.71 and PBIAS=60.3% for phosphorus calibration.

Based on the performances obtained, the model can be globally characterized as follows:

- ✓ Reliable in simulating (or predicting) the discharge with acceptable performance;
- ✓ Can be used to simulate nitrogen load;
- ✓ Presents low performance in simulating phosphorus load
- ✓ Can be used to analyze the direction of variation of discharge, nitrogen and phosphorus in other conditions (climate change and land-use change scenarios) in terms of quantity of increase or decrease.

The assessment of the future scenarios using the current model will be performed by considering these specifications. Also, they are given to provide information on the characteristics of the model that need to be improved when used for potential future works with longer period of data.

4.2. Sensitivity analysis

The sensitivity analysis has demonstrated the influence of each parameter used for the calibration (Table 15), and the results are shown in Table 16. Based on that, it can be observed that the most sensitive parameter is N_UPDIS with a p-value and t-stat of 0.00 and 35.17, respectively. GWQMN.gw is the parameter influencing the least the performance of the model.

It is important to mention the sensitivity of one specific parameter to a dependant variable, or more generally the list or sequence of sensitivity parameters, differ significantly according to the input data and the calibration characteristics such as length of historical records, fluviometric station chosen or even the number of iterations used during the analysis-sensitivity process (Moreira et al., 2018). Therefore, the sensitivity analysis provides information about the most important process-drivers in the study region, depending to local characteristics (Abbaspour et al., 2018).

Table 16 - Sensitivity analysis results

Parameter Name	t-stat	p-value	Rank
A__N_UPDIS.bsn	35.17	0.00	1 (**Most sensitive**)
A__ERORGP.hru	-23.95	0.00	2
A__ERORGN.hru	19.98	0.00	3
R__CN2.mgt	-9.30	0.00	4
A__OV_N.hru	6.37	0.00	5
V__ESCO.hru	-2.04	0.04	6
A__RCN.bsn	-1.37	0.17	7
V__GW_REVAP.gw	-1.29	0.20	8
A__REVAPMN.gw	0.93	0.35	9
A__P_UPDIS.bsn	0.85	0.40	10
V__SOL_K(..).sol	-0.78	0.43	11
A__PPERCO.bsn	-0.77	0.44	12
A__SLSUBBSN.hru	0.65	0.52	13
R__GWSOLP.gw	0.64	0.52	14
V__SOL_AWC.sol	0.48	0.63	15
A__PHOSKD.bsn	0.47	0.64	16
A__PSP.bsn	0.47	0.64	17
A__ANION_EXCL.sol	-0.43	0.67	18
R__SHALLST_N.gw	-0.30	0.76	19
V__ALPHA_BF.gw	-0.26	0.79	20
A__NPERCO.bsn	0.15	0.88	21
A__GWQMN.gw	-0.03	0.98	22 (**Least sensitive**)

4.3. Impacts of land-use change (S0o vs S1)

4.3.1. Impact on global and local outlets

As mentioned in section 3.4.2, the impact of land use change is evaluated by comparing S1 (post-development) to S0o (current conditions) at a global and local scale. The two cases differ in the repartition of the different land-use types, as illustrated in Figure 16. Considering the entire watershed, only 13.5% of the total area is urbanized with 49.7% of agricultural land, while at a local scale, the urban area represents 47.9% of the area of the sub-watershed.

Both global and local impacts are assessed by comparing the outputs in S0o and S1 at the main outlet and at the upstream outlet 46, respectively, in terms of annual maximum discharge (Figure 17) and monthly averages of discharge, nitrogen load and phosphorus load (Figure 18 & Figure 19). Monthly averages are calculated by averaging the values for a specific month during the simulation period, excluding the warmup period as the model does not include it in the outputs time series. Annual maximum boxplots are created based on the maximum discharge observed at each year of simulation. Discharge graphs are presented in cubic meters per hectare of area (the global area is 26385 ha and the local area is 1312 ha).

Globally, urbanization increased the annual average discharge and the phosphorus load by 1.57% and 26.49% respectively while a decrease of 1.88 % is observed for the annual average nitrogen load (Figure 35). The annual average discharge passed from 3.04 m^3/s in S0o (current conditions) to only 3.09 m^3/s; from 6.62 tons to 8.38 tons for annual average phosphorus load and from 871 tons to 855 tons for annual average nitrogen load. In terms of annual peak flows, urbanization impact was estimated at 0.73% increase. Therefore, these results show the phosphorus is far more sensitive to the land use change than discharge and the nitrogen at the watershed scale.

Figure 18-A & C show that the monthly averages of discharge and phosphorus load for each month follow their annual direction of change, meaning all the monthly quantities increase with no exception. However, despite the fact annual N load is lower, its monthly values (Figure 18.B) indicate that not all the months have experienced the direction of change. The decrease is mostly due to the large change during July and August, where higher amount of rainfall is observed.

As expected, peaks are unsurprisingly observed during Spring-Summer due to the higher precipitation coming from the combination of snowmelt and rainfall. Maximum quantities of flow and nitrogen load occur particularly during April (Figure 18.A) and July-August (Figure 18.B), respectively, showing that the flow is more influenced by the water quantity coming from the snowmelt while rainfall is more determinant to the nitrogen load. Two peaks are observed in the hydrograph over one year: one in April (the highest) with 8.92 m^3/s (vs 8.86 m^3/s before urbanization) and the second in July estimated at 4.98 m^3/s (vs 4.96 m^3/s in before urbanization). The average percentage of change of nitrogen load during its peak period in urbanized conditions compared to current conditions is -6.31%. In the case of phosphorus, the highest loads seemed to likely occur during April and July (peak in April, drop in May then increase again from June until the second peak in July, which is lower than the first peak). The first peak load of phosphorus was estimated at 2.13 tons after urbanization (17.03% increase compared to non-urbanized), while the second was 1.62 tons, representing 11.72%. According to these changes, phosphorus seems to be more sensitive to the land-use change than flow and nitrogen.

At the sub-watershed scale, we have the same characteristics as the global impact, such as the same directions of change for all the three variables in both monthly averages and maximums, and occurrence of peaks during Spring-Summer (especially in April and July), phosphorus more affected than discharge and nitrogen and also the sensitivity of discharge and nitrogen to the

snowmelt and the rainfall respectively (Figure 19). However, global and local impacts differ in the magnitude of the changes. The annual average changes for discharge, nitrogen load, and phosphorus are respectively 9.45% (vs. 1.57% in global), -29.00% (vs. -1.88), and 73.56% (vs. 26.49%), indicating the impact is more pronounced at the local scale. This is not surprising and is due, as illustrated in Figure 16, to the higher ratio of the urban area over the total area (13.5% in global vs 47.9% in local) and the reduction of agricultural land (from 49.7% to 10.6%). The reasons for the increase in flow are the following:

- impervious areas allow water to flow more rapidly than pervious area and have a higher potential of runoff as infiltration is limited
- the conversion to urban area reduces the travel time (time of concentration) of water and increases the surface runoff within the watershed/sub-watershed, resulting in an increase of the water quantity at the outlet.

Consequently, the annual maximum and average flow increases with urbanization and depends on the area converted. This is demonstrated by the higher water quantity increase in the upstream sub-watershed (local) with +4.76% for annual maximum flow, and as mentioned previously, +9.45% for the annual average.

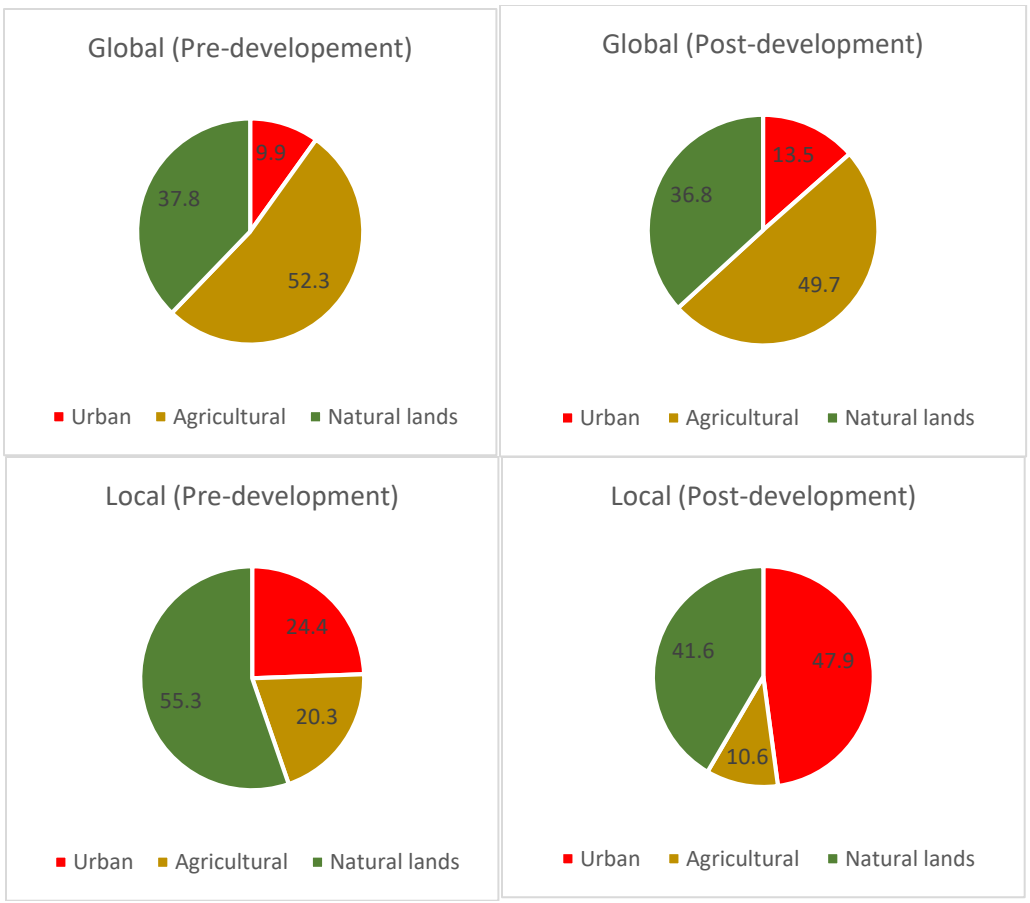

Figure 16 - Repartition of main land uses in the entire watershed (global) and the selected sub-watershed (local, sub46) under urbanization

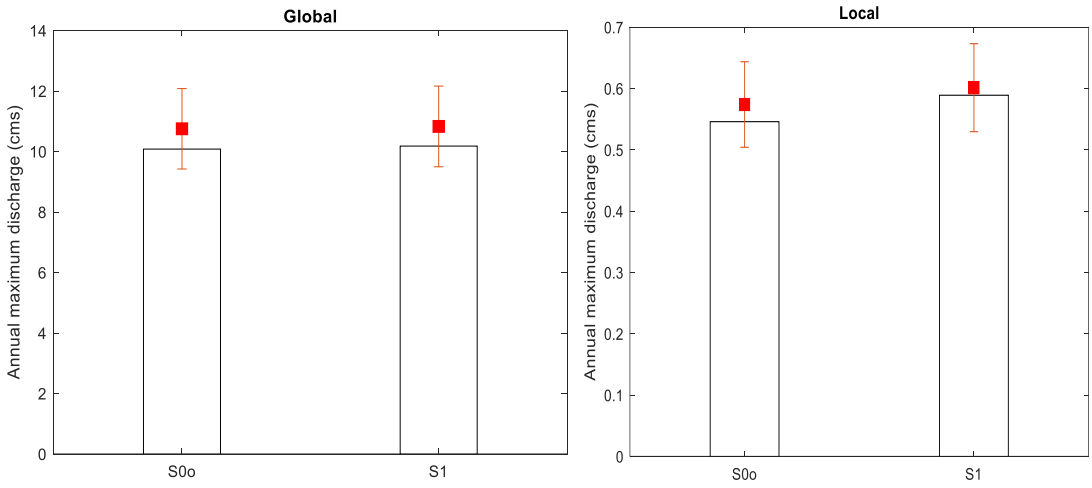

Figure 17- Global and local (sub46) impacts of land use change on annual maximum discharge. Column height corresponds to the median, top and bottom whiskers are the errors with 95% confidence; red markers represent the mean discharge

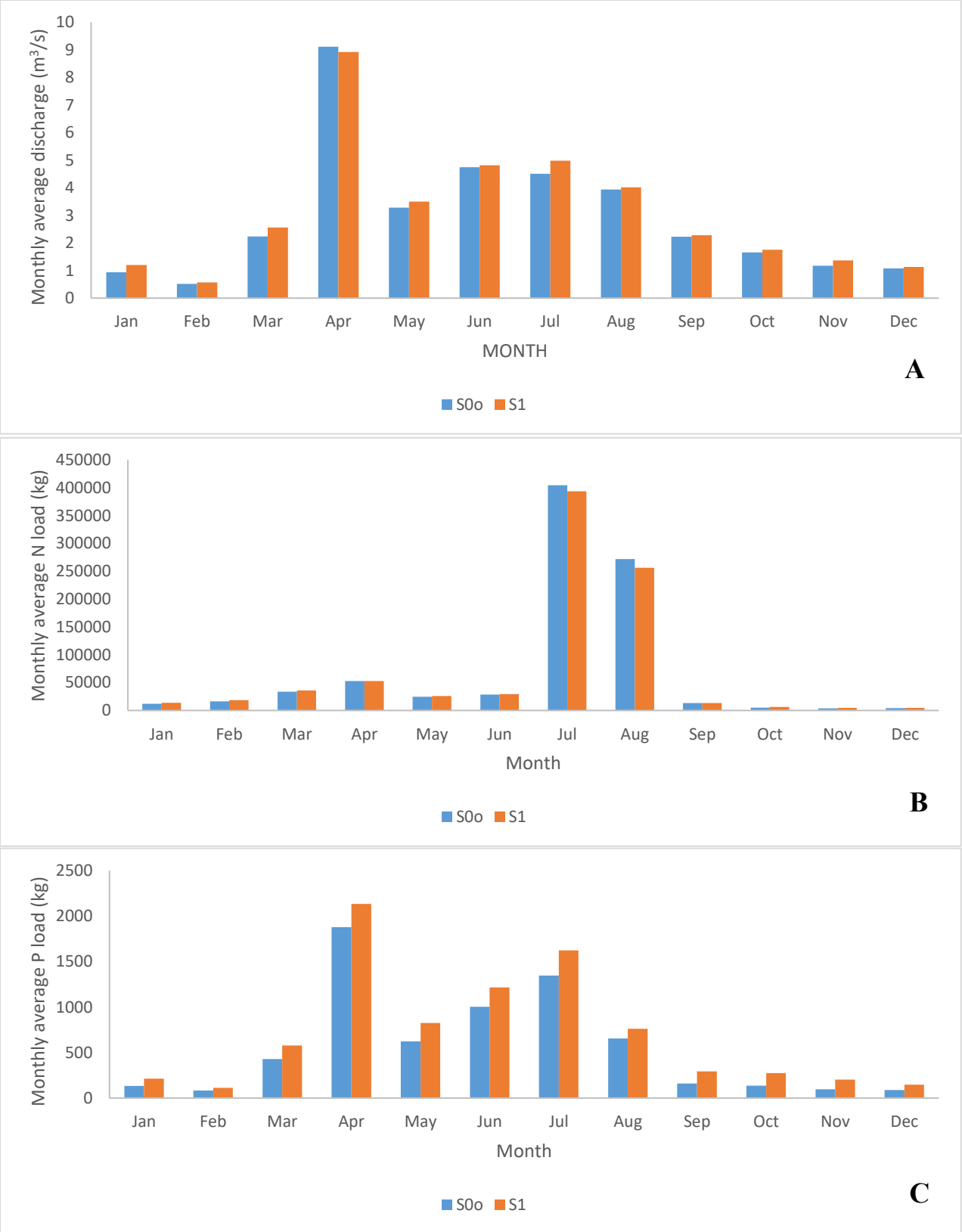

Figure 18- Global impact of land use change on monthly average discharge (A), nitrogen load (B) and phosphorus load(C)

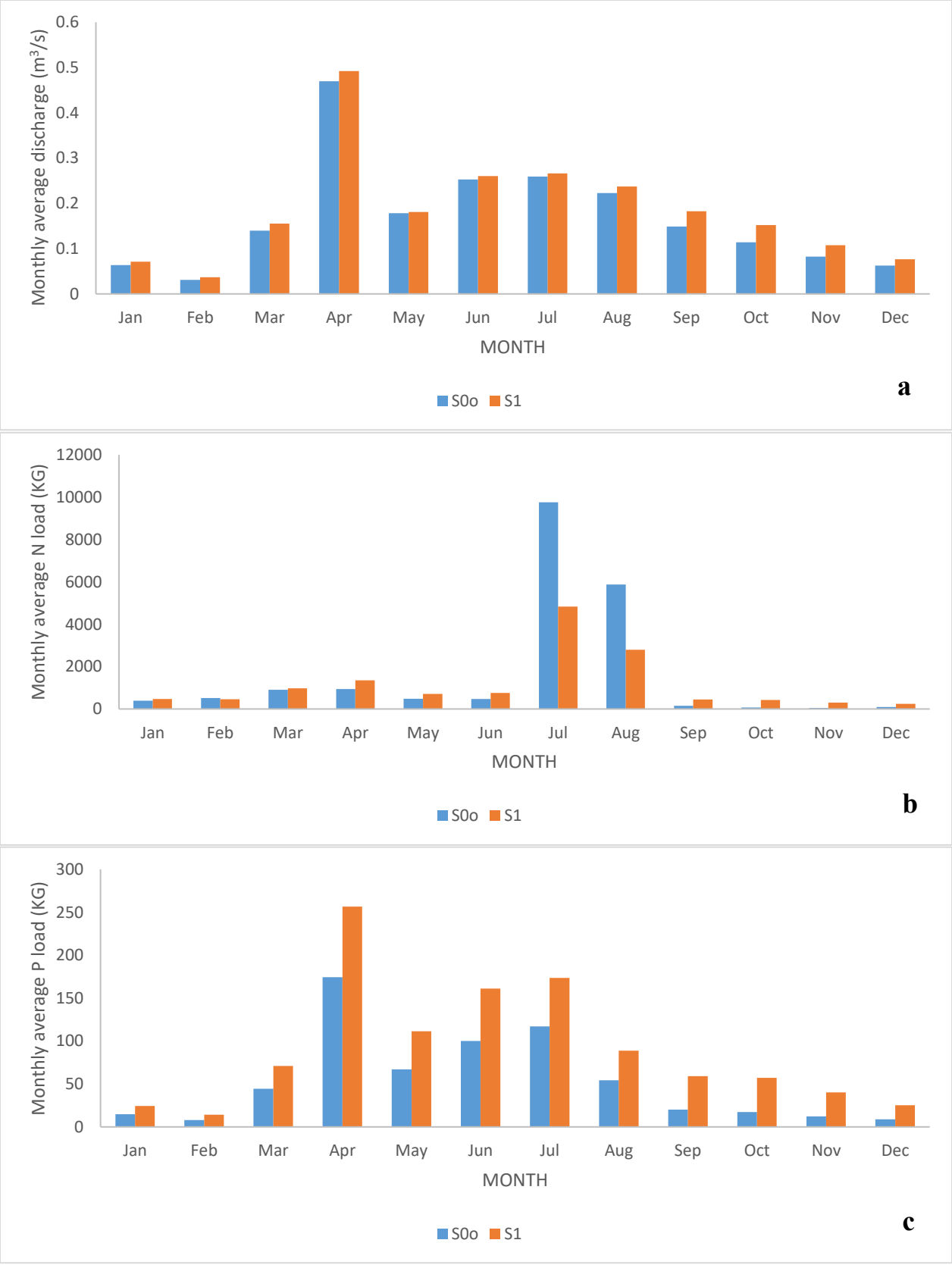

Figure 19 - Local impact (sub46) of land use change on monthly average discharge (a), nitrogen load (b) and phosphorus load (c)

4.3.2. Impact on the most and the least urbanized sub-watershed

In this section, the quantity of nutrients flowing out of the most (no. 40) and least (no. 41) urbanized sub-watersheds located upstream has been assessed to investigate their potential source of pollution and how they are transported. The percentage of occupation of these two sub-watersheds is illustrated in Figure 20, while the outputs of annual maximums are presented in Figure 21 and monthly averages of discharge, nitrogen, and phosphorus in Figure 22.

Overall, the results show that in the highly urbanized area, all the outputs increased significantly. The annual maximum discharge is higher over all the years of the simulation. The relative change (estimated by calculating the ratio of the difference between the averages of the most and the least urbanized sub-watershed over the average of the least urbanized) in the annual averages is 126.2%. Regarding the monthly average, the relative changes for all the months of the year are higher than 600% increase for discharge, nitrogen, and phosphorus. This significant increase is illustrated in Figure 22.

Based on these results, it can be observed the nutrients load drastically increased with the urbanization ratio as the loads in the sub-watershed 41 (agricultural) are completely negligible compared to the sub-watershed 40. This means that despite the agricultural lands also producing N and P, the contribution of urban areas to the loads is more dominant when the urban area ratio is very high compared to the agricultural area ratio (73.49% vs. 23.46%). Therefore, in this particular situation, N and P pollution is controlled by the urban area. However, when the urban ratio is not very high (13.5% when considering the entire watershed), only P is controlled by urban areas. At the same time, N load is driven by agricultural lands as explained in the previous section, where N decreased with the agricultural area.

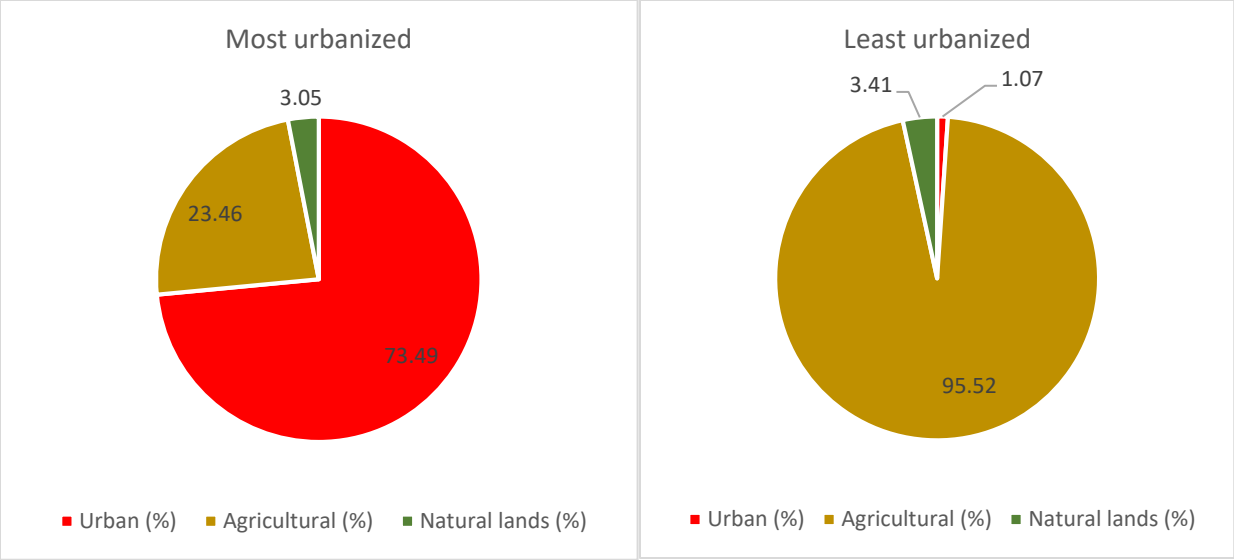

Figure 20 -Repartition of the main land uses in the most and least urbanized sub-watersheds

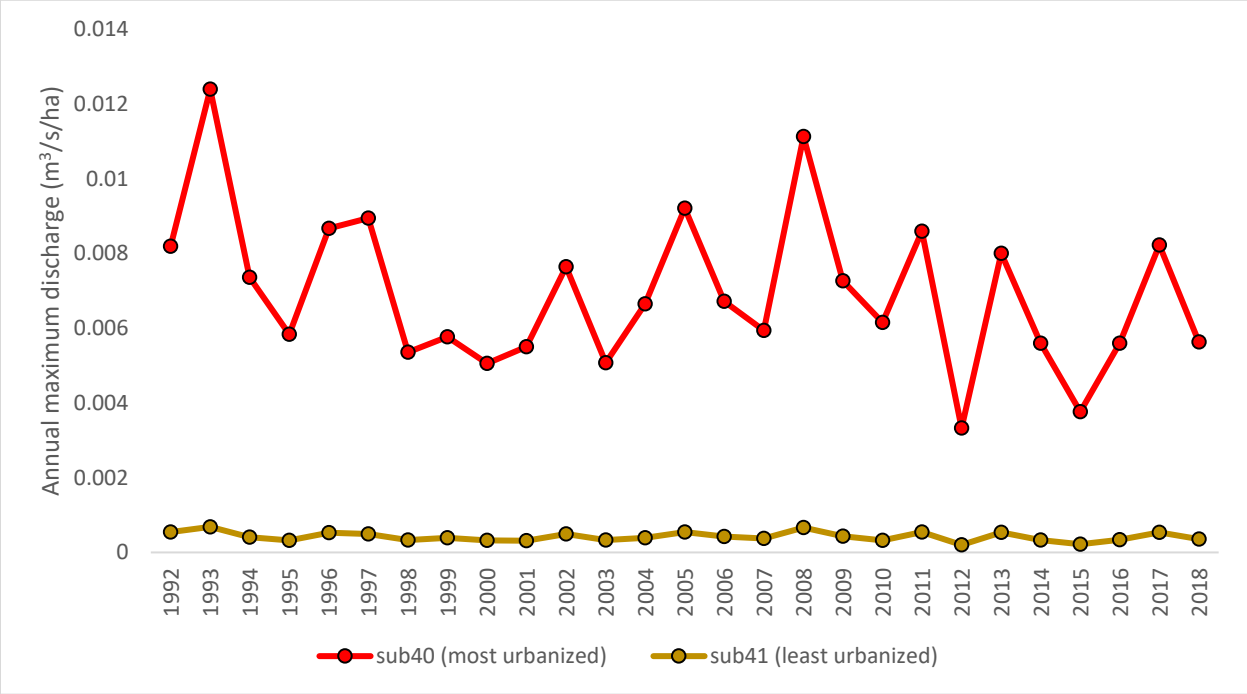

Figure 21 - Urbanization impact on annual maximum discharge

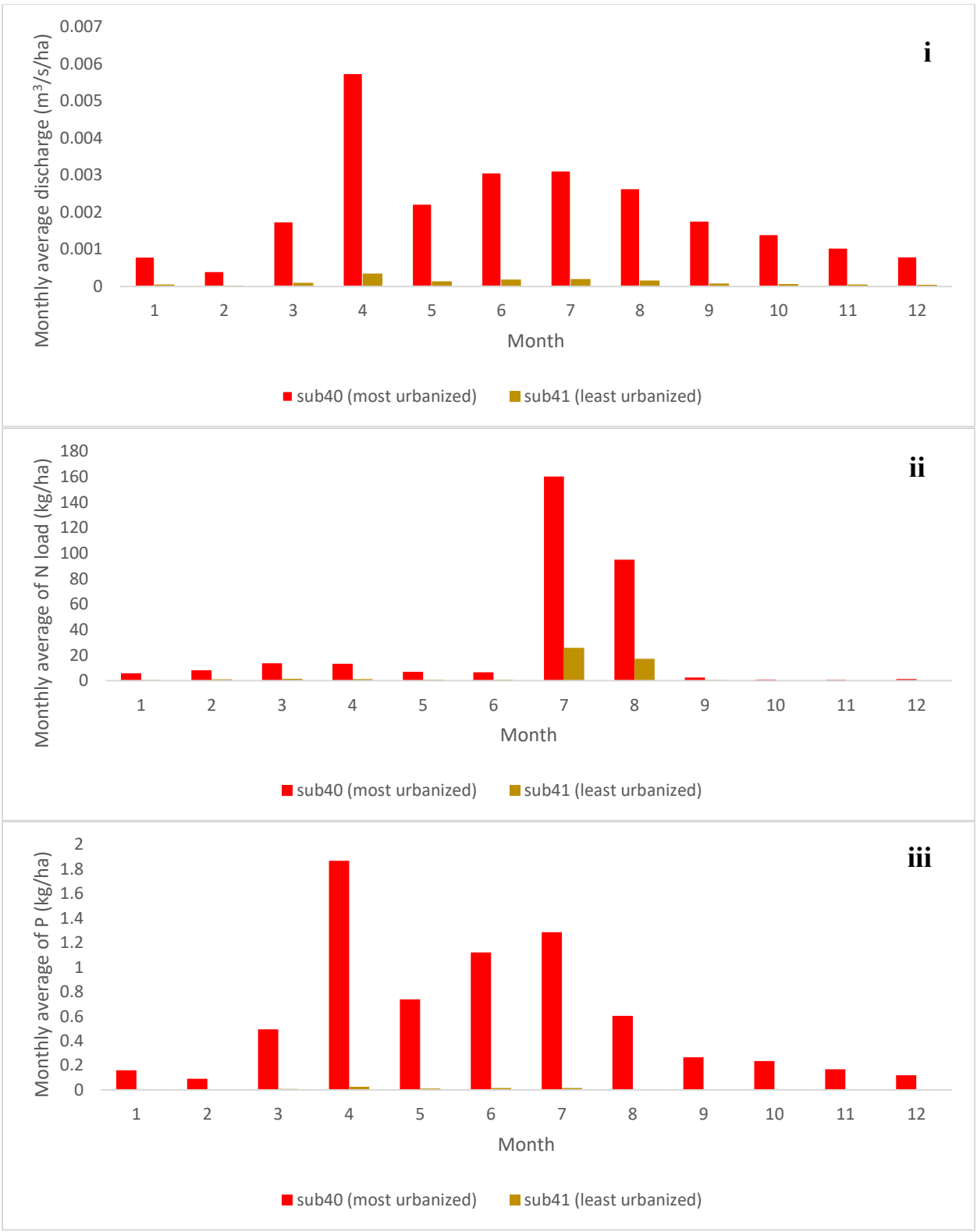

Figure 22 - Comparison of annual averages of discharge (i), nitrogen load (ii) and phosphorus (iii) between most and least urbanized sub-watersheds

4.4. Impact of climate change (S0m vs S0M45/85)

As explained in section 3.4.2, unlike in the land-use change scenario, the change is calculated compared to S0m output instead of S0o. Therefore, the S0o scenario is presented here on graphs only as a reference.

The global and local impacts of the single climate change on the Carp River watershed are presented in Figure 23, Figure 24, and Figure 25. Given that the land use map has not changed in this scenario (S0M45/85) compared to the current conditions (S0m), Figure 16 (pre-development) shows the percentage of the main types of land uses over the watershed and the sub-watershed of interest (number 46). The difference between the two repartitions is less important than that in land-use change scenario as urban area represents 9.9% and 24.4% (difference of 14.5%) at global and local scales respectively, while it was 13.5% and 47.9% (difference of 34.4%) in the land-use change scenario. However, this does not necessarily mean the impact in this scenario would be less important in the Carp River watershed, and further analysis of the results must be performed.

In terms of the annual maximum, the discharge has experienced a relatively low change under the two RCPs, as presented in Figure 23. On average, at the global scale, the maximum discharge reached 12.63 m^3/s in S0m, and the percentages of change under RCP4.5 and RCP8.5 are 3.76% and 0.90%, respectively. An opposite change is observed at a local scale with -1.06% and -3.54% in S0M45 and S0M85. Annual average discharge presented a similar dynamic in S0M45 at the global and the local scales with an increase of 5.49% and 2.61%, respectively, while in S0M85, the change was 7.52% (global) and 1.13% (local). Though an increase is observed at the year time scale for the discharge, a further investigation based on monthly averages examination shows monthly outputs do not always follow the same direction of change. This is illustrated in the monthly average graphs (Figure 24.A & Figure 25.a) where, for instance, the quantity decreases

in February, May, and September under RCP4.5 and in April under RCP8.5. The graphs also show two peaks during the year: in April and in July. The April's peak is the highest and is a direct effect of the snowmelt at the end of winter, which is around mid-March in the case of Ottawa. The peak flows are estimated at 6.80 m^3/s, 6.97 m^3/s, and 4.94 m^3/s in S0m, S0M45, and S0M85, respectively the main outlet, while in the upstream sub-watershed (local), it was 0.3567 m^3/s, 0.3531 m^3/s and 0.2437 m^3/s. The discharge starts decreasing in May before going up the next months until it reaches the second peak in July with 4.76 m^3/s, 5.17 m^3/s, and 4.98 m^3/s at the main outlet and 0.2498 m^3/s, 0.2683 m^3/s, and 0.2428 m^3/s locally, respectively in S0m, S0M45, and S0M85 scenarios. Unlike the first peak, rainfall is the main factor contributing to the second, and from these results, it can be observed the precipitations produced by the snowmelt has a more considerable impact than the rainfall precipitations in the watershed. More generally, the RCP8.5 seems to have less impact on the water quantity during the peaks as the discharge in this scenario is lower than that of RCP4.5, and in the case of the April's peak , the water quantity is even lower than that of the baseline conditions (S0m).

In terms of water quality, overall climate change seems to have a considerable impact on N in S0M45 with an increase of 29.62% (+265 tons) globally and 28.24% (+5 tons) locally, while the change is less marked in S0M85 with +2.03% (+18 tons) and -0.96% (-0.18 ton) globally and locally respectively. Annual averages in current conditions (average values the change is calculated from) are respectively 896 tons and 189 tons at the main outlet and the outlet of the sub-watershed 46. An opposite variation is observed for P, where S0M45 is the least impactful with only 1.07% increase at the global scale and 0.55% decrease at the local scale, while under S0M85, while this change is estimated at -4.49% at the main outlet and -11.19% at the local outlet. The difference between these values indicates global and local impact may differ in magnitude and in

the direction of change. At the monthly time scale, the impact on the two nutrients, illustrated in Figure 23-B & C and Figure 24-b & c, shows a clear difference in the variation over the year. Indeed, the variation of P, like in the case of the discharge, presents two peaks, and they occur in the same periods (April and July), while for N, the load is relatively small over the year (in average 21 tons in S0m, 23 tons in S0M45 and 25 tons in S0M85 per month globally) except in July and August where a sudden increase is observed. Loads in July are estimated to be 427 tons, 650 tons, and 50 tons; in August: 260 tons, 282 tons, 159 tons in S0m, S0M45, and S0M85, respectively. The graphs show an important increase of N load in July under S0M45 compared to the baseline scenario(from 427 tons to 650 tons – an increase of 52%), while in August under S0M85, the load drastically decreases by about 40% of the load in the current conditions (from 260 tons to 159 tons). They also show that the two nutrients load is lower during the peak times under S0M85 than those under S0M45, similar to the water quantity monthly variation. Though the quantities are reduced, a similar variation can be observed at the local scale, with the peaks occurring in the same period of the year. A difference is seen particularly in July, where the local P load is lower in S0M45 than in S0m (Figure 25.c), which is not the case for the global P load (Figure 24.C).

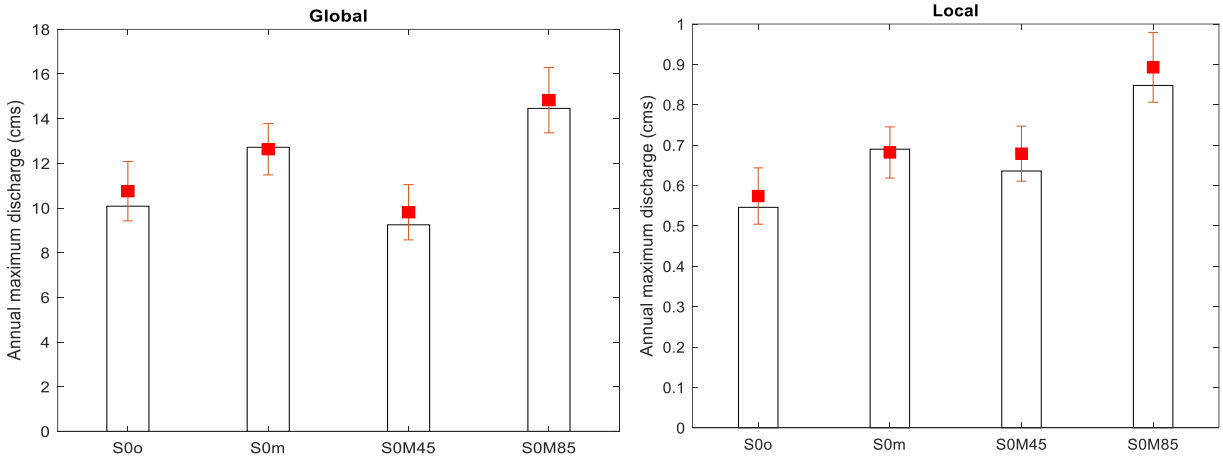

Figure 23- Global and local (sub46) impacts of climate change on annual maximum discharge under RCP4.5 and RCP8.5. Column height corresponds to the median, top and bottom whiskers are the errors with 95% confidence; red markers represent the mean discharge

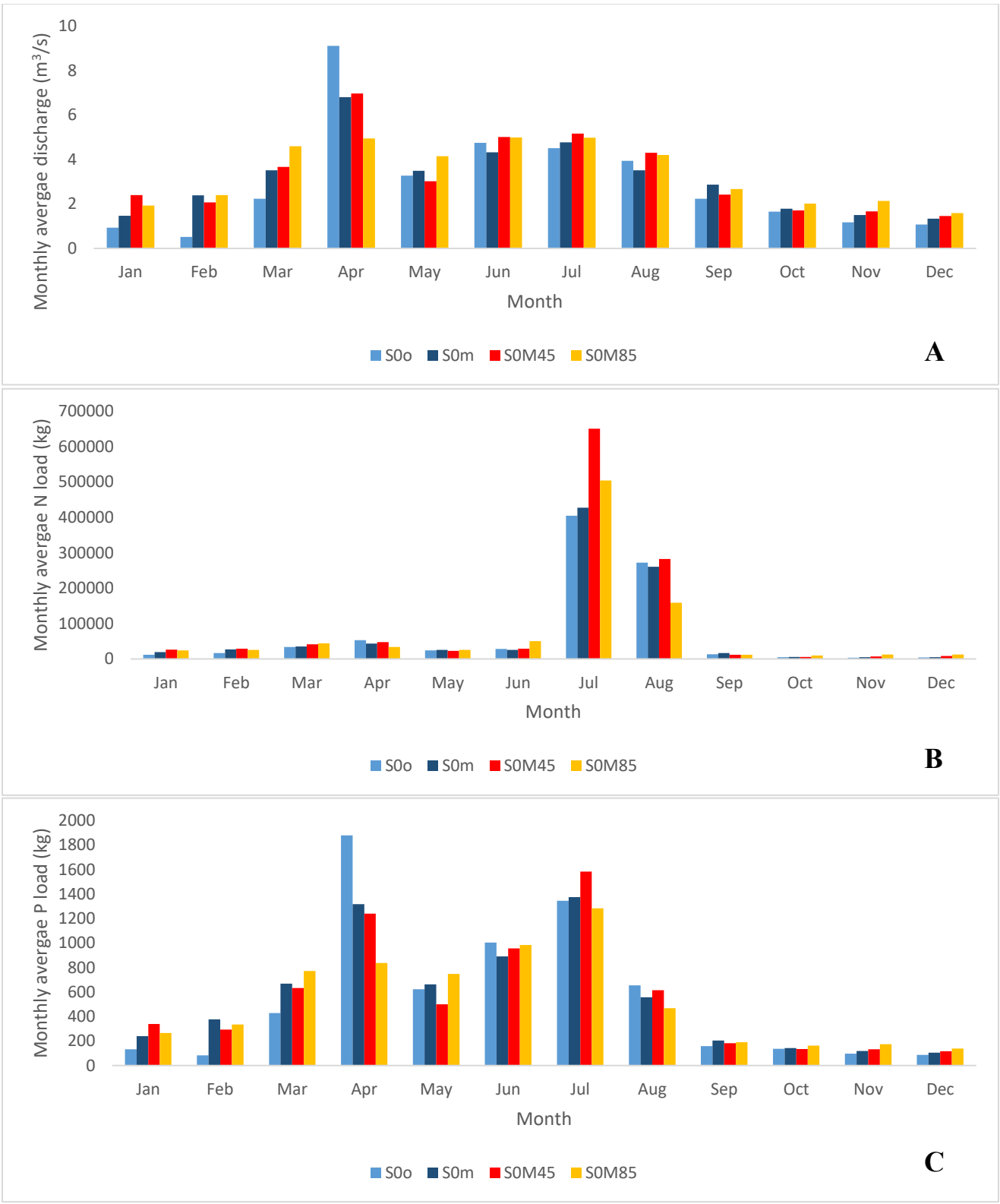

Figure 24- Global climate change impact on annual average discharge (A), nitrogen (B) and phosphorus(C) loads under RCP4.5 and RCP8.5

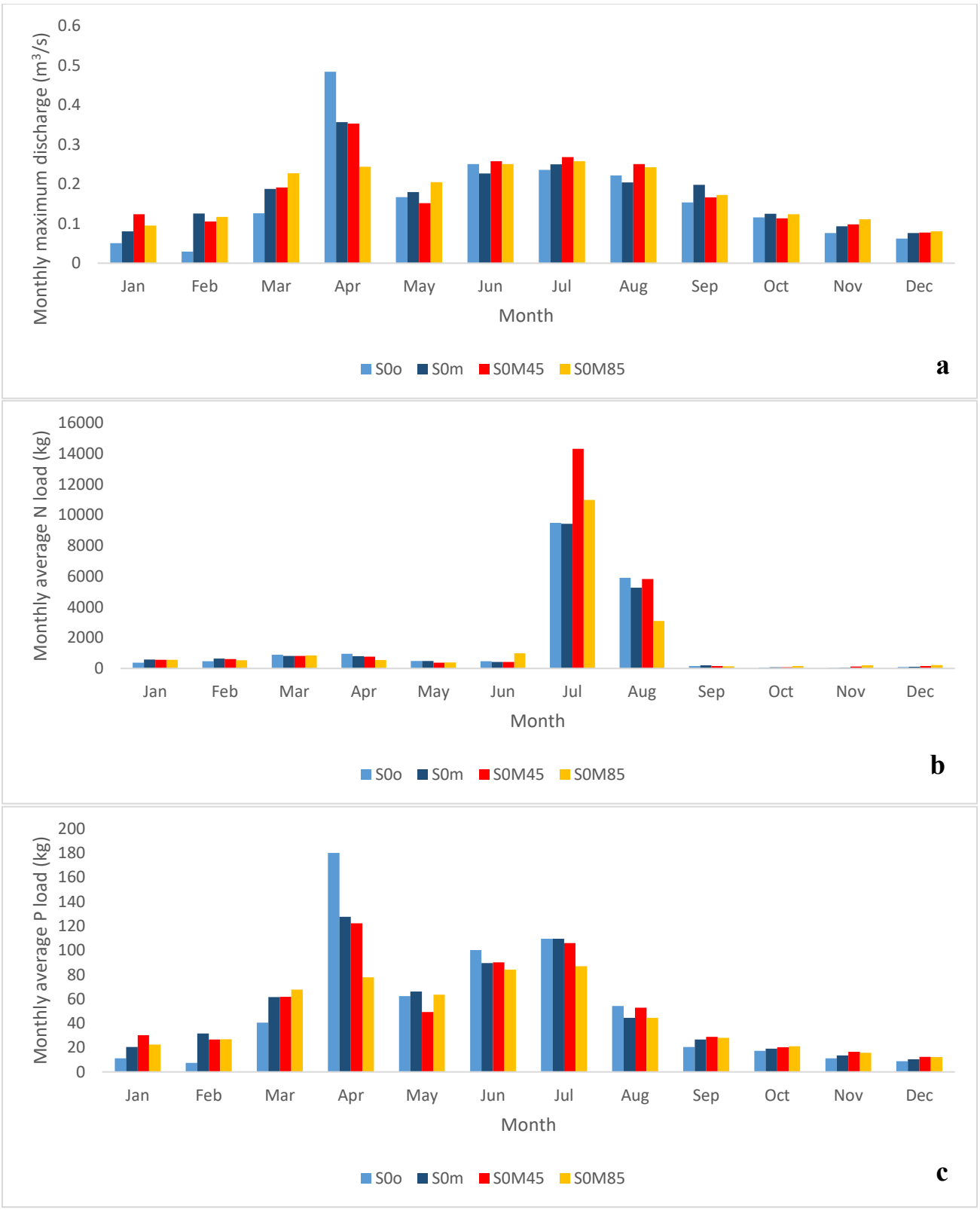

Figure 25- Local (sub46) climate change impact on annual average discharge (a), nitrogen (b), and phosphorus (c) loads under RCP4.5 and RCP8.5

4.5. Combined impact of land use and climate changes (S0m vs. S1M45/85)

Separately assessing the impacts of land-use change and climate change provides a better understanding of the level of impact caused by each of the two scenarios on the water quantity and quality. However, it is also essential to determine and quantify the most dominant scenario by evaluating the impact of the two effects. As discussed in section 3.4.2, this scenario considers the future climate conditions in a watershed over the future land use conditions (Figure 16). Therefore, the next paragraph focuses on comparing the results of this scenario with the S0m scenario (baseline scenario with historical climate data from RCMs), like in the previous section.

In terms of maximum discharge, like climate change, the combined effects of climate and land-use changes seemed not to cause a considerable impact. From Figure 26, where the maximum discharges in the different scenarios are presented as boxplots, it can be observed that the difference between the means (cross mark inside the boxes) of the scenarios S0m, S1M45, and S1M85 is relatively small, both at the global and local scale. At the global scale, the values are respectively 12.63 m^3/s, 13.13 m^3/s (+3.96%) and 12.79 m^3/s (+1.29%) in S0m, S1M45 and S1M85 while in local, they are 0.681 m^3/s, 0.692 m^3/s (+1.61%) and 0.678 m^3/s (-0.36%). Even though the impact under the two RCPs is not important, the RCP4.5 has the highest impact compared to the RCP8.5, as shown by the percentages of change.

In contrast with the maximum discharge, the annual discharge is more sensitive to the RCP8.5 than RCP4.5 in the combined effects. The annual average changed from 3.15 m^3/s in the baseline conditions to 3.44 m^3/s (+9.34%) under RCP8.5 while RCP4.5 caused an increase of 0.21 m^3/s (+6.75%). This is also the same in at the local scale where an increase of 13.07% and 11.10% is

observed under RCP8.5 and RCP4.5, respectively. By comparing these values with those of the two previous individual scenarios (S1 and S0M45/85), it emerges that the combination of land use and climate changes tends to intensify the impact (not always) on the water quantity (annual maximum and mean discharge) in the case where the impact of the individual scenarios has the same direction of change. For instance, the percentage of change of the annual mean discharge at the main outlet in S1 and S0M85 was respectively +4.76% and +7.52%, the resulting change when the two were coupled (S1M85) became +9.34%. Also, for the annual maximum discharge, the combination of +0.73% and +3.76% change was +3.97%. However, when the impacts have an opposite direction, the combined impact is attenuated as illustrated with the +1.61% (resulting from +4.78% and -1.05% changes) and -0.36% (resulting from +4.78% and -3.54% change) in the local annual maximum discharge. Based on that, it can be noted the intensification is not a systematic linear relationship where the combined effect is the summation of the individual impacts.

The impact on water quality variables presents different characteristics depending on the variable. Figure 35 shows a summary of the changes at the main outlet and at the outlet of the upstream sub-watershed. In terms of N load, overall, the coupled effect caused a reduction of the annual quantity except for S1M45, for which an important global increase of 24.84% is observed. Local impact under RCP8.5 is also likely to be important as the load decreased by 24.80% compared to the S0m scenario. However, the results indicated the annual load at the main outlet under RCP8.5 was not significantly impacted, and only a 1.20% decrease (-10.8 tons) of the baseline conditions load is expected. In contrast, the quantity of P faced a significant increase compared at the global scale to the current load and was even higher at the local outlet (in terms of percentage of change). The load increase at the main outlet was estimated at 1.6 tons (23.81%) in S1M45 and 1.3 tons in

S1M85 (19.15%), while in the upstream sub-watershed, it was 0.411 tons (66.15%) and 0.360 tons (57.97%). By comparing these results with those of the two previous scenarios (S1 and S0M45/85), the land-use change drives the P quantity as it increased like in scenario S1 although the climate change (S0M45/85) caused its reduction. Also, the impact caused by S1 is way larger than that caused by the S0M45/85.

The monthly variation of water quantity and quality in this scenario, illustrated in Figure 27 and Figure 28, presents the same characteristics as land-use change (S1) and climate change (S0M45/85). Discharge has two peaks over the year, occurring in April (the highest) and in July; N is relatively low for all the months with two exceptional peaks in July and August, while P has two peaks in April and in July, but unlike the discharge, the peak of July is the highest. The impact of this scenario under RCP4.5 was found to be more important than RCP8.5, particularly on the peaks where a more important difference is observed between the two. For instance, N's global load in August in RCP8.5 is 43.4% less (almost half) than the load in RCP4.5. In terms of discharge, there was no extraordinary monthly change. However, under RCP8.5, the scenario is expected to cause a relatively important reduction of 27.09% (-1.84 m^3/s) compared to S0m during the first peak of the year, meaning that the peak is likely to be less severe.

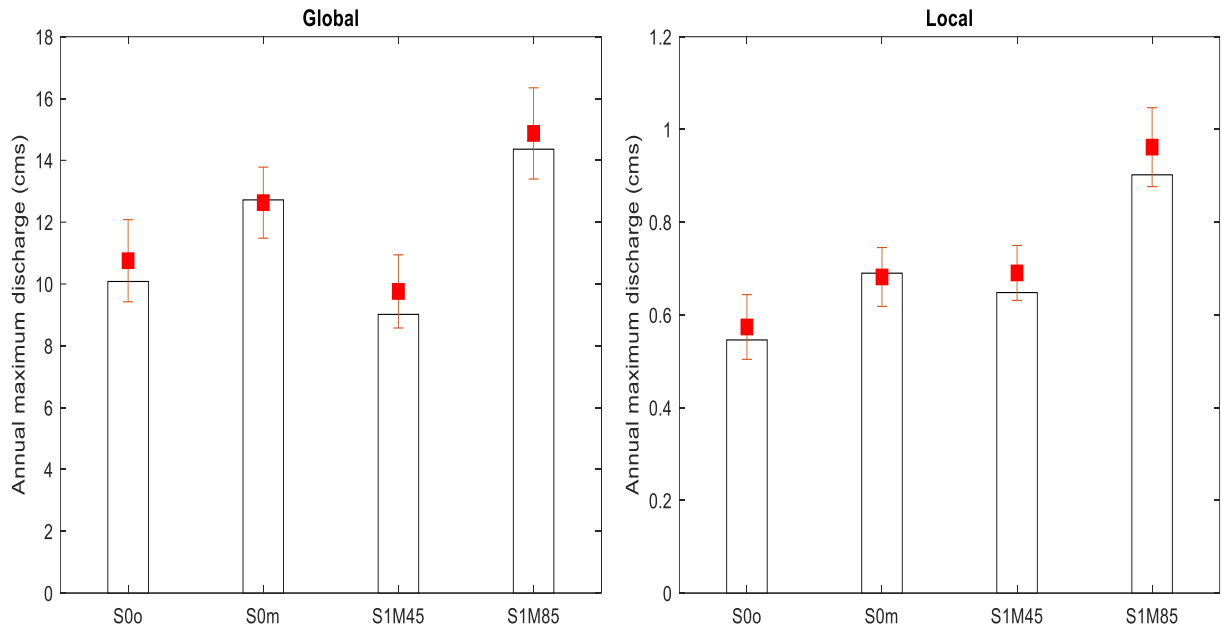

Figure 26- Global and local (sub46) impacts of combined climate and land use changes on annual maximum discharge under RCP4.5 and RCP8.5. Column height corresponds to the median, top and bottom whiskers are the errors with 95% confidence; red markers represent the mean discharge

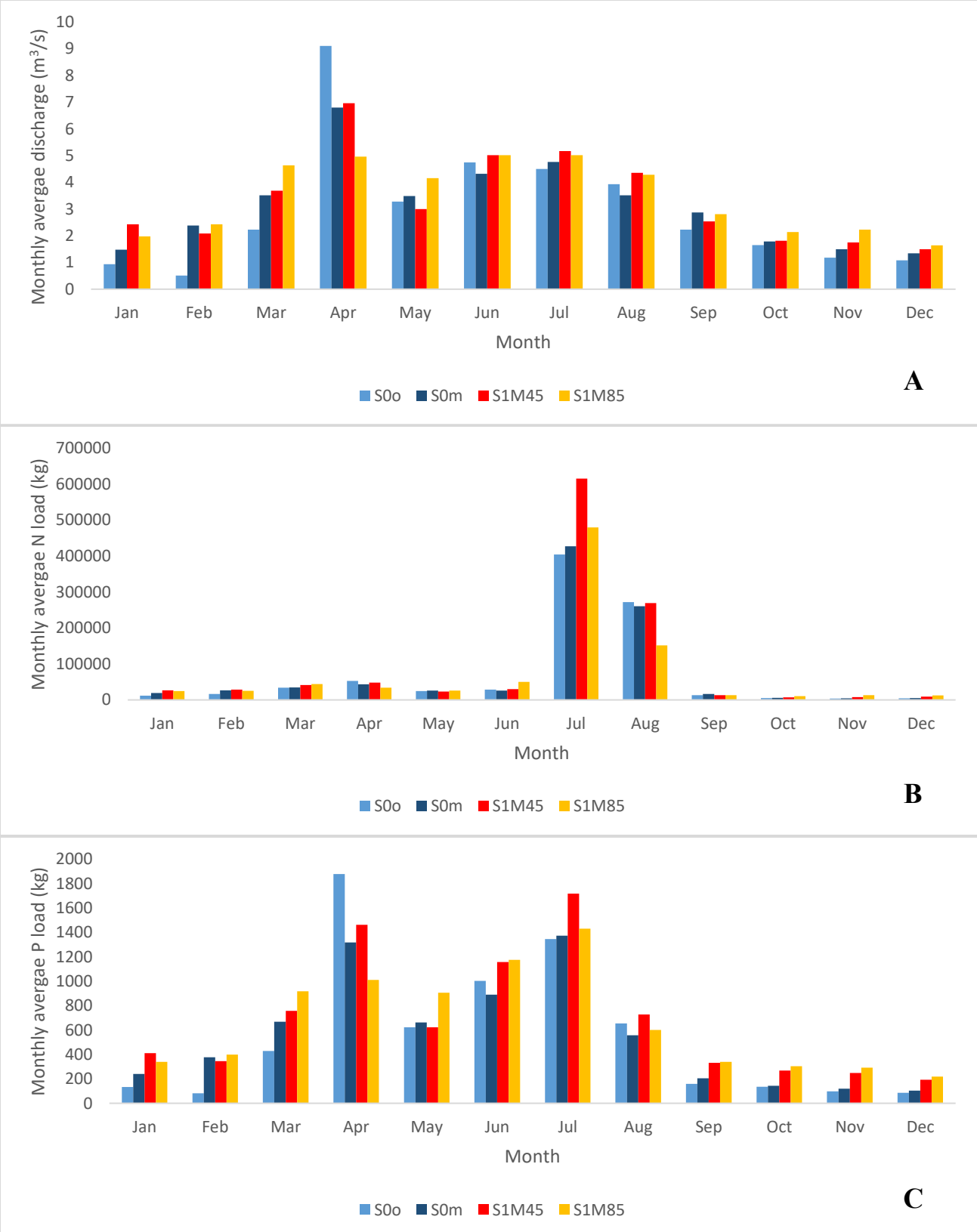

Figure 27- Global impacts of combined climate and land use changes on annual average discharge (A), nitrogen (B) and phosphorus (C) loads under RCP4.5 and RCP8.5

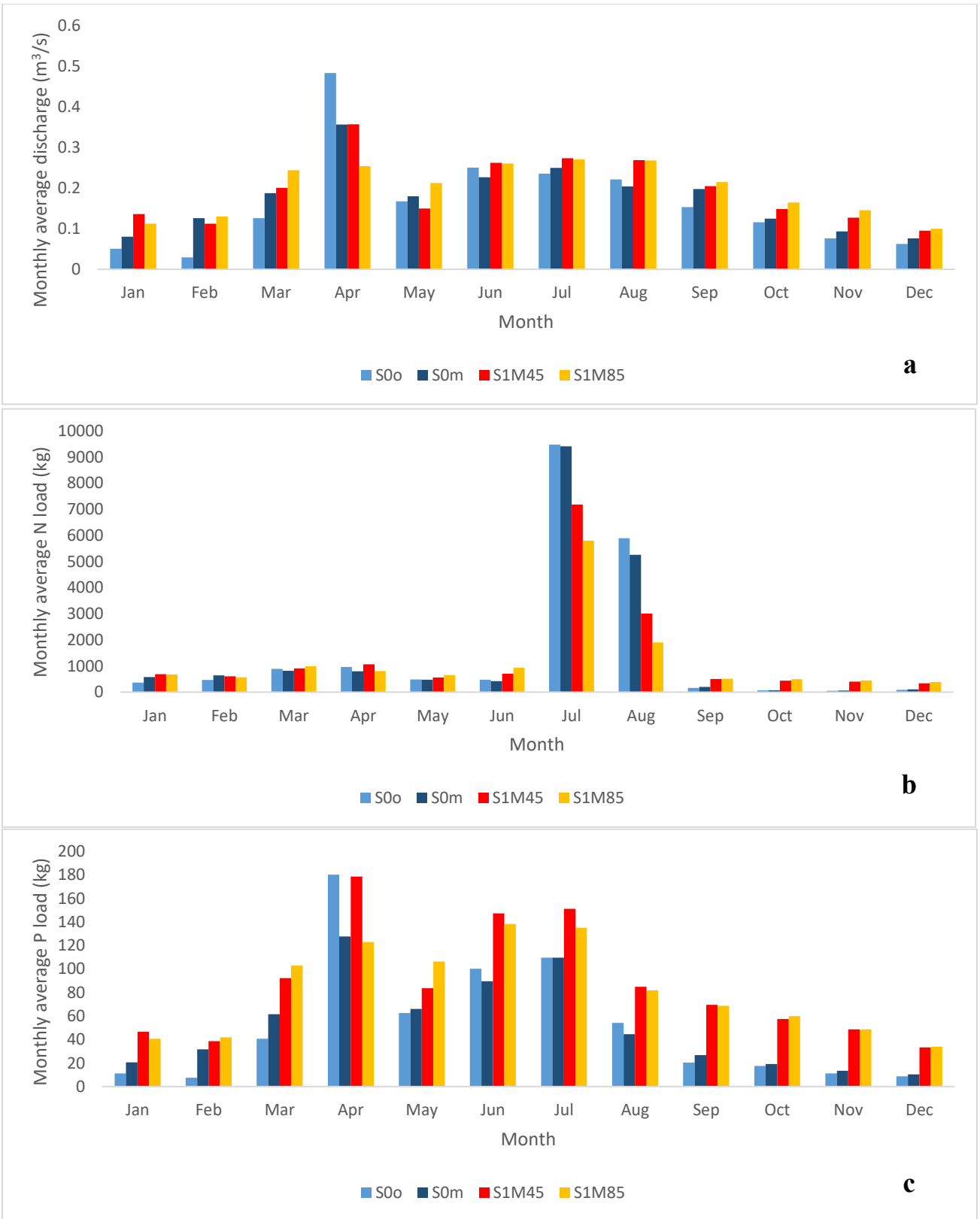

Figure 28 - Local impacts (sub46) of combined climate and land use changes on annual average discharge (a), nitrogen (b) and phosphorus (c) loads under RCP4.5 and RCP8.5

4.6. Impacts on all the sub-watersheds

This section presents the results of the different scenarios at the outlet of all the 55 sub-watersheds of the Carp River basin. Figures Figure 29, Figure 31, and Figure 33 show the variation of the quantity of flow, N, and P at the outlets, while Figure 30, Figure 32, and Figure 34show map of the percentage of change. The corresponding number of the sub-watershed on the map is indicated in Figure 10 (section 3.3.1).

Figure 29, Figure 31, and Figure 33 show how each sub-watershed is contributing to the output at the main outlet (outlet of the sub-watershed 1) and how they are impacted separately. Globally, the sub-watersheds from 32 to 55 seems to drain a relatively low quantity of water and nutrients. A significant increase is estimated at the outlet of sub-watershed 31, which is the outlet. All the previous listed sub-watersheds drain to the outlet and therefore contributes to its output. Similarly, the main outlet (sub-watershed 1) receives the discharge and nutrients of all the 54 sub-watersheds and, consequently, will be the outlet with the most important quantity (as illustrated in all the graphs, sub 1 always has the highest column).

To visualize and quantify the impact of the different scenarios, the maps in Figures Figure 30, Figure 32, and Figure 34 are used. In terms of water quantity (maximum and mean flow), the sub-watershed 50 seemed to be the most sensitive to the land-use change scenario. It experienced the highest percentage of change, estimated at +9.43% for annual maximum and +17.16% for the annual mean. The most sensitive in climate change, for annual maximum, was sub-watersheds 9 (RCP4.5) and 55 (RCP8.5) with respectively +11.77% and +4.25% while in combined land use and climate changes scenario, it was sub-watersheds 9 (RCP4.5) with +11.77% and 41 (RCP8.5) with +5.92%. For the annual mean, under climate change alone, sub-watershed 9 was the most

impacted with +9.96% in RCP4.5 and +12.21% in RCP8.5 while under S1M45 and S1M85, the most affected was sub-watersheds 50 and 41 with +20.59% and +23.53% respectively.

In terms of N, the sub-watershed 50 was the most sensitive of the basin under land-use change scenario (-73.44%) and in the combined scenario (RCP4.5: -74.17% & RCP8.5: -73.78%). The impacts of climate change were contrasted in terms of increase, and the most impacted sub-watershed depending on the RCP: under RCP4.5, it was sub 41 with +40.76%, while under RCP8.5, the downstream sub 2 was the most impacted with +7.50%.

A similar impact behavior is observed for P, as the same sub-watershed (sub 41) was the most sensitive under land-use change and combined land-use and climate change. The change was estimated as +454.73%, +470.46% and +478.37% in S1, S1M45 and S1M85, respectively. The highest impact caused by climate change was observed in sub-watersheds 32 under RCP4.5, and sub-watershed 46 under RCP8.5, with respectively -11.24% and -11.19%. Overall, although downstream sub-watersheds are the most impacted in some cases, it is obvious upstream watersheds are likely to be considerably impacted by future conditions.

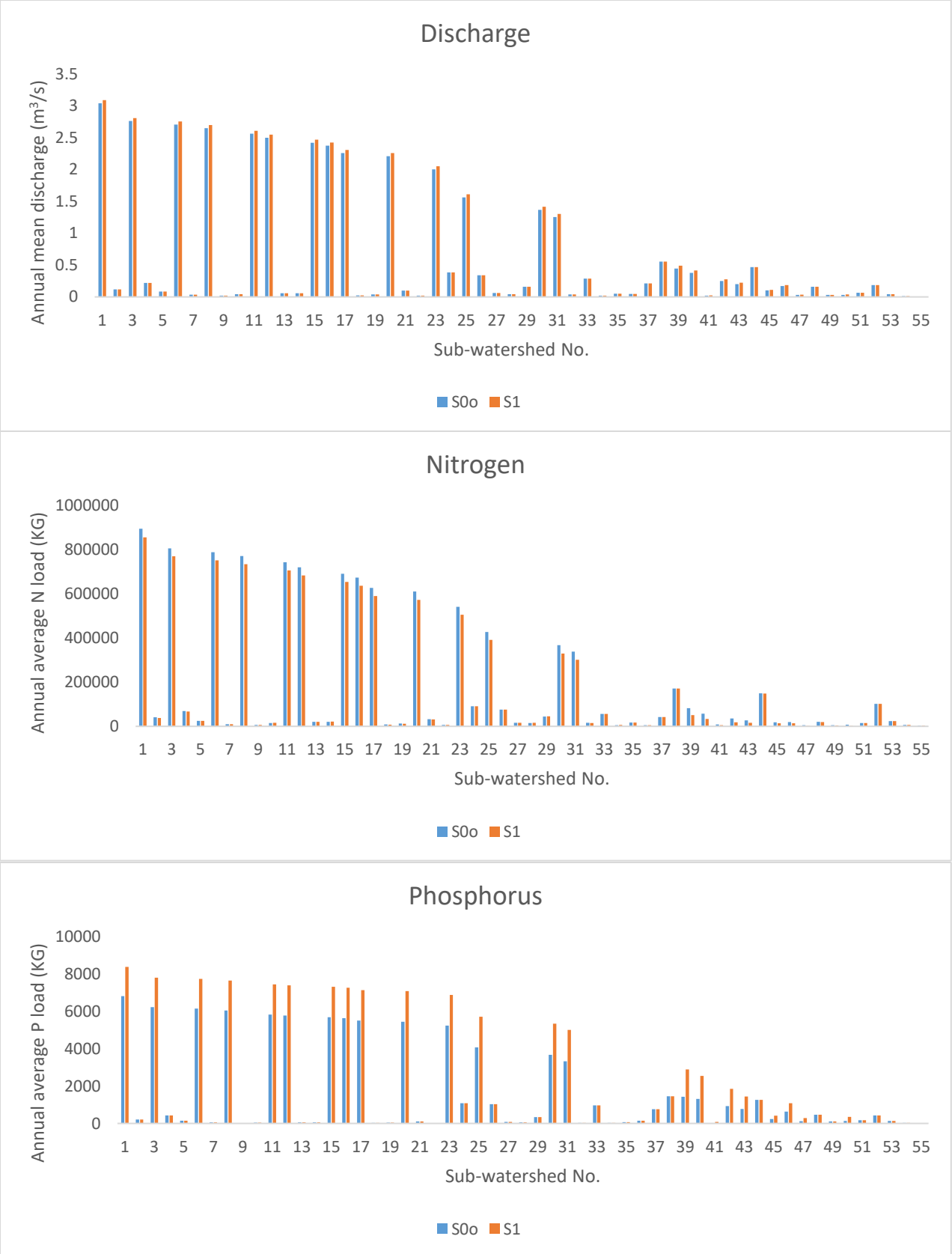

Figure 29 - Outputs comparison of all the 55 sub-watersheds in land use change scenario

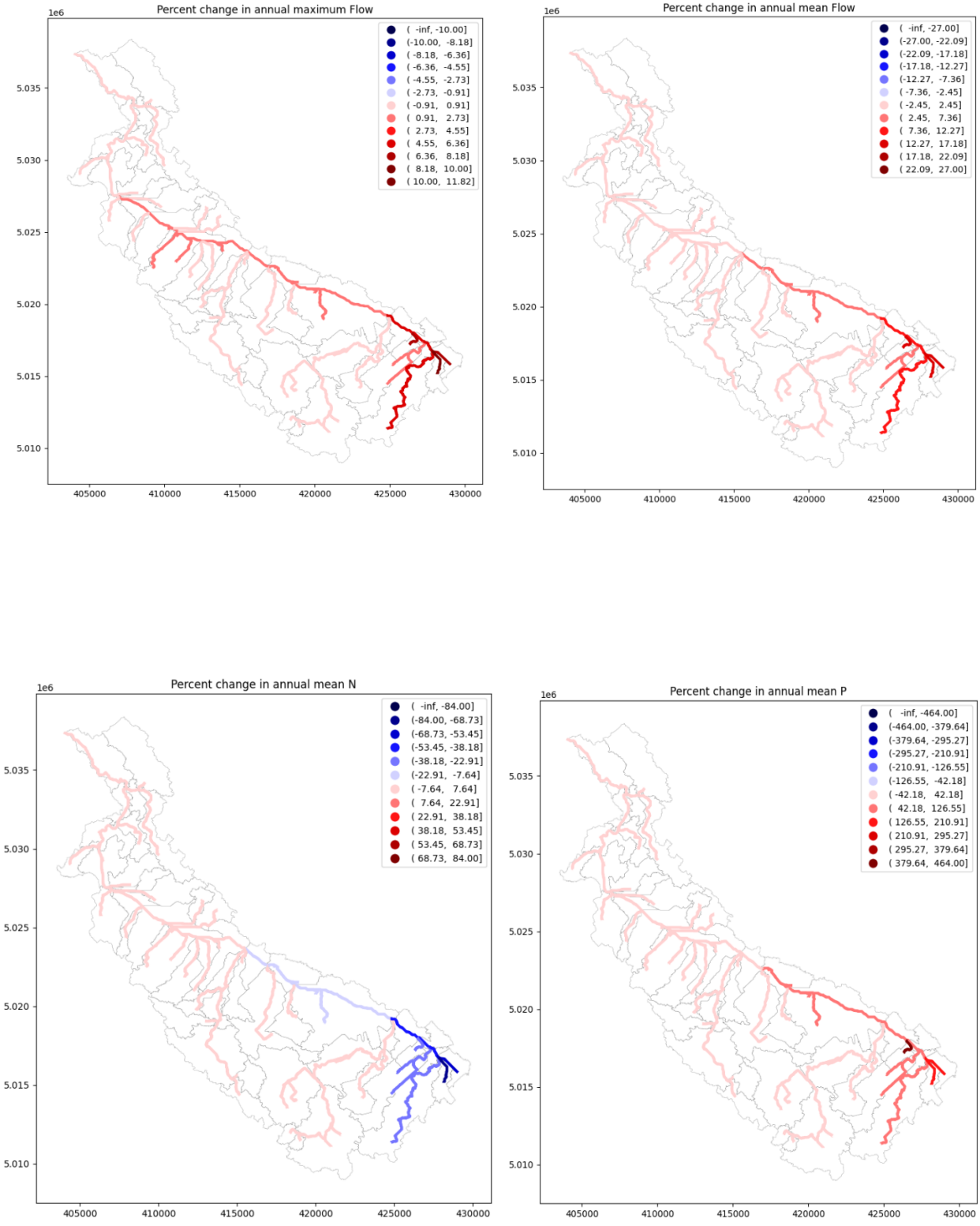

Figure 30 - Map of outputs change in land use change scenario

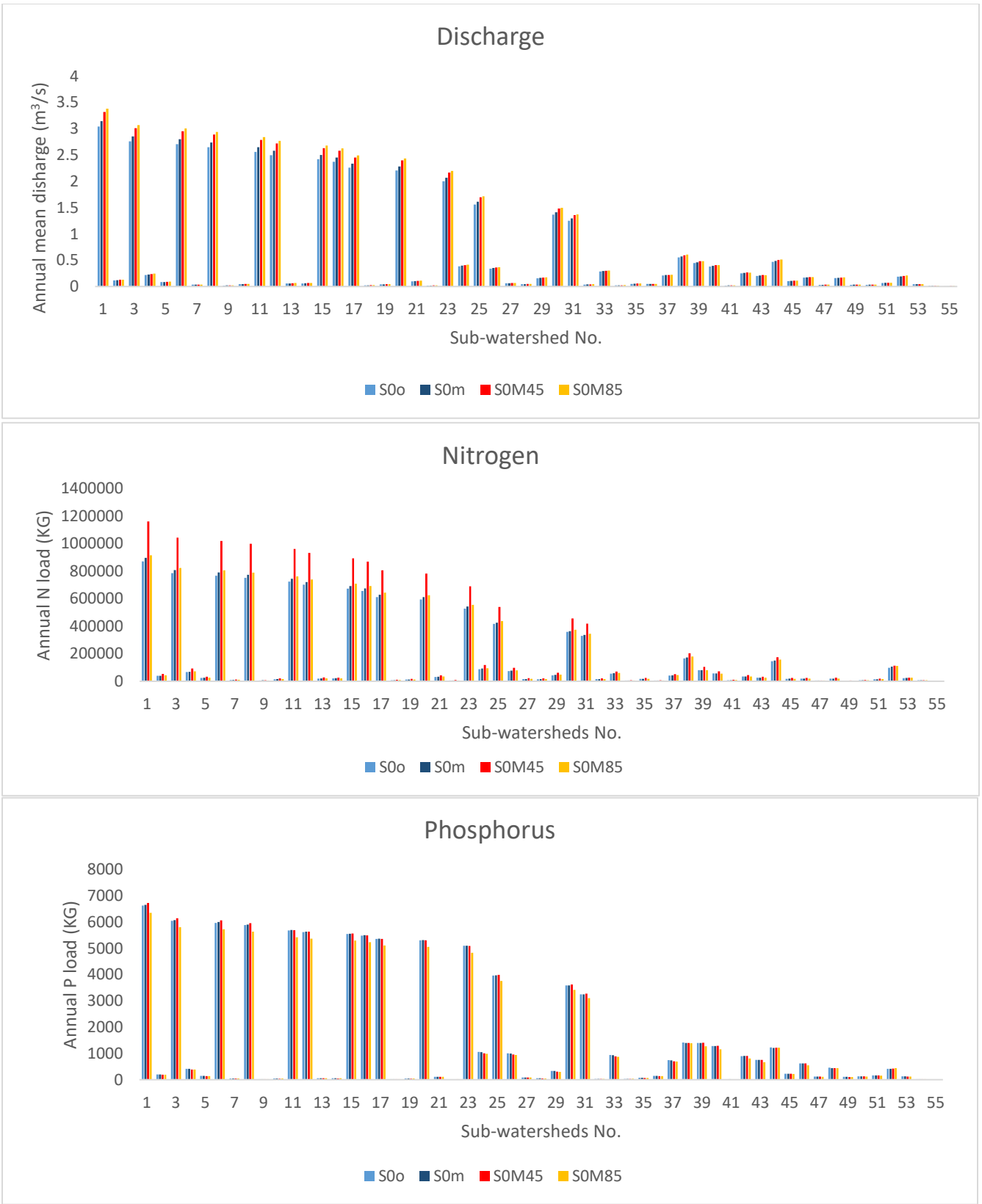

Figure 31 - Outputs comparison of all the 55 sub-watersheds in Climate Change scenario

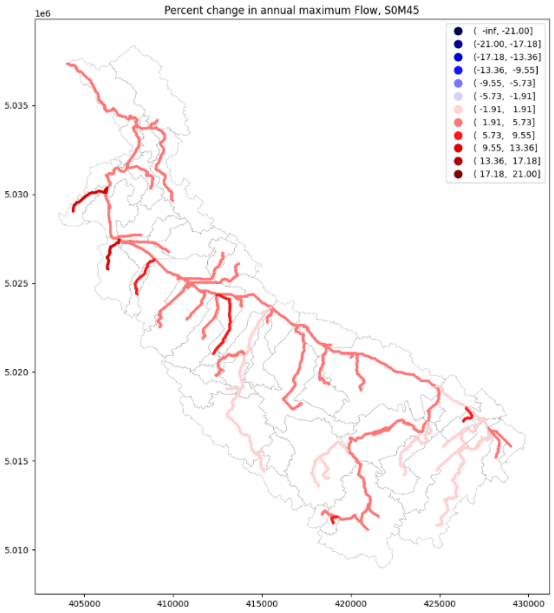
Percent change in annual maximum Flow, S0M45
1e6
(-inf, -21.00]
(-21.00, -17.18]
(-17.18, -13.36]
(-13.36, -9.55]
(-9.55, -5.73]
(-5.73, -1.91]
(-1.91, 1.91]
(1.91, 5.73]
(5.73, 9.55]
(9.55, 13.36]
(13.36, 17.18]
(17.18, 21.00]
5.035
5.030
5.025
5.020
5.015
5.010
405000
410000
415000
420000
425000
430000

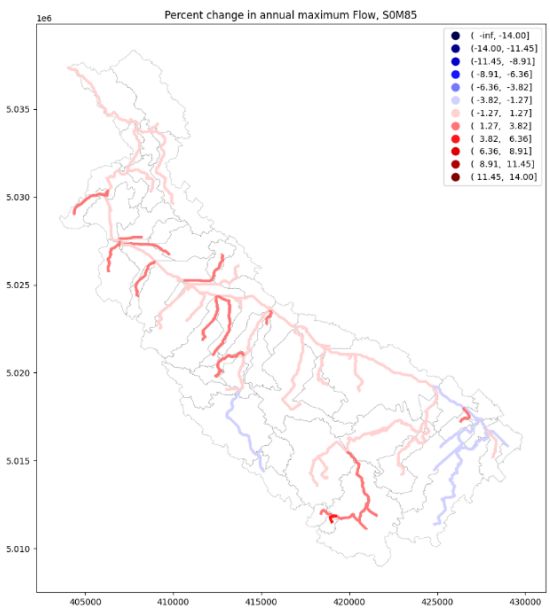
Percent change in annual maximum Flow, S0M85
1e6
(-inf, -14.00]
(-14.00, -11.45]
(-11.45, -8.91]
(-8.91, -6.36]
(-6.36, -3.82]
(-3.82, -1.27]
(-1.27, 1.27]
(1.27, 3.82]
(3.82, 6.36]
(6.36, 8.91]
(8.91, 11.45]
(11.45, 14.00]
5.035
5.030
5.025
5.020
5.015
5.010
405000
410000
415000
420000
425000
430000

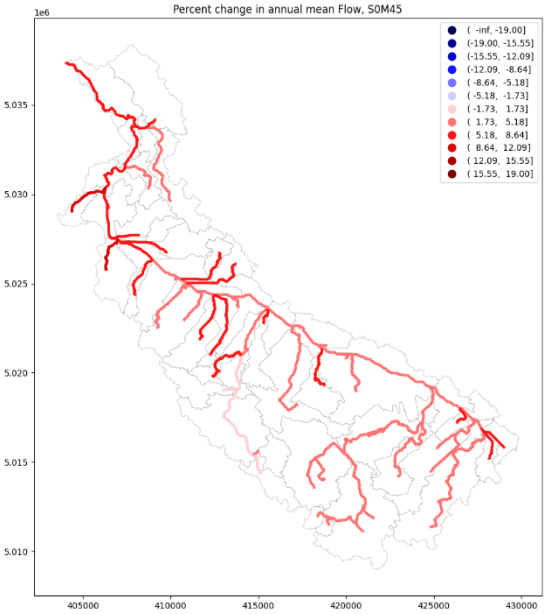
Percent change in annual mean Flow, S0M45
1e6
(-inf, -19.00]
(-19.00, -15.55]
(-15.55, -12.09]
(-12.09, -8.64]
(-8.64, -5.18]
(-5.18, -1.73]
(-1.73, 1.73]
(1.73, 5.18]
(5.18, 8.64]
(8.64, 12.09]
(12.09, 15.55]
(15.55, 19.00]
5.035
5.030
5.025
5.020
5.015
5.010
405000
410000
415000
420000
425000
430000

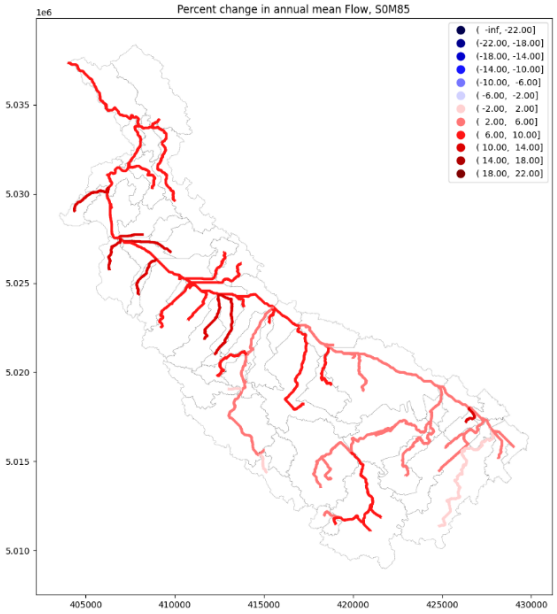
Percent change in annual mean Flow, S0M85
1e6
(-inf, -22.00]
(-22.00, -18.00]
(-18.00, -14.00]
(-14.00, -10.00]
(-10.00, -6.00]
(-6.00, -2.00]
(-2.00, 2.00]
(2.00, 6.00]
(6.00, 10.00]
(10.00, 14.00]
(14.00, 18.00]
(18.00, 22.00]
5.035
5.030
5.025
5.020
5.015
5.010
405000
410000
415000
420000
425000
430000

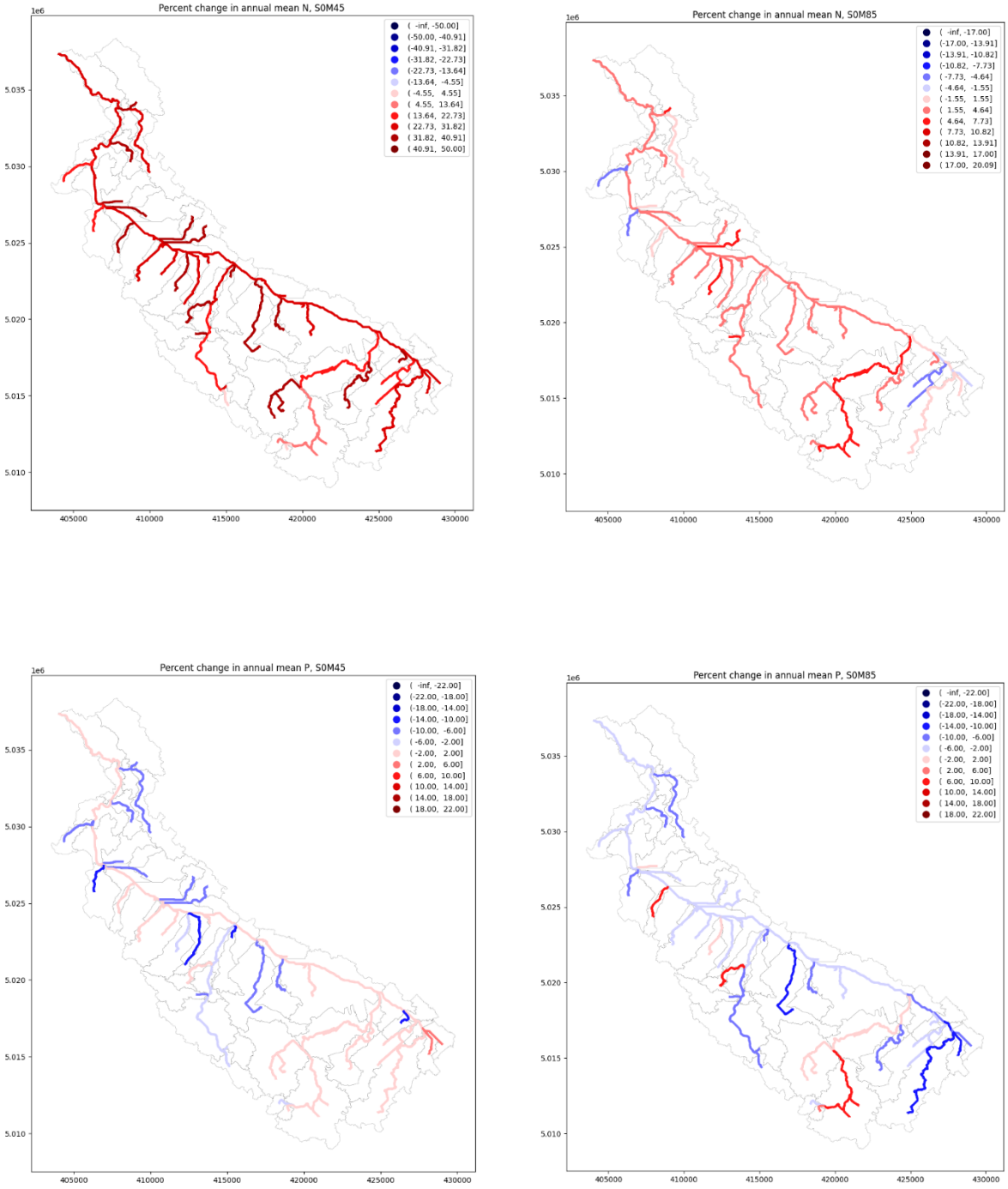

Figure 32 - Map of outputs change in Climate Change scenario

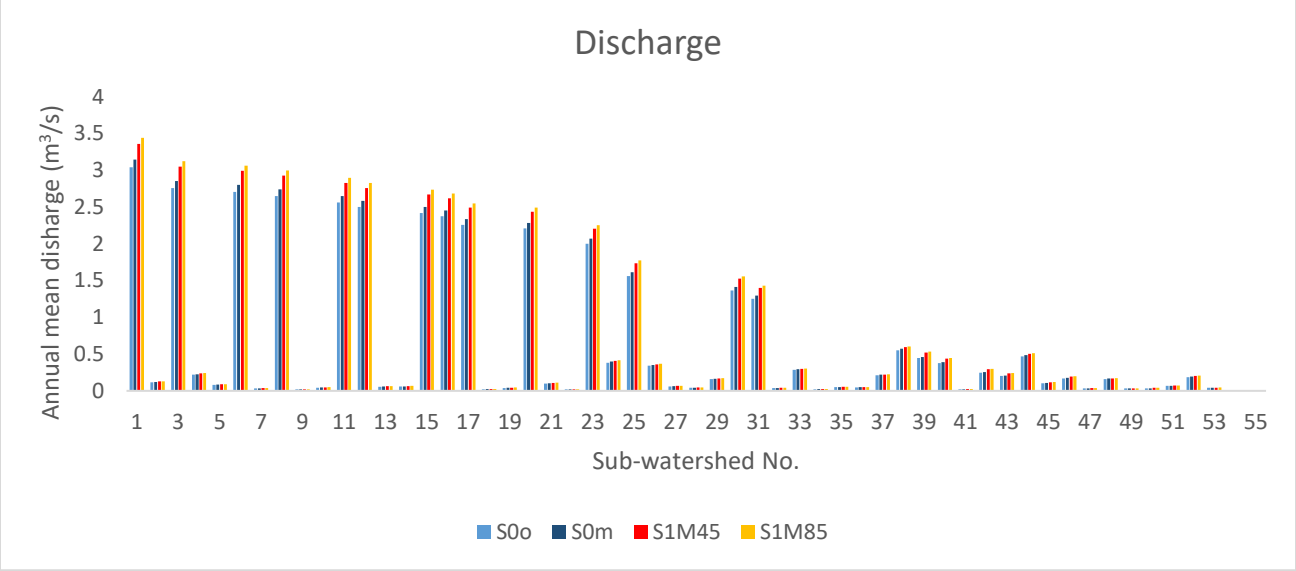

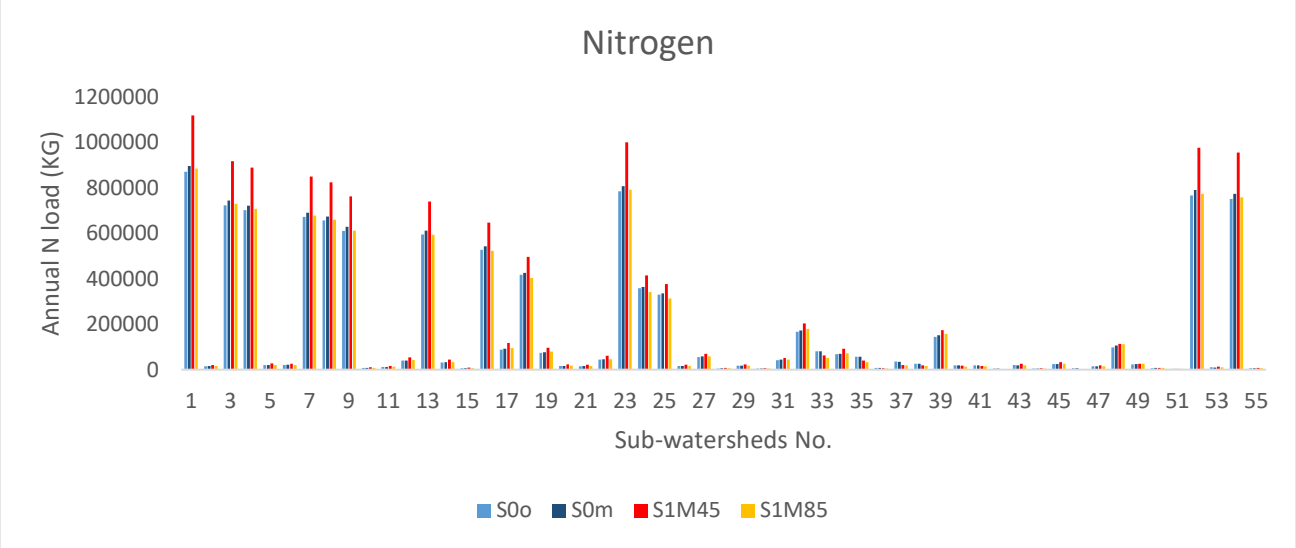

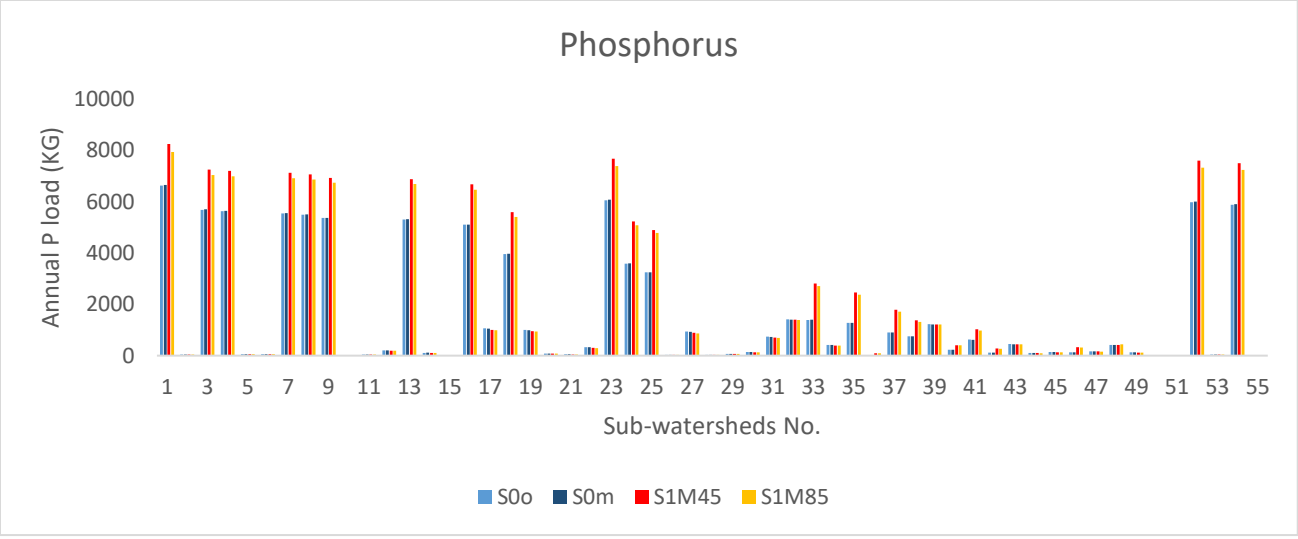

Figure 33 - Outputs comparison of all the 55 sub-watersheds in combined land use and climate changes scenario

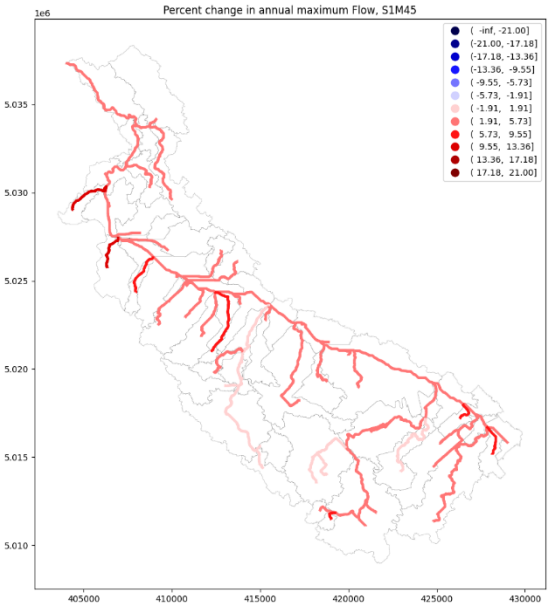
Percent change in annual maximum Flow, S1M45
1e6
(-inf, -21.00]
(-21.00, -17.18]
(-17.18, -13.36]
(-13.36, -9.55]
(-9.55, -5.73]
(-5.73, -1.91]
(-1.91, 1.91]
(1.91, 5.73]
(5.73, 9.55]
(9.55, 13.36]
(13.36, 17.18]
(17.18, 21.00]
5.035
5.030
5.025
5.020
5.015
5.010
405000
410000
415000
420000
425000
430000

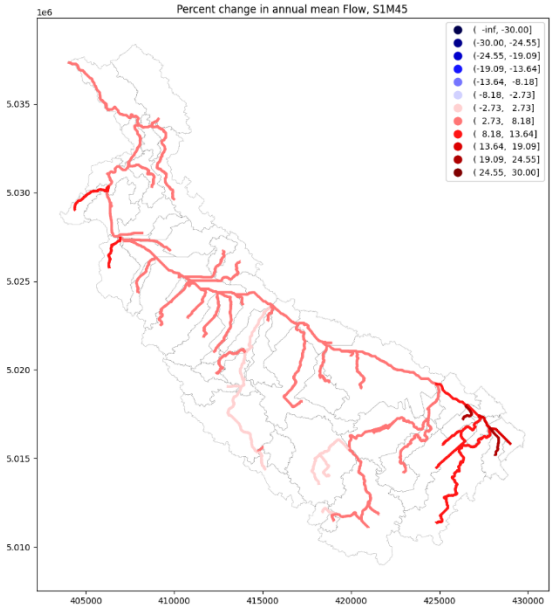
Percent change in annual mean Flow, S1M45
1e6
(-inf, -30.00]
(-30.00, -24.55]
(-24.55, -19.09]
(-19.09, -13.64]
(-13.64, -8.18]
(-8.18, -2.73]
(-2.73, 2.73]
(2.73, 8.18]
(8.18, 13.64]
(13.64, 19.09]
(19.09, 24.55]
(24.55, 30.00]
5.035
5.030
5.025
5.020
5.015
5.010
405000
410000
415000
420000
425000
430000

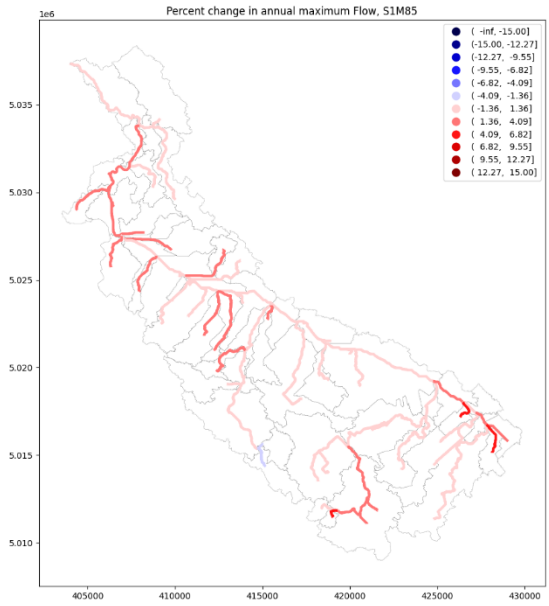
Percent change in annual maximum Flow, S1M85
1e6
(-inf, -15.00]
(-15.00, -12.27]
(-12.27, -9.55]
(-9.55, -6.82]
(-6.82, -4.09]
(-4.09, -1.36]
(-1.36, 1.36]
(1.36, 4.09]
(4.09, 6.82]
(6.82, 9.55]
(9.55, 12.27]
(12.27, 15.00]
5.035
5.030
5.025
5.020
5.015
5.010
405000
410000
415000
420000
425000
430000

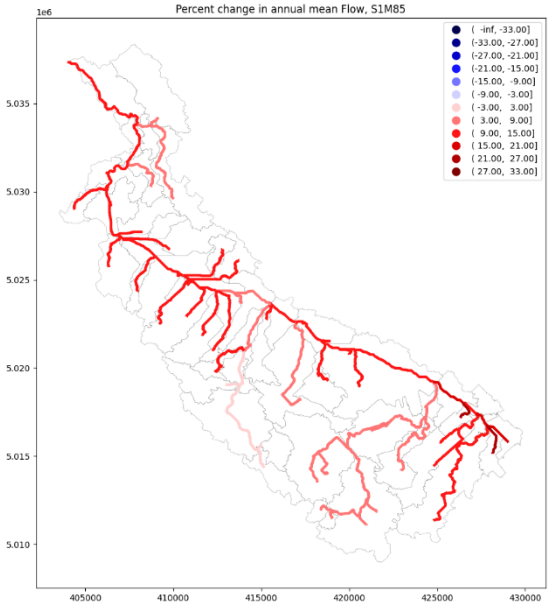
Percent change in annual mean Flow, S1M85
1e6
(-inf, -33.00]
(-33.00, -27.00]
(-27.00, -21.00]
(-21.00, -15.00]
(-15.00, -9.00]
(-9.00, -3.00]
(-3.00, 3.00]
(3.00, 9.00]
(9.00, 15.00]
(15.00, 21.00]
(21.00, 27.00]
(27.00, 33.00]
5.035
5.030
5.025
5.020
5.015
5.010
405000
410000
415000
420000
425000
430000

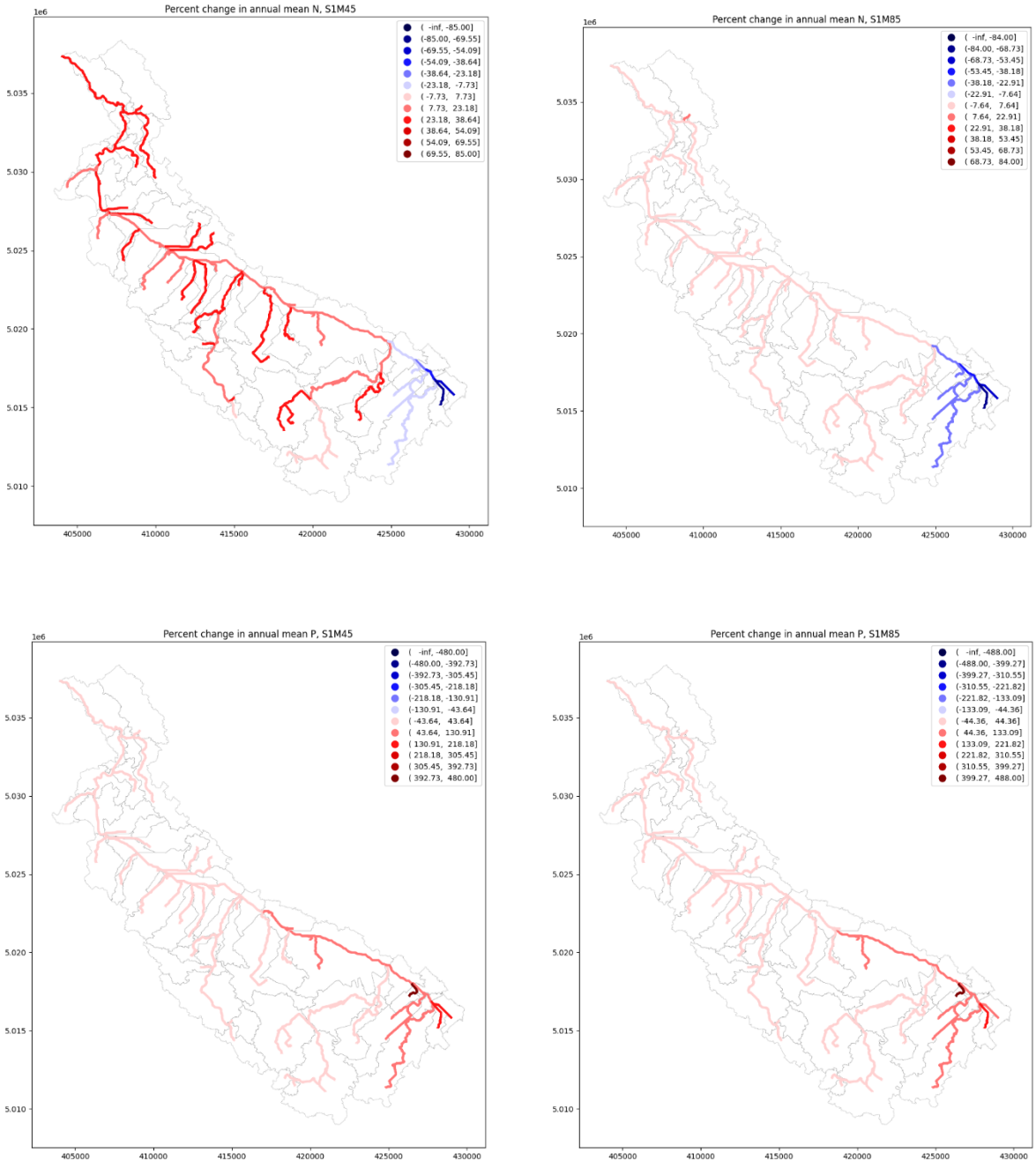

Figure 34 - Map of outputs change in combined land use and climate changes scenario

4.7. Discussion and Summary of impact results

The results presented in the previous sections provided information related to the impact level of the scenario on the water quantity and quality and the sources of pollution of nutrients. They are summarized in Table 17 with the quantities and percent changes in the local and global outlets for all the scenarios. Figure 35 presents graphically all the percent changes obtained. This section examines and discusses the different impacts observed on the discharge and water quality (N, P).

Globally, it seemed that water quantity was more sensitive to climate change than urbanization in the Carp River watershed when the scenarios are taken individually (S1 and S0M45/85). Considering the climate change effect alone in the watershed, the change in maximum discharge is expected to be within [0.90%, 3.76%] at the main outlet. In comparison, only a 0.76% increase of the maximum discharge is observed when upstream developments will be completed. The average discharge increased by 1.57% after land use change, while this change is expected to be in the interval of [5.49%, 7.42%] under climate change. Similar studies focusing on areas located in Canada have come up with the same conclusion: Kaykhosravi et al., 2020 in Montreal and Toronto; El-Khoury et al., 2015 for the South Nation watershed in Ontario. For instance, the impact caused by the land use and climate changes in the South Nation watershed was respectively +1.2% and +11.2%. Also, although the percentage of the urban area was increased in the land-use change scenario by the conversion of rural into urban (+3.64%), the agricultural lands are still dominant with 49.7% of the total area against only 13.5% for urban zones. This land-use repartition contributes to minimize the effect of the upstream developments and could explain the small impact observed in the Carp River. However, it is important to note that this is not always the case

for every Canadian watershed with agricultural dominance. The case of Montreal and Toronto illustrated it perfectly as they are also more influenced by climate change despite being among the most urbanized cities in Canada. Kaykhosravi et al. (2020) found that both climate change and urbanization have a similar impact in Vancouver. Other reasons, such as a different dynamic of land land-use change or a different location of the developments within the same watershed, may intensify the impact of urbanization on the water quantity and give a different behavior than observed in this study.

Monthly outputs analysis of historical period indicated extreme events were likely to occur at the end of the winter around April in the Carp River watershed, mainly due to the snowmelt resulting from the increase of temperatures. This is very common for cold areas as snow's contribution to the total precipitations is more than rainfall. This is also supported by the flood activities occurrence in the region. For instance, in the last two flood activities recorded in the region, one occurred at the end of March and the most recent April. According to the model, this characteristic of the watershed is not expected to change by 2050 because the predicted monthly hydrograph in the future conditions (S1M45/85) follow the same variation as the historical period (1990-2018). The peak flow variation during April is expected to be within [-27.1%, 2.38%]. Therefore, no considerable increase is expected. The peak may decrease up to 27.1% on average over the next 30 years. As discussed previously, the peak of July, due to rainfall events, is less severe than April, and results showed its variation wouldn’t exceed 8.60% on average.

In terms of water quality, the sources of pollution of N and P are generally related to land-uses types such as urban or agricultural and effluents of wastewater treatment plants. From the analysis made in section 4.3, it emerged P and N are both produced from urban and agricultural areas, but

N seemed to be more affected in July-August when agricultural activities take place. As fertilizers are generally used for these activities, it is unsurprising to observe a drastic increase during this period in the monthly graphs in all the scenarios. The N's sensitivity to agricultural activities is also demonstrated by the decrease of 1.88% of the annual total load at the main outlet in the land-use change scenario (see Table 14). The significant decrease also demonstrates it at the local scale where agricultural land ratio drastically dropped from 49.7% to 10.6%, resulting in a reduction from 1.88% to 29.00%. However, when the urban area is highly dominant (Figure 20), it seemed to contribute more to the N load than agricultural area even during July-August, as shown in Figure 22.ii, where the difference between the two outputs is considerable. In the same perspective, as the increase of urban area led to an increase of the annual P load (Figure 35.A), the pollution of P seems to be driven by the urban areas. An analysis of the impacts at the local scale shows that places with high urban area ratio experienced more increase (Figure 16). Since the type of urban occupation is primarily residential in the watershed, examples of pollution sources could include lawn fertilizers, yard and pet waste, certain soaps and detergent containing P and the chemicals used in the roads de-icing during winter and washed-off with the snowmelt in Spring which is more likely as peak N load is observed in April (Figure 18.C, Figure 19.c) with the snowmelt transporting an important quantity of chemicals into the streams.

Considering the most severe conditions in the future (S1M85), a decrease in the annual average of nitrogen load (-1.20%) is expected in opposition to an increase of 24.84% in the S1M45 scenario. Therefore, a contrasting impact on N is likely to occur under the two RCPs. As a justification, the increase of the temperatures in future conditions, especially in RCP8.5, influences the evaporation and transpiration (indispensable for the growth of plants) from natural (forests, water bodies, etc.) and agricultural lands. Given that plant cells control the openings where water is released to the

atmosphere, higher temperatures stimulate them to open, enhancing the release of water. Consequently, the rate of transpiration, defined as the water loss from living plants surfaces (Manashi, 2016), goes up with the temperature (USGS, 2020). Also, plant growth is influenced by the available amount of nitrogen, which is a vital element in the photosynthesis process. The higher the rate of plant growth, the higher the demand for nitrogen. Therefore, considering these two factors (transpiration increase and N availability), and the significant ratio of the forested area within the watershed, Nitrogen demand is expected to increase with transpiration caused by higher temperatures. This will lead to a decrease of the annual load, as observed in the S1M85 scenario) -1.20% reduction). This argument is supported by the fact that the annual evapotranspiration (ET) represents 65.65% of the total precipitations in current conditions, while this ratio is estimated at 71.91% on average under the climate change conditions. Therefore, plant growth will be more stimulated with climate change. ET and total precipitation quantities are presented at the end of this document.

This justification is also valid for the phosphorus. The increase of the load at the main outlet is smaller under the hottest scenario (S1M85: 19.15% increase) than under the coolest (S1M45: 23.81% increase). The difference is that P is less soluble than N, and consequently, it is less sensitive to temperature. This can be explained by the fact that the cycle of N has more loss processes involved than P. In Figure 2 and Figure 3, it can be observed N and P are both partially lost in plant uptake. However, in the case of N, the losses also include denitrification and volatilization. Given that temperature is a significant factor influencing the cycles of N and P, higher temperatures generally enhance their decomposition and accumulation (Y. Geng et al., 2017; Hong and Tang, 2014), meaning that denitrification and volatilization are promoted. Consequently N loss may be more important, which is the case in the Carp River watershed. Also,

it is important to mention N and P, even though having similar sources of pollution, seemed to have different transport pathways. As explained, N is more reactive (e.g., denitrification) than P, making it more soluble. N is, therefore, more likely to be retained within the watershed by infiltration into the groundwater or in the atmosphere by volatilization. At the same time, the net quantity of P is more likely to be higher in terms of ratio, especially for urbanized sub-watersheds. This was demonstrated for the Mississippi River watershed in USA (Hobbie et al., 2017), where only 22% of P inputs were retained versus 80% of the N inputs. Nieder et al. (2018) also that nitrate is the most common chemical contaminant in the world's groundwater aquifers, and surface water is particularly affected by the presence of phosphorus, confirming the findings in Carp River watershed. Therefore, although urban and agricultural lands are the main factors of nutrients pollution, the increase in temperatures due to climate has to be taken into consideration when simulating the nutrients loads. Temperature plays a very important role in their cycle and their transport from the source of pollution to the ending point (groundwater or streams).

Impact assessment at the local scale showed that the impact of urbanization become very significant when the urban area is dominant in the sub-watershed, to the point where it can even surpass the impact of climate change. For instance, at the global scale under S1 scenario, the impact on streamflow per unit hectare is 1.17E-04 $m^3/s/ha$; at the local scale, it is 1.41E-04 $m^3/s/ha$. This corresponds to 20.2 % increase. More explicitly, it means the impact on annual average flow at the local outlet is 1.2 times more intense than what occurs at the main outlet in post-development conditions. This is also confirmed in Mehdi and Lehner (2014), who mentioned that land use change could have a more important effect than climate change depending of its magnitude. This is the case of the Carp River watershed where P load and discharge experiences a higher increase

in the outlet of the upstream sub-watershed than in the main outlet in S1M45/85 scenarios (Figure 35.D & E).

The contrast in N and P variation observed in our study area differs from some published studies such as Mehdi and Lehner (2014), Eum et al. (2016), Luo et al. (2020), and El-Khoury et al. (2015) with different direction of change. For instance, El-Khoury et al. (2015) found out that P will increase regardless of the type of conditions (LUC, CC or the two combined), which is in opposition with what is observed in the Carp River watershed. This divergence indicates the impact of climate change, land-use change, or both combined must be evaluated case by case and cannot be generalized even for watershed located in the same region because every study area has different characteristics in terms of topography, land use occupation and climate conditions. Water quality is considerably affected by the entire watershed characteristics (Liu et al., 2018).

The land-use change scenario was indispensable in determining the potential sources of pollution of nutrients. As discussed in section 4.3, it emerged that N load mostly comes from agricultural land in the Carp River watershed. In contrast, phosphorus load is more affected by urban areas, and this was confirmed by the local impact assessment demonstrating the importance of the spatial distribution of land uses. Van Rompaey et al. (2007) corroborate these findings in their study by stating that the spatial distribution of land use affects the connectivity between pollution sources and sinks. Therefore, there are different contamination transport and transformation capacities in the various land-use types.

Table 17 - Summary of the results describing the impacts of land use change, climate change and combined effects

Scenario	Impact	Annual Maximum Flow		Annual Mean Flow		Annual nitrogen Load		Annual phosphorus Load	
		Value (m^3/s)	Change (%)	Value (m^3/s)	Change (%)	Value ($x10^5$ Kg)	Change (%)	Value ($x10^3$ Kg)	Change (%)
S0o	Global	10.75	-	35.40	-	8.71	-	6.62	-
	Local	0.57	-	1.97	-	0.19	-	0.62	-
S0m	Global	12.63	-	3.15	-	8.96	-	6.65	-
	Local	0.68	-	0.18	-	0.19	-	0.62	-
S1	Global	10.83	**0.73**	3.09	**1.57**	8.55	**-1.88**	8.38	**26.49**
	Local	0.60	**4.78**	0.18	**9.45**	0.14	**-29.00**	1.08	**73.56**
S0M45	Global	13.11	**3.76**	3.32	**5.49**	11.61	**29.62**	6.72	**1.07**
	Local	0.67	**-1.05**	0.18	**2.61**	0.24	**28.24**	0.62	**-0.55**
S0M85	Global	12.75	**0.90**	3.38	**7.52**	9.14	**2.03**	6.35	**-4.49**
	Local	0.66	**-3.54**	0.18	**1.13**	0.19	**-0.96**	0.55	**-11.19**
S1M45	Global	13.13	**3.97**	3.36	**6.75**	11.19	**24.84**	8.24	**23.81**
	Local	0.69	**1.61**	0.19	**11.10**	0.16	**-12.92**	1.03	**66.15**
S1M85	Global	12.79	**1.29**	3.44	**9.34**	8.85	**-1.20**	7.93	**19.15**
	Local	0.68	**-0.36**	0.20	**13.07**	0.14	**-24.80**	0.98	**57.97**

Current conditions – Observed climate

Current conditions – Simulated (RCMs) climate

Land use change scenario

Climate change scenario

Combined land use and climate changes scenario

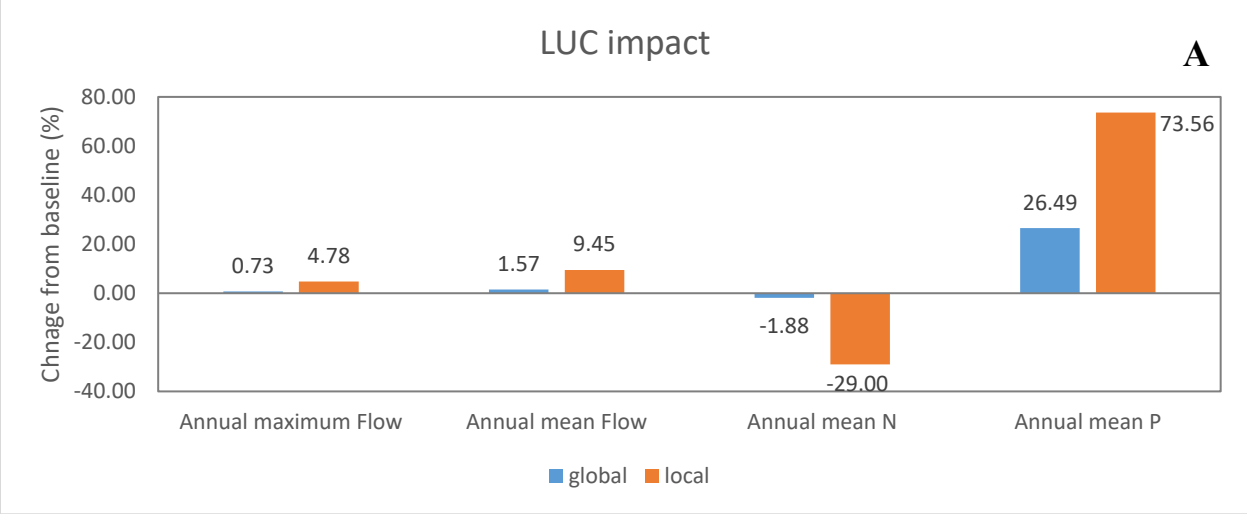
LUC impact
A
Chnage from baseline (%)
80.00
60.00
40.00
20.00
0.00
-20.00
-40.00
0.73
4.78
1.57
9.45
-1.88
-29.00
26.49
73.56
Annual maximum Flow
Annual mean Flow
Annual mean N
Annual mean P
global
local

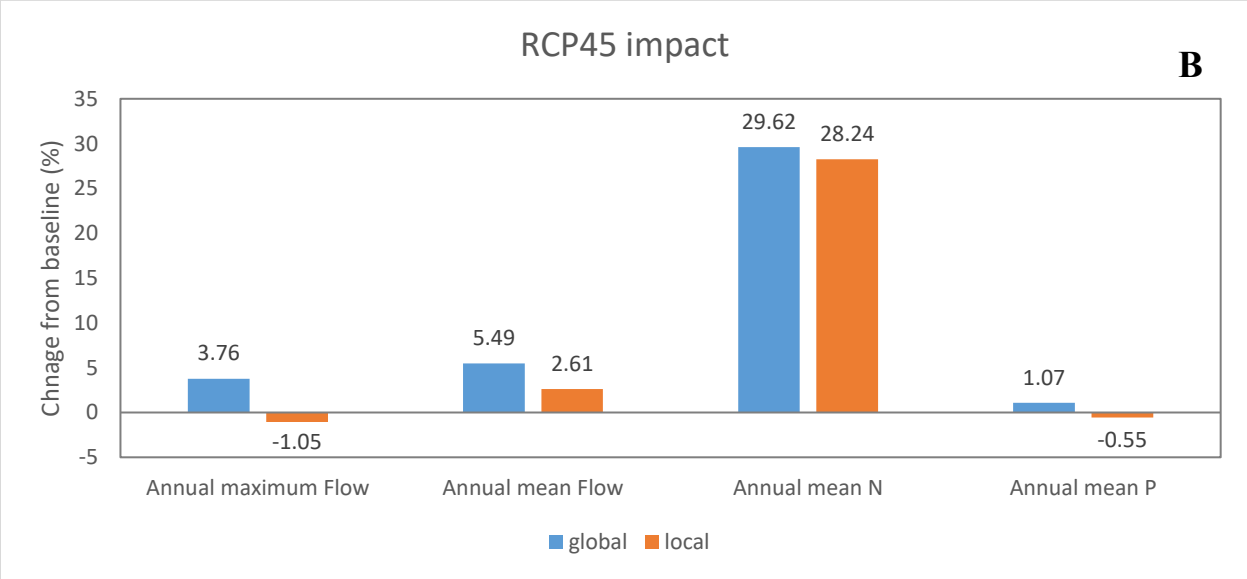
RCP45 impact
B
Chnage from baseline (%)
35
30
25
20
15
10
5
0
-5
3.76
-1.05
5.49
2.61
29.62
28.24
1.07
-0.55
Annual maximum Flow
Annual mean Flow
Annual mean N
Annual mean P
global
local

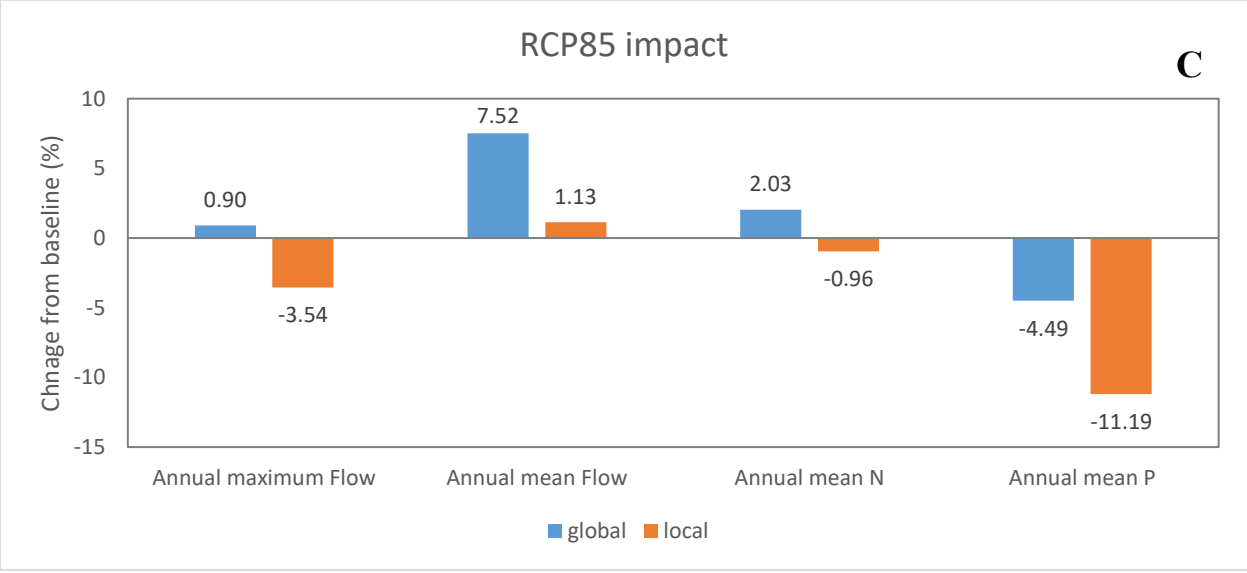
RCP85 impact
C
Chnage from baseline (%)
10
5
0
-5
-10
-15
0.90
-3.54
7.52
1.13
2.03
-0.96
-4.49
-11.19
Annual maximum Flow
Annual mean Flow
Annual mean N
Annual mean P
global
local

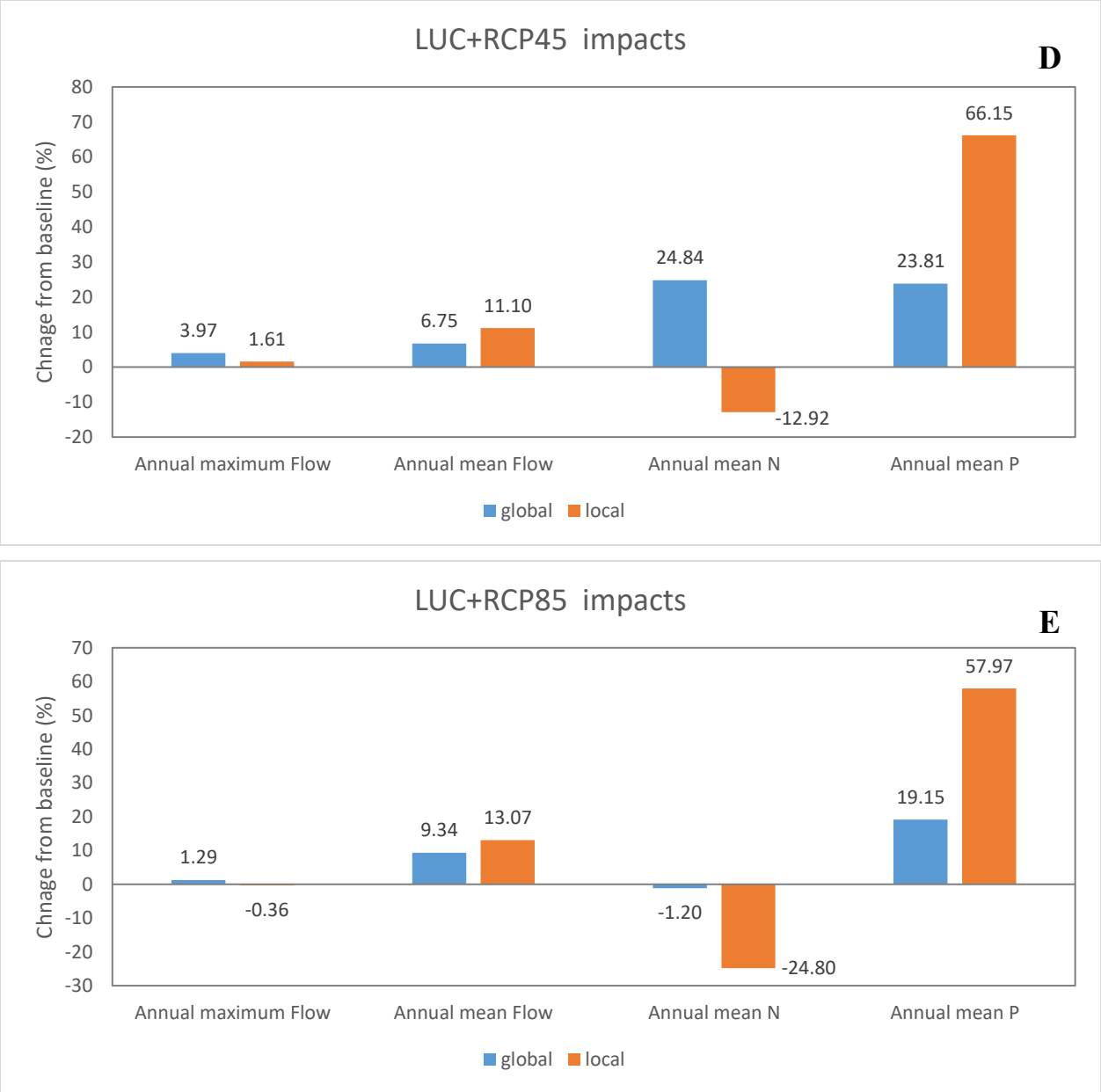

Figure 35- Changes under land use change (A), climate change (B & C) and combined effects (D &E) compared to baseline conditions

LUC= Land Use Change, CC= Climate Change

5. Conclusion and recommendations

This study examined the influence of the land-use change (urban development) and climate change individually and coupled on the watershed of the Carp River using the hydrological model SWAT. The model was developed using input data from several sources and different resolutions. It has been calibrated and validated using observed data of streamflow, N, and P, and presented overall satisfactory performance. The calibrated model showed a better performance in simulating the streamflow than the N and P, with lower performance related to the P. The impacts were evaluated by developing realistic scenarios based on the 2050 year land use map projected by the local authorities, and the future climate conditions under RCP4.5 and RCP8.5. This study's local and global approach reveals how different the impact dynamic could be at small and large scales in terms of magnitude and direction of change. Therefore, the findings suggest that not considering this aspect when conducting impacts assessment study may end up in a partial or even a misleading understanding of the results.

The conclusions that emerged from this study, as well as some recommendations, are listed as follow:

- ✓ The expected increase of the annual maximum flow at the outlet (Fitzroy Harbour) of the Carp River watershed between **1.29%** and **3.97%**
- ✓ The expected increase of the annual average flow at Fitzroy Harbour between **6.75%** and **9.34%**
- ✓ The expected variation of the annual average N load at Fitzroy Harbour between **-1.20%** and **24.84%**

- ✓ The expected variation of the annual average P load at Fitzroy Harbour between **19.15%** and **23.81%**
- ✓ Climate change is likely to be the most dominant factor affecting the flow (peaks and trend) and nitrogen while urbanization will control the phosphorus quantity in the future.
- ✓ Higher temperatures in the future will significantly affect water quality in surface (P) and ground (N) waters.
- ✓ Global and local impacts may differ significantly, and it is crucial to check the impacts at both scales.
- ✓ Local impact is found to be more significant, and small municipalities are likely to be more affected by future conditions.
- ✓ Based on the results of combined effects, impacts are not additive (e.g., 10% and 20% increase of N load in urbanization and climate change conditions respectively do not necessarily lead to a 30% increase in combined effect conditions)
- ✓ Based on the local and global approach, the correlation between impact and variable change is not linear (e.g., Increasing urbanization by 20% does not necessarily cause the same increase in the water discharge)
- ✓ Response to future conditions (land use and climate changes) differs from one watershed to another, though they are located in the same region
- ✓ For impacts assessment study, evaluating one effect alone without considering the other is incorrect and leads to a wrong understanding of the variation.
- ✓ As a recommendation, P management should emphasize reducing watershed inputs and transport from urban zones, whereas N management should reduce watershed inputs and transport from cultivated zones when active.

The future conditions will play a crucial role in modifying the hydrology of the watershed of Carp River, and it was essential to evaluate how much and in which direction they are likely going to impact. The findings from this study will inform and assist the stakeholders in planning and decision-making to limit and manage the potential consequences of the impacts, especially the flood risk, on the local communities. They will also be indispensable to future works on the watershed, especially for the hydraulic part. For example, the expected increase of water quantity could be integrated into existing or future hydraulic models and perform an adequate design/update of the local drainage system. This would guarantee the combined effect of climate change and developments are taken into consideration. The future systems will safely contain/drain the expected upcoming water quantity to protect human lives against the potential extreme events and limit the socio-economical costs that they may cause.

It is important to keep in mind that the impact assessment in this study was conducted based on the outputs of the calibrated model that presented a limited performance in simulating phosphorus. The findings of this study may differ from those of future studies on the same watershed with a different hydrological model, as explained previously. The current model would even give different dynamics of change, especially in terms of magnitude, if a different set of calibrated parameters within the fitted ranges (Table 15) were used. However, this does not diminish the value of the model developed. The methodology used, as is well known, hydrological modeling and modeling in general, always involves sources of error (described in this document) that the modeller must try to reduce as much as possible. In this context, John Tukey (1962) stated: "*Far better an approximate answer to the right question, which is often vague, than an exact answer to the wrong question, which can always be made precise*."

6. References

Abbaspour, K. (2007). *User manual for SWAT-CUP, SWAT calibration and uncertainty analysis programs.* Dübendorf, Switzerland: Swiss Federal Institute of Aquatic Science and Technology, Eawag.

Abbaspour, K., Faramarzi, M., Ghasemi, S. S., & Yang, H. (2009). Assessing the impact of climate change on water resources in Iran. *Water Resources Research, Volume 45*, Pages 1-16. Retrieved from http://dx.doi.org/10.1029/2008WR007615

Abbaspour, K., Rouholahnejad, E., Vaghefi, S., Srinivasan, R., Yang, H., & Kløve, B. (2015, May). A continental-scale hydrology and water quality model for Europe: Calibration and uncertainty of a high-resolution large-scale SWAT model. *Journal of Hydrology, 524*, 733-752. doi:https://doi.org/10.1016/j.jhydrol.2015.03.027

Abbaspour, K., Vaghefi, S. A., & Srinivasan, R. (2018). A Guideline for Successful Calibration and Uncertainty Analysis for Soil and Water Assessment: A Review of Papers from the 2016 International SWAT Conference. *Water, Volume 10*(Issue 1), Pages 6. Retrieved from https://doi.org/10.3390/w10010006

Abbaspour, K., Yang, J., Maximov, I., Siber, R., Bogner, K., Mieleitner, J., . . . Srinivasan, R. (2007). Modelling hydrology and water quality in the pre-alpine/alpine Thur watershed using SWAT. *Journal of Hydrology, Volume 333*(Issues 2–4), Pages 413-430. Retrieved from https://doi.org/10.1016/j.jhydrol.2006.09.014

Abbot, M. B., Bathurst, J. C., Cunge, J. A., O'Connell, P. E., & Rasmussen, J. (1986, October 15). An introduction to the European Hydrological System — Systeme Hydrologique

Europeen, “SHE”, 1: History and philosophy of a physically-based, distributed modelling system. *Journal of Hydrology, Volume 87*(Issues1-2), Pages 45-59. doi:https://doi.org/10.1016/0022-1694(86)90114-9

Anjum, M. N., Ding, Y., & Shangguan, D. (2019, October). Simulation of the projected climate change impacts on the river flow regimes under CMIP5 RCP scenarios in the westerlies dominated belt, northern Pakistan. *Atmospheric Research, Volume 227*, Pages 233-248. doi:https://doi.org/10.1016/j.atmosres.2019.05.017

Arnell, N., Kram, T., Carter, T., Ebi, K., Edmonds, J., Hallegatte, S., . . . Zwickel, T. (2011, August). A framework for a new generation of socioeconomic scenarios for climate change impact, adaptation, vulnerability, and mitigation research. *Climate Change*. Retrieved June 2020, from https://depts.washington.edu/iconics/wordpress/wp-content/uploads/2018/03/Scenario_FrameworkPaper_15aug11.pdf?fbclid=IwAR32cQAeziKs_L81AoPfv4TjdnQJyYUrI2vKfa03VBEZ_v2dyr9--gF5rG4

Arnold, J. G., Moriasi, D. N., Gassman, P. W., Abbaspour, K., White, M. J., Srinivasan, R., . . . Jha, M. K. (2012). SWAT: Model Use, Calibration, and Validation. *American Society of Agricultural and Biological Engineers, 55*(4), Pages 1491-1508. doi: 10.13031/2013.42256

Arnold, J., Srinivasan, P., Muttiah, R., & Williams, J. (1998, February). Large area hydrologic modeling and assessment, Part I: Model development. *Journal of the American Water Resources Association, Volume 34*(Issue 1), Pages 73-89. doi:10.1111/j.1752-1688.1998.tb05961.x

B.Karlsson, I., Sonnenborg, T. O., Refsgaard, J. C., Trolle, D., Børgesen, C. D., Olesen, J. E., . . . Jensen, K. H. (2016, August). Combined effects of climate models, hydrological model structures and land use scenarios on hydrological impacts of climate change. *Journal of Hydrology, Volume 535*, Pages 301-317. Retrieved from https://doi.org/10.1016/j.jhydrol.2016.01.069

Barringer, T., Reiser, R., & Price, C. (1994, April). Potential effects of development on flow characteristics of two New Jersey streams. *JAWRA Journal of the American Water Resources Association, Volume 30*(Issue 2), Pages 283-295. doi:10.1111/j.1752-1688.1994.tb03291.x

Beighley, R., & Moglen, G. (2002, January). Trend assessment in rainfall-runoff behavior in urbanizing watersheds. *Journal of Hydrologic Engineering, Volume 7*(Issue 1), Pages 27-34. doi:10.1061/(ASCE)1084-0699(2002)7:1(27)

Bernard Engel, D. S. (2007, August). A Hydrologic/Water Quality Model Applicati1. *Journal of the American Water Resources Association, Volume 43*(5), Pages 1223-1236. Retrieved from https://doi.org/10.1111/j.1752-1688.2007.00105.x

Bhaduri, B., Minner, M., Tatalovich, S., & Harbor, J. (2001). Long-term hydrologic impact of urbanization: A tale of two models. *Journal of Water Resources Planning and Management, Volume 127*(Issue 1), Pages 13-19. doi:10.1061/(ASCE)0733-9496(2001)127:1(13)

Blum, A., Ferraro, P., Archfield, S., & Ryberg, K. (2020, March 16). Causal Effect of Impervious Cover on Annual Flood Magnitude for the United States. *Geophysical Research Letters, Volume 47*(Issue 5). doi:10.1029/2019GL086480

Bosilovich, M., Kennedy, J., Dee, D., Allan, R., & O'Neill, A. (2013, May 8). On the Reprocessing and Reanalysis of Observations for Climate. *Climate Science for Serving Society*, 55-71. doi:https://doi.org/10.1007/978-94-007-6692-1_3

Brun, S., & Band, L. (2000, January 31). Simulating runoff behavior in an urbanizing watershed. *Computers, Environment and Urban Systems, Volume 24*(Issue 1), Pages 5-22. doi:10.1016/S0198-9715(99)00040-X

Bush, E., & Lemmen, D. S. (2019). *Canada's Changing Climate Report - Chapter 4: Changes in Temperature and Precipitation Across Canada.* Environment and Climate Change Canada. Ottawa, ON: Government of Canada. Retrieved from https://www.nrcan.gc.ca/climate-change/impacts-adaptations/canadas-changing-climate-report/21177

Čerkasova, N., Umgiesser, G., & Ertürk, A. (2018, December). Development of a hydrology and water quality model for a large transboundary river watershed to investigate the impacts of climate change – A SWAT application. *Ecological Engineering, Volume 124*, Pages 99-115.

Cheng, S.-J., & Wang, R.-Y. (2002, May). An approach for evaluating the hydrological effects of urbanization and its application. *Hydrological Processes, Volume 16*(Issue 7), Pages 1403-1418. doi:10.1002/hyp.350

Choukri, F., Raclot, D., Naimi, M., Chikhaoui, M., Nunes, J. P., Huard, F., . . . Pépin, Y. (2020, June). Distinct and combined impacts of climate and land use scenarios on water availability and sediment loads for a water supply reservoir in northern Morocco. *International Soil and Water Conservation Research, Volume 8*(Issue 2), Pages 141-153.

City of Ottawa. (2017). *Carp River PCSWMM Model Documentation - Draft Report.* Ottawa: City of Ottawa.

Debbage, N., & Shepherd, J. (2018, May). The Influence of Urban Development Patterns on Streamflow Characteristics in the Charlanta Megaregion. *Water Resources Research, Volume 54*(Issue 5), Pages 3728-3747. doi:10.1029/2017WR021594

Dosdogru, F., Kalin, L., Wang, R., & Yen, H. (2020, May). Potential impacts of land use/cover and climate changes on ecologically relevant flows. *Journal of Hydrology, Volume 584*.

Du, J., Qian, L., Rui, H., Zuo, T., Zheng, D., Xu, Y., & Xu, C.-Y. (2012, September 25). Assessing the effects of urbanization on annual runoff and flood events using an integrated hydrological modeling system for Qinhuai River basin, China. *Journal of Hydrology, Volume 464-465*, Pages 127-139. doi:10.1016/j.jhydrol.2012.06.057

Dunn, S., Brown, I., Sample, J., & Post, H. (2012, April). Relationships between climate, water resources, land use and diffuse pollution and the significance of uncertainty in climate change. *Journal of Hydrology, Volumes 434–435*, Pages 19-35. Retrieved from https://doi.org/10.1016/j.jhydrol.2012.02.039

Ehsani, N., Vörösmarty, C. J., Fekete, B. M., & Stakhiv, E. Z. (2017, December). Reservoir operations under climate change: Storage capacity options to mitigate risk. *Journal of Hydrology, Volume 555*, Pages 435-446.

El-Khoury, A., Seidou, O., Lapen, D. R., Que, Z., Mohammadian, M., Sunohara, M., & Bahram, D. (2015, March). Combined impacts of future climate and land use changes on discharge, nitrogen and phosphorus loads for a Canadian river basin. *Journal of*

Environmental Management, Volume 151, Pages 76-86. Retrieved from https://doi.org/10.1016/j.jenvman.2014.12.012

Environment and Natural Resources. (2013, July 22). *Flooding events in Canada*. Retrieved November 29, 2020, from Environment and Natural Resources: https://www.canada.ca/en/environment-climate-change/services/water-overview/quantity/floods/events-canada.html

Environment and Natural Resources. (2018, July 5). *National Weather Data Archive: HYDAT*. Retrieved from Environment and Natural Resources: https://www.canada.ca/en/environment-climate-change/services/water-overview/quantity/monitoring/survey/data-products-services/national-archive-hydat.html

Environment and natural resources Canada. (2019, Novemeber 28). *Causes and effects of climate change*. Retrieved from Government of Canada: https://www.canada.ca/en/services/environment/weather/climatechange/causes-effects.html

Environment and Natural Resources Canada. (2020, September). *Historical Climate data*. Retrieved from Environment and Natural Resources Canada: https://climate.weather.gc.ca/

Environmental Systems Research Institute (ESRI) - ArcGis for Desktop. (2016). *Projected Coordinate Systems*. Retrieved April 2020, from Environmental Systems Research Institute

ESRI. (2020, January 7). *Geographic vs Projected Coordinate Systems*. Retrieved from esri: https://www.esri.com/arcgis-blog/products/arcgis-pro/mapping/gcs_vs_pcs/

Eum, H.-I., Dibike, Y., & Prowse, T. (2016, December). Comparative evaluation of the effects of climate and land-cover changes on hydrologic responses of the Muskeg River, Alberta, Canada. *Journal of Hydrology: Regional Studies, Volume 8*, Pages 198-221.

Food and Agricultural Organization, UNESCO. (2019, November). *FAO/UNESCO Soil Map of the World*. Retrieved from Food and Agricultural Organization: http://www.fao.org/soils-portal/soil-survey/soil-maps-and-databases/faounesco-soil-map-of-the-world/en/

Gassman, P. W., Reyes, M. R., Green, C. H., & Arnold, J. G. (2007). The Soil and Water Assessment Tool: Historical Development, Applications, and Future Research Directions. *American Society of Agricultural and Biological Engineers, Volume 50*(Issue 4), Pages 1211-1250. doi:10.13031/2013.23637

Geng, Y., Baumann, F., Song, C., Zhang, M., Shi, Y., Kühn, P., . . . He, J.-S. (2017, March). Increasing temperature reduces the coupling between available nitrogen and phosphorus in soils of Chinese grasslands. *Sci. Rep.*, 7: 43524. doi:10.1038/srep43524

Geomatic Solutions. (2017). *Datum: World Geodetic System 1984*. Retrieved May 16, 2020, from GeoRepository: https://georepository.com/datum_6326/World-Geodetic-System-1984.html

Geza, M., & Mccray, J. E. (2008). Effects of Soil Data Resolution on SWAT Model Streamflow and Water Quality Predictions. *Journal of Environmental Management, Volume 88*(Issue 3), Pages 393-406. doi:10.1016/j.jenvman.2007.03.016

Government of Canada. (2018, 10 24). *Scenarios and climate models*. Retrieved from https://www.canada.ca/en/environment-climate-change/services/climate-change/canadian-centre-climate-services/basics/scenario-models.html

Gumbo, B., Munyamba, N., Sithole, G., & Savenije, H. H. (2002). Coupling of digital elevation model and rainfall-runoff model in storm drainage network design. *Physics and Chemistry of the Earth, Parts A/B/C, Volume 27*(Issues 11–22), Pages 755-764. doi:https://doi.org/10.1016/S1474-7065(02)00063-3

Guo, Y., Fang, G., Xu, Y.-P., Tian, X., & Xie, J. (2020, March). Identifying how future climate and land use/cover changes impact streamflow in Xinanjiang Basin, East China. *Science of The Total Environment, Volume 710*, Article 136275. Retrieved from https://doi.org/10.1016/j.scitotenv.2019.136275

Gupta, H. V., Kling, H., Yilmaz, K. K., & Martinez, G. F. (2009, October 20). Decomposition of the mean squared error and NSE performance criteria: Implications for improving hydrological modelling. *Journal of Hydrology, Volume 377*(Issues 1–2), Pages 80-91.

Gupta, H., Sorooshian, S., & Yapo, P. (1998, April). Toward improved calibration of hydrologic models: Multiple and noncommensurable measures of information. *Water Resources Research, Volume 34*(4), 751-763.

Harmel, R. D., & Smith, P. K. (2007, April 30). Consideration of measurement uncertainty in the evaluation of goodness-of-fit in hydrologic and water quality modeling. *Journal of Hydrology, Volume 337*(Issues 3–4), Pages 326-336. Retrieved from https://doi.org/10.1016/j.jhydrol.2007.01.043

Havrylenko, S. B., Bodoque, J. M., Srinivasan, R., Zucarelli, G. V., & Mercuri, P. (2016, Fevrier). Assessment of the soil water content in the Pampas region using SWAT. *CATENA*, Pages 298-309. doi:https://doi.org/10.1016/j.catena.2015.10.001

Hayes, N., & Vanni, M. (2018, July). Microcystin concentrations can be predicted with phytoplankton biomass and watershed morphology. *Inland Waters, Volume 8*(Issue 3), Pages 273-283. doi:10.1080/20442041.2018.1446408

Heo, J., Yu, J., Giardino, J., & Cho, H. (2015). Water resources response to climate and land-cover changes in a semi-arid watershed, New Mexico, USA. *Terrestrial, Atmospheric and Oceanic Sciences, Volume 26*(Issue 4), Pages 463-474.

Hessami, M., Gachon, P., Ouarda, T. B., & St-Hilaire, A. (2008, June). Automated regression-based statistical downscaling tool. *Environmental Modelling & Software, Volume 23*(Issue 6), Pages 813-834. doi:https://doi.org/10.1016/j.envsoft.2007.10.004

Hobbie, S. E., Finlay, J. C., Janke, B. D., Nidzgorski, D. A., Millet, D. B., & Baker, L. A. (2017, April). Contrasting nitrogen and phosphorus budgets in urban watersheds and implications for managing urban water pollution. (A. S. B. L. Turner, Ed.) *National Academy of Sciences, 114*(16).

Holvoet, K., Van Griensven, A., Seuntjens, P., & Vanrolleghem, P. (2005). Sensitivity analysis for hydrology and pesticide supply towards the river in SWAT. *Physics and Chemistry of the Earth, Parts A/B/C, Volume 30*(Issues 8–10), Pages 518-526. Retrieved from https://doi.org/10.1016/j.pce.2005.07.006

Hong, F., & Tang, J. (2014). *Influence of temperature and moisture on nitrogen cycling in soils from experimentally heated and control plots at the Harvard Forest, MA.* Mount Holyoke College. Chicago: Marine Biological Laboratory. Retrieved December 2020, from https://www.mbl.edu/ses/files/2015/04/Fangyuan-Hong.pdf

Hong, Y., Liao, Q., Bonhomme, C., & Chebbo, G. (2019, September 15). Physically-based urban stormwater quality modelling: An efficient approach for calibration and sensitivity analysis. *Journal of Environmental Management, Volume 246*, Pages 462-471. doi:https://doi.org/10.1016/j.jenvman.2019.06.003

Huo, A., & Li, H. (2013). Assessment of climate change impact on the stream-flow in a typical debris flow watershed of Jianzhuangcuan catchment in Shaanxi Province, China. *Environmental Earth Sciences, 69*, 1931–1938.

Huo, W., Li, Z., Zhang, K., Wang, J., & Yao, C. (2020, March). GA-PIC: An improved Green-Ampt rainfall-runoff model with a physically based infiltration distribution curve for semi-arid basins. *Journal of Hydrology, Volume 586*. doi:https://doi.org/10.1016/j.jhydrol.2020.124900

International Association of Oil and Gas Producer. (2020, April 30). *About the EPSG Dataset*. Retrieved May 16, 2020, from International Association of Oil and Gas Producer: http://www.epsg.org/

IPCC (Intergovernmental Panel on Climate Change). (2019). *IPCC Special Report on Climate Change, Desertification, Land Degradation, Sustainable Land Management, Food Security, and Greenhouse gas fluxes in Terrestrial Ecosystems.* The World Meteorological Organization & United Nations Environment Programme, Geneva, Switwerland. Retrieved from https://www.ipcc.ch/site/assets/uploads/2019/08/4.-SPM_Approved_Microsite_FINAL.pdf

IPCC. (2014). *Climate Change 2014 - Synthesis Report.* Geneva, Switzerland.

Ishida, K., Ercan, A., Trinh, T., Kavvas, M. L., Ohara, N., Carr, K., & Anderson, M. L. (2018, December 15). Analysis of future climate change impacts on snow distribution over mountainous watersheds in Northern California by means of a physically-based snow distribution model. *Science of The Total Environment, Volume 645*, Pages 1065-1082. doi:https://doi.org/10.1016/j.scitotenv.2018.07.250

J.Hung, C.-L., James, L. A., Carbone, G. J., & Williams, J. M. (2020, January). Impacts of combined land-use and climate change on streamflow in two nested catchments in the Southeastern United States. *Ecological Engineering, Volume 143*, Article 105665. Retrieved from https://doi.org/10.1016/j.ecoleng.2019.105665

Jajarmizadeh, M., Sidek, L. M., Harun, S., & Salarpour, M. (2017). Optimal Calibration and Uncertainty Analysis of SWAT. *Air, Soil and Water Research, Volume 10*, Pages 1-14. doi:https://doi.org/10.1177%2F1178622117731792

Jha, M. K., & Gassman, P. W. (2014, February 28). Changes in hydrology and stream flow as predicted by a modeling experiment forced with climate models. *Hydrological Processes, Volume28* (Issue 5), Pages 2772-2781. doi: https://doi.org/10.1002/hyp.9836

Judd, J. H. (1970, August). Lake stratification caused by runoff from street deicing. *Water Research, Volume 4*(Issue 8), Pages 521-532. Retrieved from https://doi.org/10.1016/0043-1354(70)90002-3

Kaykhosravi, S., Khan, U. T., & Jadidi, M. A. (2020). The Effect of Climate Change and Urbanization on the Demand for Low Impact Development for Three Canadian Cities. *Water*, 12, 1280.

Khalid, K., Ali, M. F., Rahman, N. F., Mispan, M. R., Haron, S. H., Othman, Z., & Bachok, M. F. (2016). Sensitivity analysis in watershed model using SUFI-2 algorithm. *Procedia Engineering, Volume 162*, Pages 441 – 447.

Khoiab, D. N., & Thomb, V. T. (2015, October 28). Global Ecology and Conservation. *Parameter uncertainty analysis for simulating streamflow in a river catchment of Vietnam, Volume 4*, pp. 538-548. doi:https://doi.org/10.1016/j.gecco.2015.10.007

Kingston, D., & Taylor, R. (2010). Sources of uncertainty in climate change impacts on river discharge and groundwater in a headwater catchment of the Upper Nile Basin. *Hydrology and Earth System Sciences, Volume 14*(Issue 7), Pages 1297-1308.

Kitaka, N. (2000). *PHOSPHORUS SUPPLY TO A SHALLOW TROPICAL LAKE AND ITS CONSEQUENCES - LAKE NAIVASHA, KENYA.* PhD Thesis, University of Leicester (UK), Department of Biology.

Kundu, S., Khare, D., & Mondal, A. (2017, August). Individual and combined impacts of future climate and land use changes on the water balance. *Ecological Engineering, Volume 105*, Pages 42-57. doi:10.1016/j.ecoleng.2017.04.061

Lewis, E., Birkinshaw, S., Kilsby, C., & Fowler, H. J. (2018, October). Development of a system for automated setup of a physically-based, spatially-distributed hydrological model for catchments in Great Britain. *Environmental Modelling & Software, Volume 108*, Pages 102-110. doi:https://doi.org/10.1016/j.envsoft.2018.07.006

Liang, K., Jiang, Y., Qi, J., Nyiraneza, J. F., & Meng, F.-R. (2020). Characterizing the impacts of land use on nitrate load and water yield in an agricultural watershed in Atlantic Canada.

Science of the Total Environment, Volume 729, Article number 138793. doi:10.1016/j.scitotenv.2020.138793

Liu, L., Ma, C., Huo, S., Xi, B., He, Z., Zhang, H., . . . Xia, X. (2018, August). Impacts of climate change and land use on the development of nutrient criteria. *Journal of Hydrology, Volume 563*, Pages 533-542.

Liu, Y. q., Long, H., Li, T., & Tu, S. (2015). Land use transitions and their effects on water environment in Huang-Huai-Hai Plain, China. *Land Use Policy, 47*, Pages 293-301.

Lobell, D. B., Burke, M. B., Tebaldi, C., Mastrandrea, M. D., Falcon, W. P., & Naylor, R. L. (2008, February 01). Prioritizing Climate Change Adaptation Needs for Food Security in 2030. *Science, Volume 319*(Issue 5863), pages 607-610. doi:10.1126/science.1152339

Luo, C., Li, Z., Liu, H., Li, H., Wan, R., Pan, J., & Chen, X. (2020, February). Differences in the responses of flow and nutrient load to isolated and coupled future climate and land use changes. *Journal of Environmental Management, Volume 256*, 109918.

Manashi, P. (2016). *Impacts of land use and climate changes on hydrological processes in South Dakota watersheds.* South Dakota State University, Agricultural and Biosystems Engineering. ProQuest Dissertations Publishing. Retrieved from https://search.proquest.com/docview/1837118008?pq-origsite=summon

Marshall, S. J. (2014). The Water Cycle. *Reference Module in Earth Systems and Environmental Sciences*.

Mbonimpa, E. G., Yuan, Y., Mehaffey, M. H., & Jackson, M. A. (2012, July). SWAT Model Application to Assess the Impact of Intensive Corn-farming on Runoff, Sediments and

Phosphorous loss from an Agricultural Watershed in Wisconsin. *Journal of Water Resource and Protection*, Pages 423-431.

Mehdi, B. B., & Lehner, B. (2014). *Scenarios and implications of land use and climate change on water quality in mesoscale agricultural watersheds.* McGill University, Department of Geography. Montreal: McGill University.

Mengistu, A. G., Van Rensburg, L. D., & Woyessa, Y. E. (2019, October). Techniques for calibration and validation of SWAT model in data scarce arid and semi-arid catchments in South Africa. *Journal of Hydrology: Regional Studies, Volume 25*, Article no. 100621.

Ministry of Natural Resources and Forestry. (2017, May 23). User Guide for Ontario Flow Assessment Tool (OFAT) . Ottawa, Ontario, Canada.

Ministry of Natural Resources and Forestry. (2019, November). *Ontario Flow Assessment Tool*. Retrieved from Ontario Flow Assessment Tool: http://www.gisapplication.lrc.gov.on.ca/OFAT/Index

Moreira, L. L., Schwamback, D., & Rigo, D. (2018). Sensitivity analysis of the Soil and Water Assessment Tools (SWAT) model in streamflow modeling in a rural river basin. *Rev. Ambient. Água, vol.13*(6). Retrieved from http://dx.doi.org/10.4136/ambi-agua.2221

Moriasi, D., Arnold, J., Van Liew, M., Bingner, R., Harmel, R., & Veith, T. (2007, May). Model evaluation guidelines for systematic quantification of accuracy in watershed simulations. *Transactions of the ASABE, Volume 50*(3), 885-900.

Moss, R., Babiker, M., Brinkman, S., Calvo, E., Carter, T., Edmonds, J., . . . Hibbard, K. (2008). *Towards New Scenarios For Analysis Of Emissions, Climate Change, Impacts, And*

Response Strategies - IPCC Expert Meeting Report on New Scenarios. IPCC (Intergovernmental Panel on Climate Change).

Mukundan, R., Radcliffe, D. E., & Risse, L. M. (2010). Spatial resolution of soil data and channel erosion effects on SWAT model predictions of flow and sediment. *Journal of Soil and Water Conservation, Volume 65*(Issue 2), Pages 92-104. doi:https://doi.org/10.2489/jswc.65.2.92

Muluneh, A. (2020). Impact of climate change on soil water balance, maize production, and potential adaptation measures in the Rift Valley drylands of Ethiopia. *Journal of Arid Environments, Volume 179*, Article 104195. Retrieved from https://doi.org/10.1016/j.jaridenv.2020.104195

Nash, J., & Sutcliffe, J. (1970, April). River flow forecasting through conceptual models part I — A discussion of principles. *Journal of Hydrology, Volume 10*(3), 282-290.

Natural Resources Canada. (2016, August 25). *The UTM Grid - Universal Transverse Mercator Projection*. Retrieved May 16, 2020, from Government of Canada: https://www.nrcan.gc.ca/earth-sciences/geography/topographic-information/maps/utm-grid-map-projections/utm-grid-universal-transverse-mercator-projection/9779

Neitsch, S. L., Arnold, J. G., Kiniry, J. R., & Williams, J. R. (2009). *Soil and Water Assessment Tool Theoritical Documentation Version 2009.* Grassland, Soil and Water Research Laboratory - Agricultural Research Service - Blackland Research Center - Texas AgriLife Research , US Department of Agriculture. Texas Water Research Institue. Retrieved from https://swat.tamu.edu/media/99192/swat2009-theory.pdf

Neitsch, S., Arnold, J., Kiniry, J., Williams, J., & King, K. (2005). Soil and water assessment tool theoretical documentation—version 2005. *Soil and Water Research Laboratory, Agricultural Research Service, US Department of Agriculture, Temple*.

Nieder, R., Benbi, D. K., & Reichl, F. X. (2018). Reactive Water-Soluble Forms of Nitrogen and Phosphorus and Their Impacts on Environment and Human Health. *Soil Components and Human Health*, 223-255.

O'Connell, P. (1991). A historical perspective. (O. P. Bowles D.S., Ed.) *Recent Advances in the Modeling of Hydrologic Systems*, Pages 3-30.

Oeurnga, C., Sauvage, S., & Sánchez-Pérez, J.-M. (2011, May 3). Assessment of hydrology, sediment and particulate organic carbon yield in a large agricultural catchment using the SWAT model. *Journal of Hydrology, Volume 401*(Issues 3–4), Pages 145-153. doi:https://doi.org/10.1016/j.jhydrol.2011.02.017

Parker, W. S. (2016, October). Reanalyses and Observations: What's the Difference? *American Meteorological Society*, 1565-1572. doi:https://doi.org/10.1175/BAMS-D-14-00226.1

Penjor, U., Wangdi, S., Tandin, T., & Macdonald, D. W. (2020, October). Vulnerability of mammal communities to the combined impacts of anthropic land-use and climate change in the Himalayan conservation landscape of Bhutan. *Ecological Indicators*, Article 107085. Retrieved from https://doi.org/10.1016/j.ecolind.2020.107085

Persaud, E., Levison, J., MacRitchie, S., Berg, S. J., Erler, A. R., Parker, B., & Sudicky, E. (2020, May). Integrated modelling to assess climate change impacts on groundwater and surface water in the Great Lakes Basin using diverse climate forcing. *Journal of Hydrology, Volume 584*. Retrieved from https://doi.org/10.1016/j.jhydrol.2020.124682

Prowse, T., Beltaos, S., Gardner, J., Gibson, J., Granger, R., Leconte, R., . . . Toth, B. (2006, February). Climate change, flow regulation and land-use effects on the hydrology of the Peace-Athabasca-Slave system: findings from the northern rivers ecosystem initiative. *Environmental Monitoring and Assessment, Volume 113*(Issue 1-3), pages 167-197.

Riahi, K., Rao, S., Krey, V., Cho, C., Chirkov, V., Fischer, G., . . . Rafaj, P. (2011, August). RCP 8.5 - A scenario of comparatively high greenhouse gas emissions. *Climatic Change, 109*.

Rokaya, P., Morales-Marin, L., & Lindenschmidt, K.-E. (2020, May). A physically-based modelling framework for operational forecasting of river ice breakup. *Advances in Water Resources, Volume 139*. doi:https://doi.org/10.1016/j.advwatres.2020.103554

Rossman, L. A. (2015, September). *Storm Water Management Model User's Manual Version 5.1.* Environmental Protection Agency.

Royle, J. A., Chandler, R. B., Sollmann, R., & Gardner, B. (2014). Chapter 3 - GLMs and Bayesian Analysis. *Spatial Capture-recapture*, Pages 47-85. doi:https://doi.org/10.1016/B978-0-12-405939-9.00003-7

Samaras, A. G., & Koutitas, C. G. (2014, September). Modeling the impact of climate change on sediment transport and morphology in coupled watershed-coast systems: A case study using an integrated approach. *International Journal of Sediment Research, Volume 29*(Issue 3), Pages 304-315.

Santhi, C., Arnold, J. G., Williams, J. R., Dugas, W. A., Srinivasan, R., & Hauck, L. M. (2001, October). Validation of the SWAT Model on a Large River Basin with Point and Nonpoint Sources. *Journal of the American Water Resources Association, Volume 37*(5), 1169 - 1188. Retrieved from https://doi.org/10.1111/j.1752-1688.2001.tb03630.x

Shrestha, B., Cochrane, T. A., Caruso, B. S., Arias, M. E., & Piman, T. (2016, September). Uncertainty in flow and sediment projections due to future climate scenarios for the 3S Rivers in the Mekong Basin. *Journal of Hydrology, Volume 540*, Pages 1088-1104.

Shrestha, N. K., Du, X., & Wang, J. (2017, December 1). Assessing climate change impacts on fresh water resources of the Athabasca River Basin, Canada. *Science of The Total Environment, Volumes 601–602*, Pages 425-440. Retrieved from https://doi.org/10.1016/j.scitotenv.2017.05.013

Shrestha, N. K., Rudra, R. P., Daggupati, P., Goel, P. K., & Shukla, R. (2021). A comparative evaluation of the continuous and event-based modelling approaches for identifying critical source areas for sediment and phosphorus losses. *Journal of Environmental Management, Volume 277*, Article 111427. Retrieved from https://doi.org/10.1016/j.jenvman.2020.111427

Skala, V., Dohnal, M., Votrubova, J., Vogel, T., Dusek, J., Sacha, J., & Jelinkova, V. (2020, February). Hydrological and thermal regime of a thin green roof system evaluated by physically-based model. *Urban Forestry & Urban Greening, Volume 48*. doi:https://doi.org/10.1016/j.ufug.2020.126582

South Dakota Department of Water and Natural Resources. (1990, October). *Minimizing the Environmental Impact From Snow Disposal - Guidance for Municipalities*. Retrieved from South Dakota Department of Water and Natural Resources: https://denr.sd.gov/dfta/wp/snow.aspx

Taranu, Z., Gregory-Eaves, I., Steele, R., Beaulieu, M., & Legendre, P. (2017, June). Predicting microcystin concentrations in lakes and reservoirs at a continental scale: A new

framework for modelling an important health risk factor. *Global Ecology and Biogeography, Volume 26*(Issue 6), Pages 625-637. doi:10.1111/geb.12569

Tiruneh, B. A. (2004). *Modelling Water Quality Using Soil and Water Assessment Tool (SWAT) - A Case Study in Lake Naivasha Basin, Kenya.* International Institute for Geo-information Science and Earth Observation . International Institute for Geo-information Science and Earth Observation .

Tirupathi, C., & Shashidhar, T. (2020, June). Investigating the impact of climate and land-use land cover changes on hydrological predictions over the Krishna river basin under present and future scenarios. *Science of The Total Environment, Volume 721*, Article 137736. Retrieved from https://doi.org/10.1016/j.scitotenv.2020.137736

Trang, N. T., Shrestha, S., Shrestha, M., Datta, A., & Kawasaki, A. (2017, January 17). Evaluating the impacts of climate and land-use change on the hydrology and nutrient yield in a transboundary river basin: A case study in the 3S River Basin (Sekong, Sesan, and Srepok). *Science of The Total Environment, Volume 576*, Pages 586-598.

Tu, J. (2009). Combined impact of climate and land use changes on streamflow and water quality in eastern Massachusetts, USA. *Journal of Hydrology, Volume 379*(Issues 3–4), Pages 268-283. Retrieved from https://doi.org/10.1016/j.jhydrol.2009.10.009

Tukey, J. W. (1962). The future of data analysis. : . *Annals of Mathematical Statistics, 33*, 1-67.

U.S. EPA. (2019, February 4). *Nutrient Pollution*. Retrieved May 2020, from United States Environmental Protection Agency: https://www.epa.gov/nutrientpollution/issue

UCAR Community Program. (2012). *Network Common Data Form (NetCDF)*. Retrieved December 14, 2019, from UCAR/Unidata: https://www.unidata.ucar.edu/software/netcdf/

UNESCO, FAO. (2007). *Soil Map of the World 1: 5 000 000, Volume II, North America.* Paris.

United Nations. (2019). *World Population Prospects 2019 - Volume II: DemographicProfiles.* Economic and Social Affairs, PopulationDivision. United Nations. Retrieved May 2020, from https://population.un.org/wpp/Publications/Files/WPP2019_Volume-II-Demographic-Profiles.pdf

USGS. (2020). *Water Science School - Evapotranspiration and the Water Cycle*. Retrieved 12 05, 2020, from USGS - Science for a Changing World: https://www.usgs.gov/special-topic/water-science-school/science/evapotranspiration-and-water-cycle?qt-science_center_objects=0#qt-science_center_objects

Van Rompaey, A., Krasa, J., & Dostál, T. (2007, July). Modelling the impact of land cover changes in the Czech Republic on sediment delivery. *Land Use Policy. 24. 576-583., Volume 24*(Issue 3), Pages 576-583. doi:10.1016/j.landusepol.2005.10.003

Verhagen, A. P., Ostelo, R. W., & Rademaker, A. (2004). Is the p value really so significant?*. *Australian Journal of Physiotherapy, Volume 50*(Issue 4), Pages 261-262. Retrieved from https://doi.org/10.1016/S0004-9514(14)60122-7

Vuuren, D. P., Edmonds, J., Kainuma, M., Riahi, K., Thomson, A., Hibbard, K., . . . Rose, S. J. (2011, August). The representative concentration pathways: an overview. *Climatic Change, 109*.

Vuuren, D. P., Stehfest, E., Elzen, M. G., Kram, T., Vliet, J. v., Deetman, S., . . . Ruijven, R. O. (2011). RCP2.6: exploring the possibility to keep global mean temperature increase below 2°C. *Climate Change, 109*.

Wang, Q., Xu, Y., Wang, Y., Zhang, Y., Xiang, J., Xu, Y., & Wang, J. (2020, May). Individual and combined impacts of future land-use and climate conditions on extreme hydrological events in a representative basin of the Yangtze River Delta, China. *Atmospheric Research, Volume 236*, 104805. Retrieved from https://doi.org/10.1016/j.atmosres.2019.104805

Wayne, G. (2013, August). *The Beginner's Guide to Representative Concentration Pathways.* Retrieved from Skeptical Science: https://www.skepticalscience.com/docs/RCP_Guide.pdf

Weedom, G., Balsamo, G., Bellouin, N., Gomes, S., Best, M., & Viterbo, P. (2014). The WFDEI meteorological forcing data set: WATCH Forcing Data methodology applied to ERA-Interim reanalysis data. *Water Resources Research, 50*. doi:10.1002/2014WR015638

Wilby, R., Charles, S., Zorita, E., Timbal, B., Whetton, P., & Mearns, L. (2004). *Guidelines for use of climate scenarios developed from statistical downscaling methods.* Retrieved October 18, 2020, from https://www.academia.edu/download/31092390/dgm_no2_v1_09_2004.pdf

Wu, H., & Chen, B. (2015, March). Evaluating uncertainty estimates in distributed hydrological modeling for the Wenjing River watershed in China by GLUE, SUFI-2, and ParaSol methods. *Ecological Engineering, Volume 76*, Pages 110-121. doi:https://doi.org/10.1016/j.ecoleng.2014.05.014

Yang, J., Reichert, P., Abbaspour, K., Xia, J., & Yang, H. (2008, August). Comparing uncertainty analysis techniques for a SWAT application to the Chaohe Basin in China. *Journal of Hydrology, Volume 358*(Issues 1–2), Pages 1-23. doi:https://doi.org/10.1016/j.jhydrol.2008.05.012

Ye, X., Zhang, Q., & Viney, N. R. (2010, December). The effect of soil data resolution on hydrological processes modelling in a large humid watershed. *Hydrological processes, Volume 25*(Isssue 1), Pages 130-140. doi: https://doi.org/10.1002/hyp.7823

Yu, Z. (2015). HYDROLOGY, FLOODS AND DROUGHTS | Modeling and Prediction. *Encyclopedia of Atmospheric Sciences (Second Edition)*.

Appendices

A. Model calibration and validation: Comparison of model performance before and after calibration

OUTLET 8

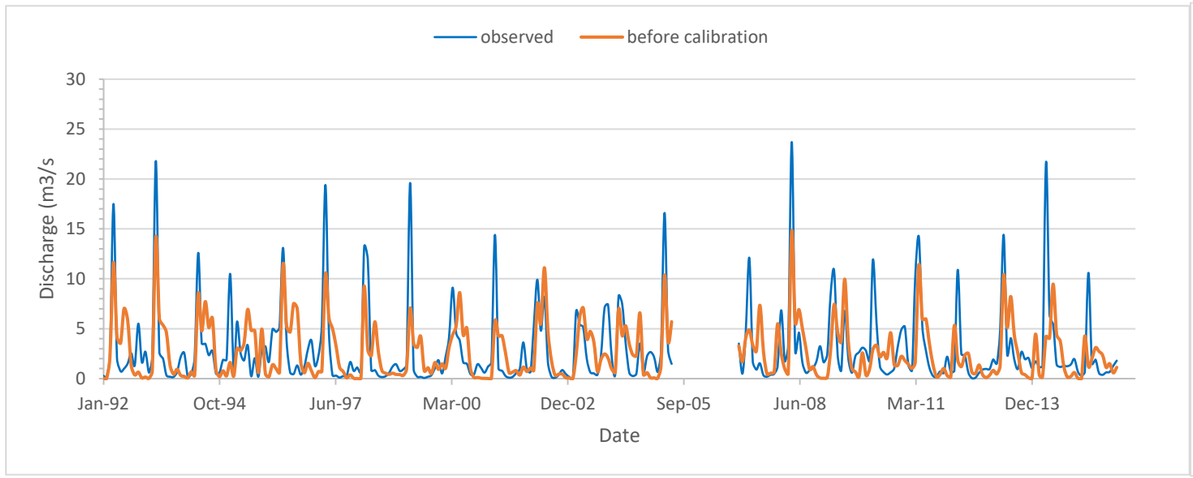

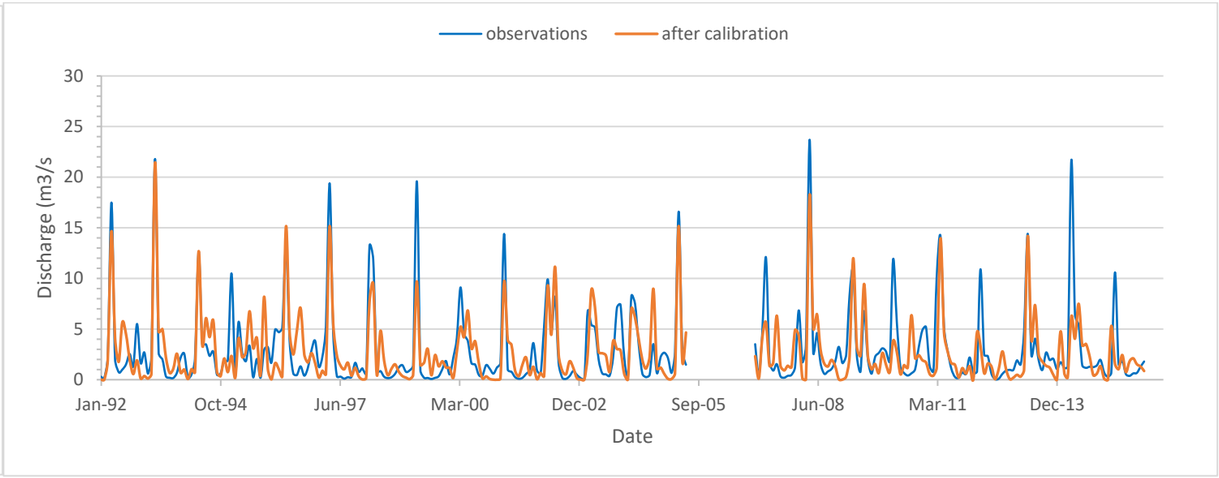

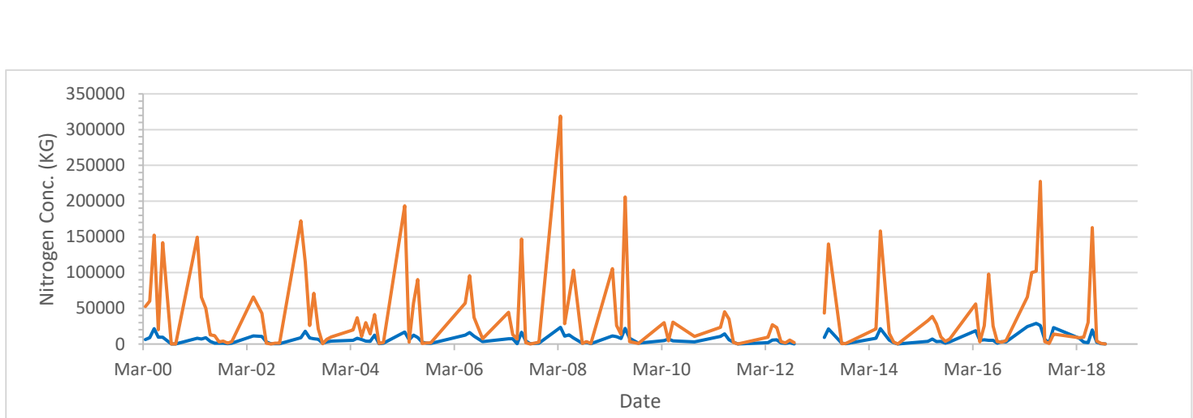

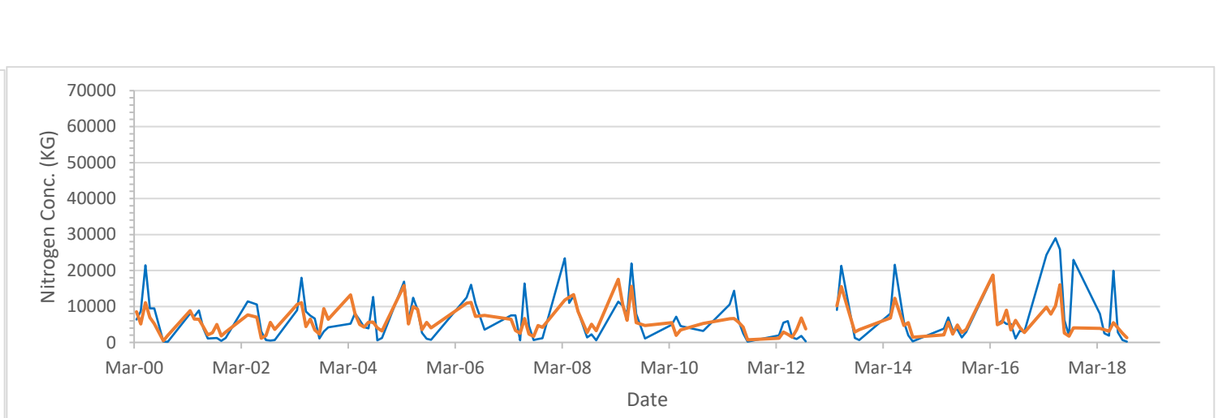

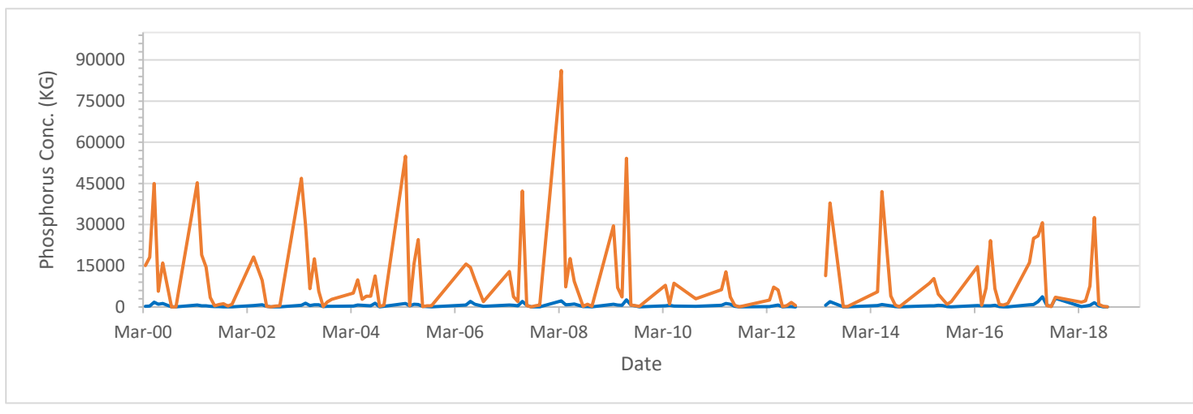

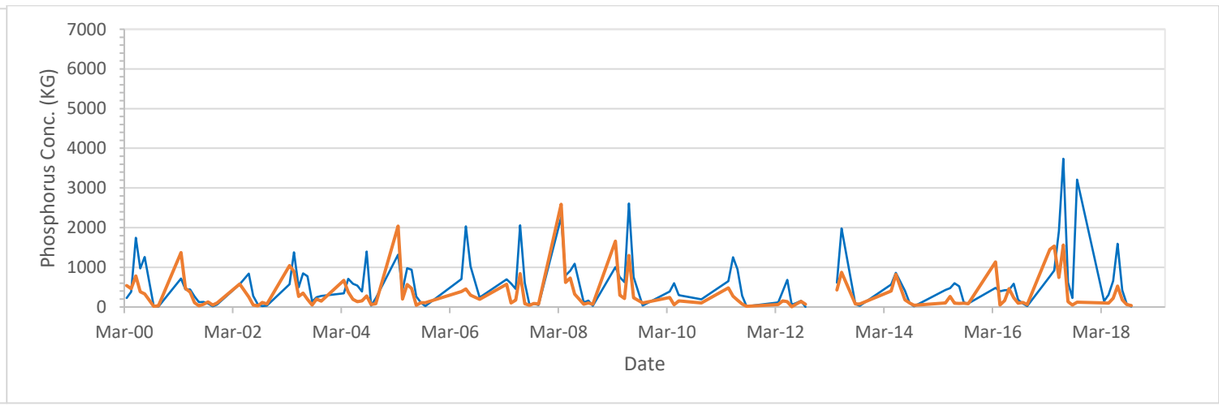

OUTLET 30

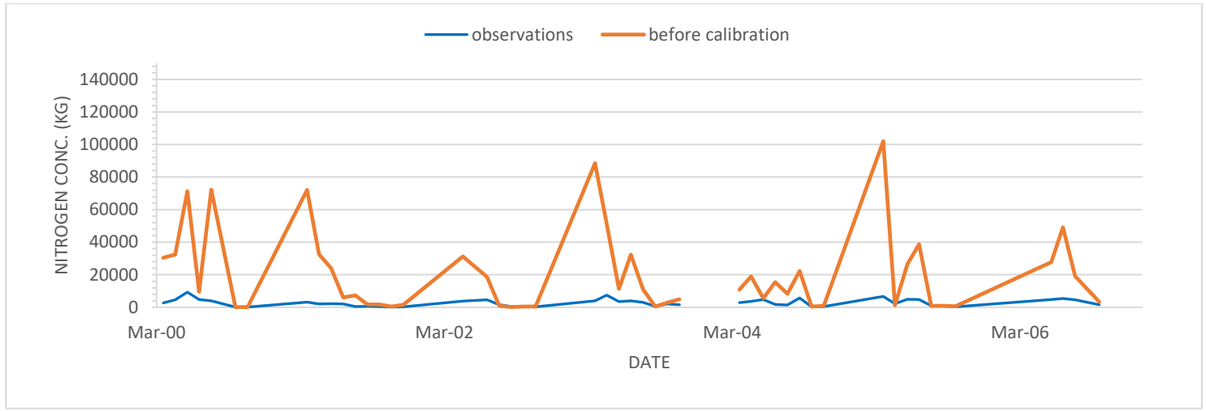
observations
before calibration
NITROGEN CONC. (KG)
140000
120000
100000
80000
60000
40000
20000
0
Mar-00
Mar-02
Mar-04
Mar-06
DATE

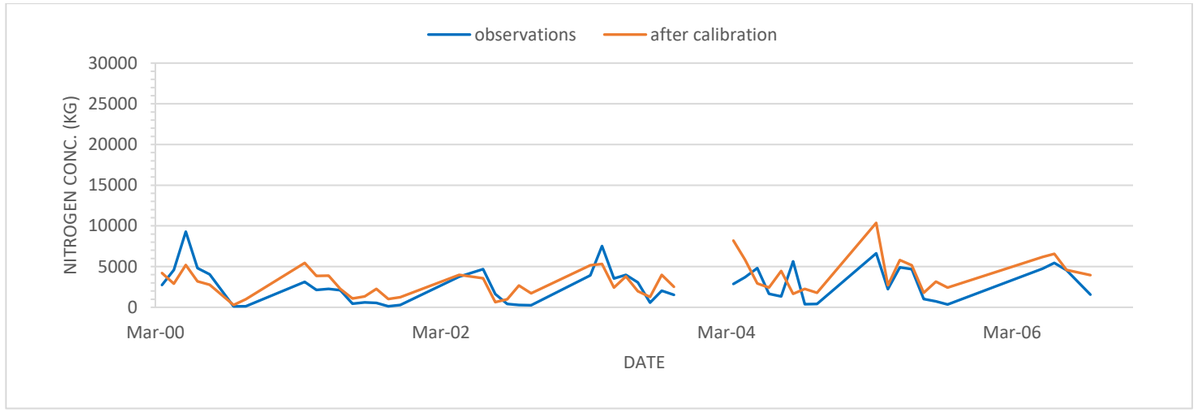
observations
after calibration
NITROGEN CONC. (KG)
30000
25000
20000
15000
10000
5000
0
Mar-00
Mar-02
Mar-04
Mar-06
DATE

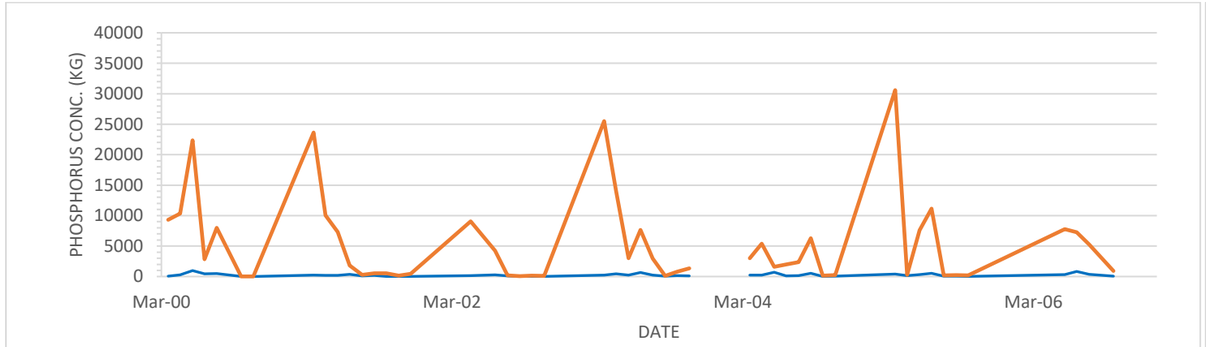
PHOSPHORUS CONC. (KG)
40000
35000
30000
25000
20000
15000
10000
5000
0
Mar-00
Mar-02
Mar-04
Mar-06
DATE

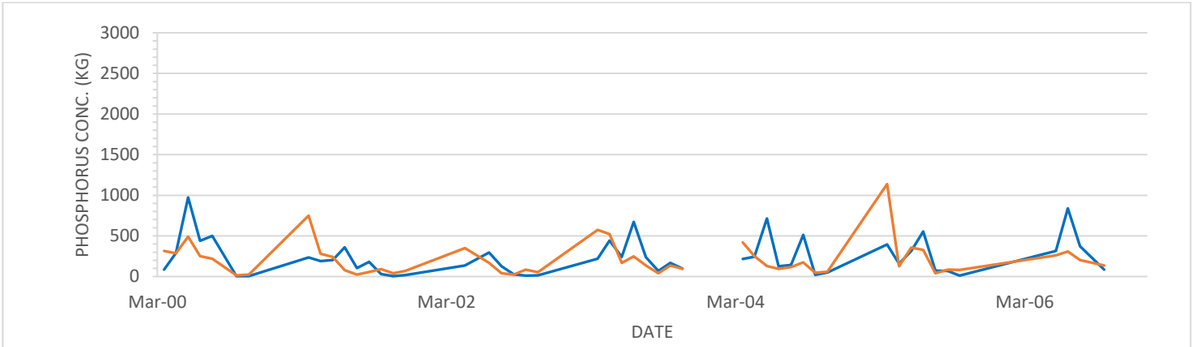
PHOSPHORUS CONC. (KG)
3000
2500
2000
1500
1000
500
0
Mar-00
Mar-02
Mar-04
Mar-06
DATE

B. Impact assessment outputs

B.1. Monthly averages of discharge, nitrogen and phosphorus at global scale

SCENARIO S0o

MONTH	Average of FLOW_OUT (cms)	Average of TOT N (kg)	Average of TOT P (kg)
Jan	0.93487818	12046.35	133.4605
Feb	0.51508558	16592.47	82.70004
Mar	2.2348448	33959.04	428.4668
Apr	9.107632	52782.4	1877.696
May	3.278172	24457.68	621.9592
Jun	4.74556	28398.8	1002.408
Jul	4.503672	404510	1344.336
Aug	3.935068	271843.6	653.6984
Sep	2.230392	13205.36	159.3204
Oct	1.6538692	5285.888	135.8694
Nov	1.177734	3661.909	97.01316
Dec	1.07885346	4386.774	86.75275
Annual=	35.3957612	871130.3	6623.681

SCENARIO S0m

MONTH	Average of FLOW_OUT (cms)	Average of TOT N (kg)	Average of TOT P (kg)
Jan	1.475019	19167.56	240.0431
Feb	2.383247	26782.84	376.2648
Mar	3.511442	34951.27	667.3573
Apr	6.804265	43319.64	1317.524
May	3.491836	25845.96	661.7348
Jun	4.323476	25932.83	889.9409
Jul	4.766913	427469.6	1373.22
Aug	3.514081	260381.2	556.8187
Sep	2.870277	16420.72	203.9892
Oct	1.789256	5942.496	142.7746
Nov	1.497233	4722.392	119.1135
Dec	1.342933	5062.115	104.3745
Annual=	37.76998	895998.6	6653.155

SCENARIO S1

MONTH	Average of FLOW_OUT (cms)	Average of TOT N (kg)	Average of TOT P (kg)
Jan	1.203896	13673.4	213.3092
Feb	0.567514	18405.9	112.4687
Mar	2.557393	35973.11	577.3222
Apr	8.918667	52745	2132.633
May	3.497593	25753.74	825.3
Jun	4.816296	29221.11	1215.926
Jul	4.981285	393768.5	1623.37
Aug	4.015541	256193	761.5296
Sep	2.278537	13405.63	292.7296
Oct	1.749078	6199.993	273.9889
Nov	1.36714	4642.53	203.3274
Dec	1.126369	4763.628	146.36
Annual=	37.07931	854745.5	8378.265

SCENARIO S0M45

MONTH	Average of FLOW_OUT (cms)	Average of TOT N (kg)	Average of TOT P (kg)
Jan	2.395513	26337.4	339.8484
Feb	2.071895	28800.45	293.4691
Mar	3.667786	41511.66	632.5928
Apr	6.970057	47250.46	1239.693
May	3.018315	22640.6	499.9603
Jun	5.009885	29053.77	956.5845
Jul	5.166613	649987.2	1583.111
Aug	4.299067	282259.2	613.9976
Sep	2.417526	11966.25	182.2714
Oct	1.708507	6016.48	134.6821
Nov	1.665043	7054.776	131.8515
Dec	1.453267	8510.152	116.18
Annual=	39.84347	1161388	6724.242

SCENARIO S0M85

MONTH	Average of FLOW_OUT (cms)	Average of TOT N (kg)	Average of TOT P (kg)
Jan	1.927303	24485.71	265.4365
Feb	2.398262	25609.97	335.7323
Mar	4.598779	44381.03	771.8266
Apr	4.942989	33596.11	836.7343
May	4.145189	25758.14	747.3392
Jun	4.994203	50311.22	983.0754
Jul	4.984125	504212.6	1282.203
Aug	4.204679	158827.8	468.5298
Sep	2.676321	12124.35	189.8869
Oct	2.019034	9821.907	161.8766
Nov	2.131662	12834.76	174.0925
Dec	1.588226	12244.22	137.8725
Annual=	40.61077	914207.9	6354.606

SCENARIO S1M45

MONTH	Average of FLOW_OUT (cms)	Average of TOT N (kg)	Average of TOT P (kg)
Jan	2.425428	26423.59	409.7372
Feb	2.086801	28485.34	344.9631
Mar	3.687668	41385.61	756.5902
Apr	6.966054	47851.49	1461.906
May	3.003159	23002.83	622.5995
Jun	5.014869	29750.72	1156.572
Jul	5.176826	615650.3	1717.433
Aug	4.358402	269084.5	726.7925
Sep	2.541833	12918.76	330.9117
Oct	1.814182	7224.901	268.6308
Nov	1.74688	7830.618	248.0482
Dec	1.498025	8944.961	193.3062
Annual=	40.32013	1118554	8237.49

SCENARIO S1M85

MONTH	Average of FLOW_OUT (cms)	Average of TOT N (kg)	Average of TOT P (kg)
Jan	1.972735	24457.58	338.7786
Feb	2.432332	25360.3	398.8707
Mar	4.637739	44086.36	916.5716
Apr	4.960159	33940.16	1009.76
May	4.158867	26270.02	904.6017
Jun	5.014506	49846.86	1175.118
Jul	5.018824	479391.8	1430.169
Aug	4.287177	151896.4	601.4129
Sep	2.810949	13315.68	338.9609
Oct	2.140251	10719.87	302.7354
Nov	2.226895	13373.22	292.5062
Dec	1.638816	12577.17	217.6373
Annual=	41.29925	885235.4	7927.122

B.2. Monthly averages of discharge, nitrogen and phosphorus at local scale

SCENARIO S0

MONTH	Average of FLOW_OUT (cms)	Average of TOT N (kg)	Average of TOT P (kg)
Jan	0.05053287	369.528	11.22544
Feb	0.02916616	469.6052	7.403424
Mar	0.12623104	888.832	40.6286
Apr	0.4837852	963.524	180.0528
May	0.167316	483.624	62.42596
Jun	0.2504552	473.504	100.1804
Jul	0.235608	9476.652	109.5028
Aug	0.2215864	5896.828	54.1296
Sep	0.153386	163.2088	20.46012
Oct	0.11588776	67.838	17.41148
Nov	0.07619032	51.0284	11.22824

Dec	0.06235929	91.65341	8.714867
Annual=	1.97250424	19395.83	623.3637

SCENARIO S0m

MONTH	Average of FLOW_OUT (cms)	Average of TOT N (kg)	Average of TOT P (kg)
Jan	0.080268	581.4682	20.54643
Feb	0.125729	645.358	31.53982
Mar	0.187754	813.6282	61.50523
Apr	0.356695	802.956	127.6281
May	0.179875	480.728	66.032
Jun	0.226762	422.396	89.57827
Jul	0.249757	9417.999	109.6037
Aug	0.204347	5259.199	44.56871
Sep	0.19799	199.1279	26.67889
Oct	0.124785	73.24653	19.1244
Nov	0.093142	60.07325	13.50159
Dec	0.076261	105.8903	10.35249
Annual=	2.103365	18862.07	620.6596

SCENARIO S1

MONTH	Average of FLOW_OUT (cms)	Average of TOT N (kg)	Average of TOT P (kg)
Jan	0.071109	466.2907	24.27002
Feb	0.036937	459.0399	14.21921
Mar	0.155328	972.9	70.92544
Apr	0.492416	1359.315	256.4785
May	0.18087	707.6259	111.3448
Jun	0.260311	763.2815	161.2341
Jul	0.266307	4832.811	173.6533
Aug	0.237374	2797.804	88.68407
Sep	0.182791	451.5519	59.23815
Oct	0.151774	421.8704	57.11222
Nov	0.107636	301.5778	40.07222

Dec	0.07392	236.3846	24.66328
Annual=	2.216774	13770.45	1081.895

SCENARIO S0M45

MONTH	Average of FLOW_OUT (cms)	Average of TOT N (kg)	Average of TOT P (kg)
Jan	0.123906	565.1336	30.17356
Feb	0.105214	605.6329	26.56148
Mar	0.19126	814.6391	61.85179
Apr	0.353072	762.5276	122.2472
May	0.151552	374.7447	49.35483
Jun	0.257991	417.0437	90.1819
Jul	0.268275	14298.14	105.8964
Aug	0.250731	5826.377	52.92374
Sep	0.166688	163.2434	28.84275
Oct	0.113539	80.64264	20.3071
Nov	0.098358	118.1002	16.54127
Dec	0.077703	162.7483	12.36822
Annual=	2.15829	24188.97	617.2502

SCENARIO S0M85

MONTH	Average of FLOW_OUT (cms)	Average of TOT N (kg)	Average of TOT P (kg)
Jan	0.095148	566.782	22.48363
Feb	0.117055	530.8893	26.84079
Mar	0.227526	849.4893	67.68821
Apr	0.243709	555.0241	77.86407
May	0.204752	395.9859	63.62784
Jun	0.250834	982.1892	84.19497
Jul	0.257855	10979.66	86.94311
Aug	0.242804	3091.689	44.53659
Sep	0.172424	142.0194	27.98183
Oct	0.123663	157.6233	21.02946

Nov	0.111134	205.6722	15.77434
Dec	0.080236	224.889	12.23263
Annual=	2.127141	18681.91	551.1975

SCENARIO S1M45

MONTH	Average of FLOW_OUT (cms)	Average of TOT N (kg)	Average of TOT P (kg)
Jan	0.136162	688.4288	46.49111
Feb	0.112246	608.3962	38.51413
Mar	0.200766	911.5368	92.24626
Apr	0.357467	1063.444	178.4614
May	0.149623	555.2791	83.67294
Jun	0.262472	708.3218	147.1774
Jul	0.273902	7184.46	151.1357
Aug	0.268719	3014.397	84.8469
Sep	0.204937	508.4379	69.38575
Oct	0.148313	441.3437	57.47733
Nov	0.12729	399.7609	48.52709
Dec	0.094993	341.1592	33.2714
Annual=	2.33689	16424.97	1031.207

SCENARIO S1M85

MONTH	Average of FLOW_OUT (cms)	Average of TOT N (kg)	Average of TOT P (kg)
Jan	0.112648	683.3693	40.69011
Feb	0.130405	571.9817	41.891
Mar	0.244306	996.1144	102.8543
Apr	0.253802	809.3149	122.831
May	0.212418	652.7485	106.3856
Jun	0.260354	932.7713	138.2954
Jul	0.270928	5800.808	134.9438
Aug	0.268538	1904.453	81.64961
Sep	0.215031	509.5489	68.73239
Oct	0.164441	495.3705	59.8158

Nov	0.145519	446.1155	48.4977
Dec	0.099869	381.283	33.84445
Annual=	2.378259	14183.88	980.4312

B.3. Annual maximum discharge at global scale

Year	S0	S0m	S1	S0M45	S0M85	S1M45	S1M85
3	13.53	11.74	13.74	24.34	9.832	24.42	9.895
4	18.74	9.088	18.96	15.03	13.47	15.09	13.45
5	10.89	11.21	10.98	12.13	15.04	12.19	15.09
6	8.021	10.09	8.241	18.41	8.808	18.33	8.883
7	13.6	12.72	13.69	10.91	14.7	10.97	14.75
8	13.63	9.366	13.73	18.57	15.17	18.57	15.16
9	8.01	13.03	8.018	9.081	14.69	9.09	14.65
10	9.011	10.13	9.144	10.8	13.66	10.85	13.71
11	8.237	8.59	8.295	10.78	8.792	10.85	8.835
12	7.423	14.88	7.621	13.03	13.86	13.09	14.16
13	12.41	12.81	12.42	14.8	11.37	14.83	11.56
14	7.803	14.02	7.878	10.31	14.28	10.38	14.35
15	10.08	15.96	10.18	9.296	9.562	9.298	9.515
16	13.77	16.29	13.85	9.822	9.731	9.891	9.805
17	10.83	15.18	10.78	10.47	12.98	10.51	12.98
18	9.489	7.386	9.496	17.95	13.12	18.02	13.35
19	17.64	11.81	17.7	11.97	8.829	11.97	8.903
20	11.41	12.59	11.47	23.08	15.69	23.13	15.77
21	8.51	7.203	8.718	11.13	11.07	11.15	11.23
22	13.95	16.38	13.98	15.22	14.73	15.28	14.74
23	4.958	14.9	5.017	6.104	18.42	6.173	18.44
24	12.89	13.63	13.03	7.26	10.95	7.286	10.94
25	8.685	18.05	8.724	15.67	11.56	15.53	11.66
26	5.455	16.85	5.529	9.664	11.76	9.722	11.83
27	8.909	11.88	8.775	18.15	15.61	18.12	15.47
28	13.48	12.08	13.47	11.83	10.41	11.74	10.48

29	8.936	13.18	8.973	14.63	11.27	14.62	11.22
AVERAGE	10.75	12.63	10.83	13.11	12.75	13.13	12.79

**The first 2 years of warmup period are not included

B.4. Annual maximum discharge at local scale

Year	S0	S0m	S1	S0M45	S0M85	S1M45	S1M85
3	0.67	0.66	0.74	1.22	0.55	1.26	0.57
4	1.06	0.50	1.11	0.78	0.71	0.80	0.70
5	0.62	0.59	0.65	0.62	0.76	0.65	0.79
6	0.49	0.54	0.55	0.95	0.46	0.93	0.50
7	0.71	0.66	0.74	0.60	0.76	0.62	0.78
8	0.75	0.51	0.78	0.96	0.75	0.96	0.76
9	0.45	0.70	0.46	0.46	0.76	0.47	0.75
10	0.45	0.52	0.50	0.53	0.70	0.55	0.72
11	0.41	0.47	0.44	0.53	0.43	0.56	0.45
12	0.44	0.77	0.50	0.63	0.84	0.66	0.93
13	0.63	0.69	0.64	0.72	0.54	0.73	0.61
14	0.41	0.73	0.44	0.58	0.73	0.60	0.76
15	0.57	0.87	0.59	0.54	0.47	0.59	0.48
16	0.75	0.89	0.79	0.50	0.47	0.54	0.50
17	0.55	0.80	0.54	0.53	0.68	0.56	0.68
18	0.50	0.41	0.50	0.89	0.79	0.92	0.85
19	0.92	0.61	0.94	0.62	0.49	0.62	0.52
20	0.61	0.61	0.63	1.17	0.77	1.20	0.80
21	0.53	0.39	0.59	0.58	0.63	0.59	0.68
22	0.70	0.86	0.72	0.75	0.76	0.79	0.77
23	0.27	0.77	0.29	0.34	0.94	0.39	0.96
24	0.64	0.72	0.69	0.41	0.55	0.44	0.55
25	0.46	0.96	0.48	0.79	0.55	0.76	0.59
26	0.31	0.96	0.33	0.53	0.59	0.55	0.62
27	0.46	0.62	0.42	0.91	0.78	0.91	0.74

28	0.69	0.85	0.69	0.60	0.51	0.58	0.53
29	0.46	0.75	0.48	0.74	0.58	0.74	0.58
AVERAGE	0.57	0.68	0.60	0.67	0.66	0.69	0.68

B.5. Annual maximum flow for all the sub-watersheds (m^3/s)

Sub #	S0	S0m	S1	S0M45	S0M85	S1M45	S1M85
1	10.75	12.63	10.83	13.11	12.75	13.13	12.79
2	0.42	0.49	0.42	0.51	0.50	0.51	0.50
3	9.71	11.41	9.80	11.83	11.51	11.86	11.56
4	0.78	0.92	0.78	0.95	0.92	0.95	0.92
5	0.29	0.34	0.29	0.35	0.34	0.35	0.34
6	9.51	11.17	9.59	11.59	11.28	11.61	11.33
7	0.12	0.14	0.12	0.15	0.14	0.14	0.14
8	9.29	10.90	9.37	11.30	11.00	11.32	11.05
9	0.07	0.09	0.07	0.11	0.10	0.11	0.10
10	0.15	0.18	0.15	0.19	0.18	0.19	0.18
11	8.97	10.51	9.05	10.88	10.60	10.91	10.65
12	8.75	10.25	8.83	10.59	10.33	10.62	10.38
13	0.20	0.23	0.20	0.24	0.24	0.24	0.24
14	0.21	0.26	0.21	0.29	0.27	0.29	0.27
15	8.47	9.92	8.55	10.25	10.00	10.28	10.05
16	8.31	9.73	8.39	10.04	9.80	10.07	9.85
17	7.91	9.27	7.99	9.55	9.32	9.58	9.37
18	0.08	0.09	0.08	0.10	0.09	0.10	0.09
19	0.14	0.16	0.14	0.17	0.17	0.17	0.17
20	7.73	9.06	7.81	9.33	9.11	9.36	9.16
21	0.34	0.40	0.34	0.43	0.42	0.43	0.42
22	0.07	0.08	0.07	0.08	0.08	0.08	0.08
23	7.00	8.20	7.08	8.42	8.22	8.45	8.27
24	1.37	1.61	1.37	1.63	1.61	1.63	1.61
25	5.43	6.36	5.51	6.53	6.37	6.56	6.42
26	1.22	1.44	1.22	1.45	1.43	1.45	1.43
27	0.21	0.25	0.21	0.27	0.26	0.27	0.26
28	0.15	0.17	0.15	0.18	0.17	0.18	0.17
29	0.55	0.64	0.55	0.66	0.65	0.66	0.65
30	4.75	5.56	4.83	5.71	5.57	5.74	5.62
31	4.36	5.11	4.44	5.24	5.12	5.27	5.17
32	0.13	0.15	0.13	0.16	0.15	0.16	0.15
33	1.02	1.21	1.03	1.21	1.20	1.21	1.20
34	0.08	0.09	0.08	0.10	0.10	0.10	0.10
35	0.18	0.21	0.18	0.22	0.21	0.22	0.21

36	0.17	0.20	0.17	0.20	0.20	0.20	0.20
37	0.75	0.89	0.75	0.89	0.88	0.89	0.88
38	1.98	2.35	1.98	2.40	2.36	2.40	2.36
39	1.51	1.75	1.58	1.78	1.73	1.82	1.78
40	1.27	1.48	1.34	1.50	1.45	1.53	1.50
41	0.07	0.08	0.07	0.08	0.08	0.09	0.08
42	0.84	0.98	0.89	0.99	0.96	1.02	1.00
43	0.68	0.80	0.72	0.80	0.78	0.83	0.81
44	1.69	2.01	1.69	2.05	2.02	2.05	2.02
45	0.35	0.40	0.36	0.41	0.40	0.41	0.40
46	0.57	0.67	0.60	0.67	0.66	0.69	0.68
47	0.10	0.12	0.11	0.12	0.12	0.12	0.12
48	0.58	0.69	0.58	0.70	0.69	0.69	0.69
49	0.11	0.13	0.11	0.13	0.13	0.13	0.13
50	0.11	0.13	0.12	0.13	0.12	0.13	0.13
51	0.23	0.27	0.23	0.27	0.27	0.27	0.27
52	0.69	0.83	0.69	0.86	0.85	0.86	0.85
53	0.15	0.18	0.15	0.17	0.17	0.17	0.17
54	0.04	0.05	0.04	0.05	0.05	0.05	0.05
55	0.02	0.03	0.02	0.03	0.03	0.03	0.03

B.6. Annual mean discharge for all the 55 sub-watersheds (m^3/s)

Sub #	S0	S0m	S1	S0M45	S0M85	S1M45	S1M85
1	3.04	3.15	3.09	3.32	3.38	3.36	3.44
2	0.12	0.12	0.12	0.13	0.13	0.13	0.13
3	2.76	2.86	2.81	3.01	3.07	3.05	3.13
4	0.22	0.23	0.22	0.24	0.24	0.24	0.24
5	0.08	0.08	0.08	0.09	0.09	0.09	0.09
6	2.71	2.80	2.76	2.95	3.01	2.99	3.07
7	0.03	0.03	0.03	0.04	0.04	0.04	0.04
8	2.65	2.74	2.70	2.89	2.94	2.93	3.00
9	0.02	0.02	0.02	0.02	0.02	0.02	0.02
10	0.04	0.04	0.04	0.05	0.05	0.05	0.05
11	2.56	2.65	2.61	2.79	2.84	2.83	2.90
12	2.50	2.59	2.55	2.72	2.77	2.76	2.83
13	0.06	0.06	0.06	0.06	0.06	0.06	0.06
14	0.06	0.06	0.06	0.07	0.07	0.07	0.07
15	2.42	2.50	2.47	2.63	2.68	2.67	2.74
16	2.38	2.46	2.42	2.58	2.63	2.62	2.68
17	2.26	2.34	2.31	2.45	2.49	2.49	2.55
18	0.02	0.02	0.02	0.02	0.03	0.02	0.03
19	0.04	0.04	0.04	0.04	0.04	0.04	0.04
20	2.21	2.29	2.26	2.40	2.44	2.44	2.49
21	0.10	0.10	0.10	0.11	0.11	0.11	0.11
22	0.02	0.02	0.02	0.02	0.02	0.02	0.02
23	2.00	2.07	2.05	2.17	2.20	2.21	2.26
24	0.38	0.40	0.38	0.41	0.42	0.41	0.42
25	1.56	1.62	1.61	1.70	1.72	1.74	1.77
26	0.34	0.35	0.34	0.36	0.37	0.36	0.37
27	0.06	0.06	0.06	0.07	0.07	0.07	0.07
28	0.04	0.04	0.04	0.05	0.05	0.05	0.05
29	0.16	0.16	0.16	0.17	0.17	0.17	0.17
30	1.37	1.41	1.42	1.49	1.50	1.53	1.56
31	1.25	1.30	1.30	1.36	1.37	1.40	1.43
32	0.04	0.04	0.04	0.04	0.04	0.04	0.04
33	0.29	0.30	0.29	0.30	0.31	0.30	0.31
34	0.02	0.02	0.02	0.02	0.02	0.02	0.02
35	0.05	0.05	0.05	0.06	0.06	0.06	0.06
36	0.05	0.05	0.05	0.05	0.05	0.05	0.05
37	0.21	0.22	0.21	0.22	0.22	0.22	0.22
38	0.55	0.57	0.55	0.60	0.61	0.59	0.61
39	0.45	0.46	0.49	0.48	0.48	0.52	0.53
40	0.38	0.39	0.42	0.41	0.40	0.44	0.45
41	0.02	0.02	0.02	0.02	0.02	0.02	0.02

42	0.25	0.26	0.28	0.27	0.26	0.29	0.30
43	0.20	0.21	0.22	0.22	0.21	0.24	0.24
44	0.47	0.49	0.47	0.50	0.51	0.50	0.51
45	0.10	0.11	0.11	0.11	0.11	0.12	0.12
46	0.17	0.18	0.18	0.18	0.18	0.19	0.20
47	0.03	0.03	0.04	0.03	0.03	0.04	0.04
48	0.16	0.17	0.16	0.17	0.17	0.17	0.17
49	0.03	0.03	0.03	0.04	0.03	0.04	0.03
50	0.03	0.03	0.04	0.04	0.04	0.04	0.04
51	0.07	0.07	0.07	0.07	0.07	0.07	0.07
52	0.19	0.19	0.19	0.20	0.21	0.20	0.21
53	0.04	0.04	0.04	0.04	0.04	0.04	0.04
54	0.01	0.01	0.01	0.01	0.01	0.01	0.01
55	0.01	0.01	0.01	0.01	0.01	0.01	0.01

B.7. Annual mean N load for all the sub-watersheds (tons)

Sub #	S0	S0m	S1	S0M45	S0M85	S1M45	S1M85
1	894.04	896.00	854.75	1161.39	914.21	1118.55	885.24
2	40.53	39.83	38.08	53.38	42.82	53.42	42.91
3	805.55	807.09	768.90	1043.23	822.89	1000.26	792.33
4	69.33	69.36	67.27	91.98	72.39	91.90	73.10
5	24.49	25.18	24.87	32.89	25.32	32.80	25.91
6	787.19	789.74	750.78	1018.71	805.19	975.66	773.98
7	9.98	9.67	10.04	13.17	9.85	12.94	9.99
8	770.30	773.07	733.99	998.24	789.32	955.03	758.06
9	6.31	6.40	6.31	7.27	5.97	7.28	5.98
10	14.97	15.85	15.68	20.93	15.93	20.72	15.47
11	741.81	743.97	705.34	960.42	760.64	917.08	729.85
12	719.63	720.83	682.82	932.55	738.75	889.27	708.00
13	20.35	20.19	20.63	27.22	20.97	27.60	20.97
14	20.92	21.88	21.25	26.15	20.60	26.13	20.51
15	690.07	690.95	652.87	892.77	707.96	849.00	677.53
16	672.88	673.70	635.61	868.69	690.76	824.49	659.54
17	626.24	628.23	588.96	805.88	642.92	762.51	611.05
18	8.05	7.96	7.72	10.62	8.21	10.59	8.09
19	12.32	12.25	12.24	17.12	12.86	16.66	12.75
20	609.93	611.74	572.31	782.76	625.77	739.88	593.73
21	32.32	32.53	31.37	43.49	33.87	44.22	33.21
22	6.19	6.32	6.10	8.63	6.36	8.47	6.63
23	540.26	542.37	504.75	690.10	554.57	646.45	522.28
24	90.49	92.61	91.39	118.05	95.08	117.47	95.16
25	427.20	426.05	390.59	539.84	436.64	496.55	403.17
26	75.94	77.17	75.75	97.12	79.52	96.46	78.93
27	16.44	16.57	16.33	22.69	17.58	22.70	17.15
28	14.57	15.47	15.66	20.96	15.59	21.04	16.26
29	44.80	45.88	45.54	62.24	47.62	61.54	46.11
30	367.29	364.22	329.52	456.80	373.27	414.09	341.70
31	338.23	336.26	301.02	419.12	344.68	377.12	313.44
32	15.79	15.87	14.95	20.67	16.19	21.40	15.97
33	56.70	57.63	56.18	70.51	59.75	70.24	58.78
34	5.65	5.76	5.85	7.80	5.87	7.78	6.05
35	17.54	17.48	17.34	23.85	18.09	23.03	17.68
36	4.86	4.73	4.85	6.39	5.03	6.29	4.85
37	42.07	43.69	41.80	51.23	44.78	50.76	43.86
38	171.18	172.06	170.62	203.13	180.17	203.50	178.81
39	82.10	80.67	50.36	105.06	79.97	62.49	50.87
40	57.63	57.01	33.23	72.09	55.25	39.70	33.48
41	7.98	7.97	4.97	11.21	8.23	6.66	5.08

42	35.89	34.62	18.17	44.83	34.37	20.59	18.42
43	26.83	25.79	15.67	33.30	25.60	18.22	16.00
44	149.30	150.78	148.66	174.27	158.24	173.99	157.08
45	18.63	19.41	13.71	23.81	18.14	17.84	13.77
46	19.72	18.86	13.77	24.19	18.68	16.42	14.18
47	5.25	4.95	1.70	6.32	4.80	1.61	1.64
48	20.16	19.34	19.46	25.77	20.01	26.21	19.17
49	4.72	4.62	4.62	5.92	4.58	5.82	4.57
50	7.02	6.84	1.86	9.01	6.83	1.77	1.79
51	14.79	14.47	15.01	19.52	15.02	19.61	14.70
52	101.65	105.51	101.72	112.75	111.99	112.88	111.58
53	23.99	24.97	24.04	26.02	25.55	26.07	25.50
54	6.70	6.97	6.71	7.34	7.26	7.35	7.26
55	2.85	2.95	2.85	3.01	3.11	3.02	3.11

B.8. Annual mean P load for all the sub-watersheds (tons)

Sub #	S0	S0m	S1	S0M45	S0M85	S1M45	S1M85
1	6.81	6.65	8.38	6.72	6.35	8.24	7.93
2	0.21	0.20	0.21	0.19	0.19	0.19	0.19
3	6.22	6.08	7.80	6.15	5.80	7.67	7.39
4	0.43	0.41	0.43	0.39	0.39	0.39	0.39
5	0.15	0.14	0.15	0.13	0.13	0.13	0.13
6	6.14	6.00	7.73	6.06	5.73	7.60	7.32
7	0.05	0.05	0.05	0.04	0.04	0.04	0.04
8	6.05	5.90	7.64	5.96	5.64	7.50	7.23
9	0.02	0.02	0.02	0.02	0.02	0.02	0.02
10	0.04	0.04	0.04	0.04	0.04	0.04	0.04
11	5.83	5.70	7.44	5.69	5.42	7.25	7.04
12	5.77	5.63	7.38	5.64	5.37	7.20	6.98
13	0.06	0.06	0.06	0.05	0.05	0.05	0.05
14	0.05	0.06	0.05	0.05	0.05	0.05	0.05
15	5.69	5.56	7.31	5.57	5.29	7.12	6.91
16	5.63	5.50	7.25	5.49	5.23	7.06	6.85
17	5.50	5.36	7.13	5.35	5.11	6.93	6.73
18	0.02	0.02	0.02	0.02	0.02	0.02	0.02
19	0.05	0.04	0.05	0.04	0.04	0.04	0.04
20	5.44	5.31	7.08	5.30	5.05	6.88	6.68
21	0.11	0.11	0.11	0.11	0.11	0.11	0.11
22	0.01	0.01	0.01	0.01	0.02	0.01	0.02
23	5.23	5.10	6.87	5.09	4.83	6.67	6.46
24	1.09	1.05	1.09	1.00	0.99	1.00	0.99
25	4.06	3.97	5.71	3.99	3.76	5.58	5.41
26	1.03	1.00	1.03	0.95	0.94	0.95	0.94
27	0.08	0.08	0.08	0.08	0.08	0.08	0.08
28	0.05	0.05	0.05	0.05	0.05	0.05	0.05
29	0.34	0.33	0.34	0.30	0.30	0.30	0.30
30	3.67	3.59	5.33	3.63	3.42	5.23	5.07
31	3.33	3.25	5.00	3.28	3.11	4.89	4.78
32	0.03	0.03	0.03	0.03	0.03	0.03	0.03
33	0.97	0.93	0.97	0.89	0.87	0.89	0.87
34	0.03	0.03	0.03	0.03	0.03	0.03	0.03
35	0.07	0.07	0.07	0.07	0.07	0.07	0.07
36	0.15	0.14	0.15	0.13	0.13	0.13	0.13
37	0.76	0.73	0.76	0.70	0.69	0.70	0.69
38	1.45	1.40	1.45	1.40	1.39	1.40	1.39
39	1.43	1.40	2.89	1.41	1.27	2.81	2.70

40	1.31	1.28	2.54	1.29	1.16	2.46	2.37
41	0.02	0.02	0.09	0.01	0.02	0.09	0.09
42	0.92	0.90	1.85	0.91	0.81	1.79	1.71
43	0.77	0.75	1.44	0.75	0.67	1.37	1.31
44	1.26	1.21	1.26	1.22	1.22	1.22	1.21
45	0.23	0.23	0.41	0.23	0.22	0.41	0.40
46	0.64	0.62	1.08	0.62	0.55	1.03	0.98
47	0.12	0.12	0.28	0.12	0.11	0.28	0.27
48	0.47	0.44	0.47	0.44	0.44	0.44	0.44
49	0.11	0.11	0.11	0.10	0.10	0.10	0.10
50	0.13	0.13	0.35	0.13	0.11	0.33	0.32
51	0.17	0.17	0.17	0.17	0.16	0.16	0.16
52	0.43	0.41	0.43	0.42	0.44	0.42	0.44
53	0.13	0.13	0.13	0.12	0.12	0.12	0.12
54	0.02	0.02	0.02	0.02	0.02	0.02	0.02
55	0.01	0.01	0.01	0.01	0.01	0.01	0.01

B.9. Monthly total precipitations and ET in scenarios S0M45/85

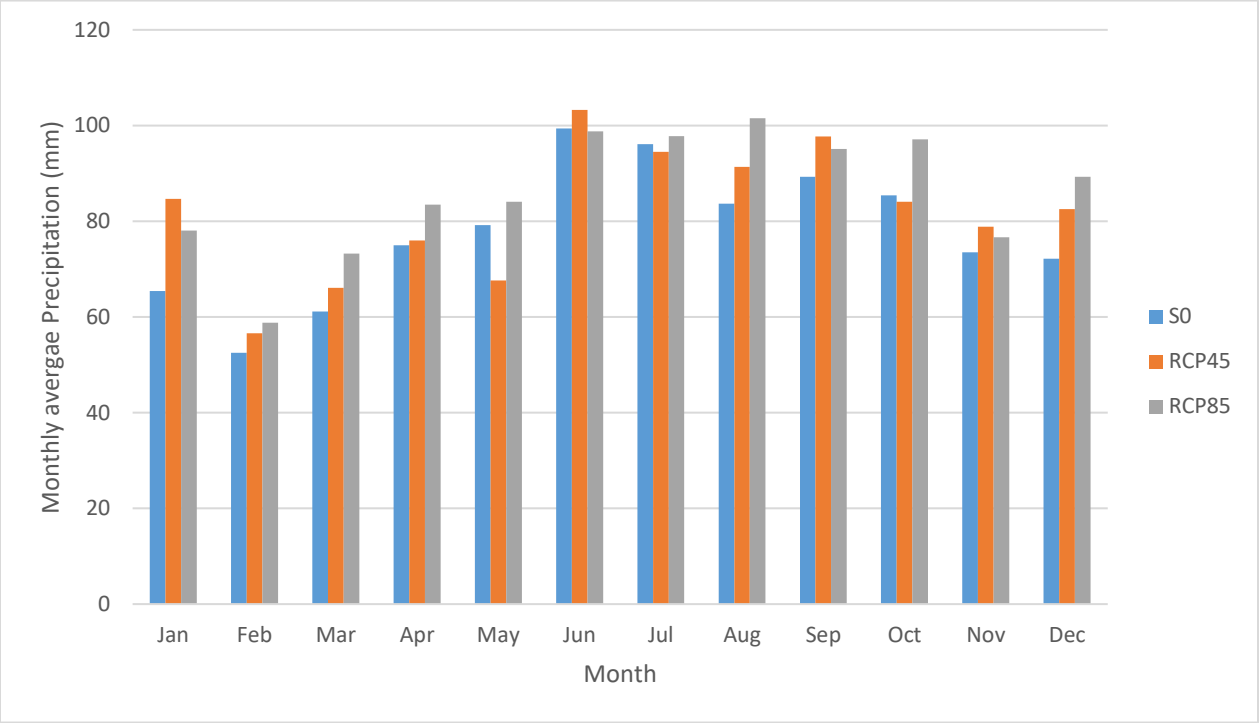

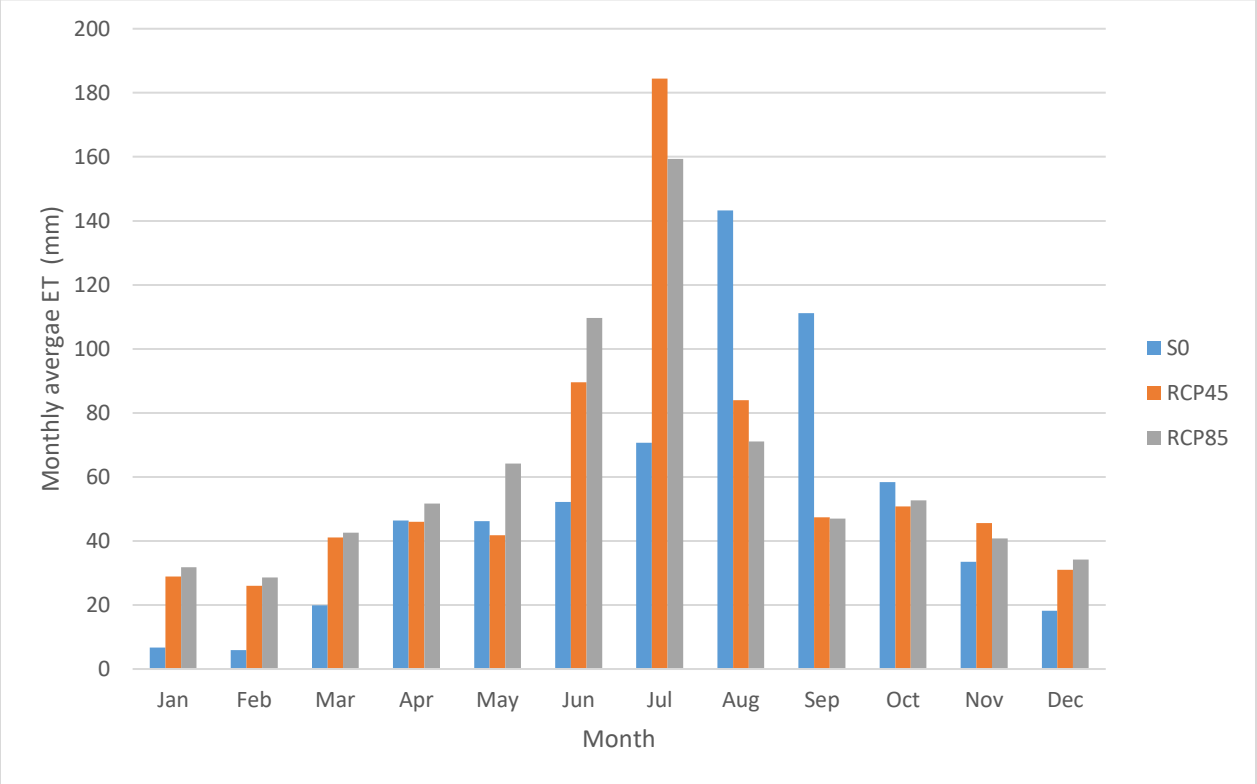

B.10. Monthly Total precipitations and ET in scenarios S1M45/85

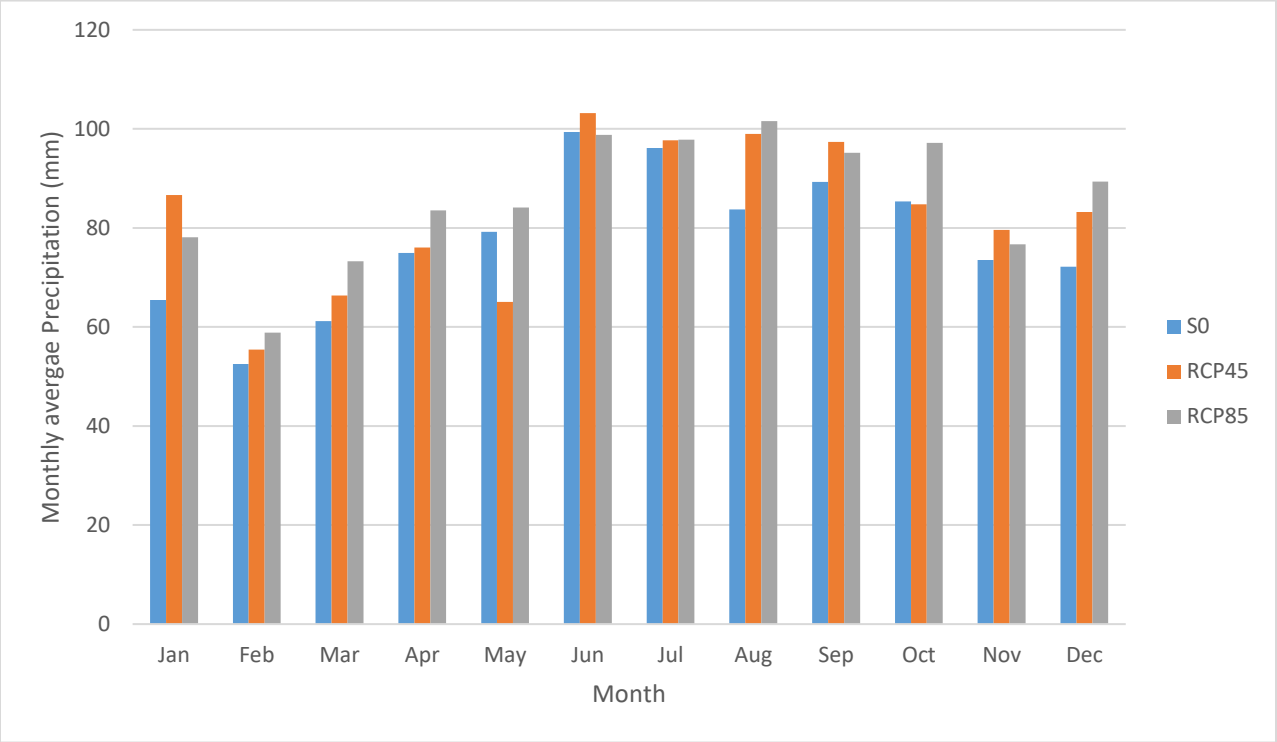

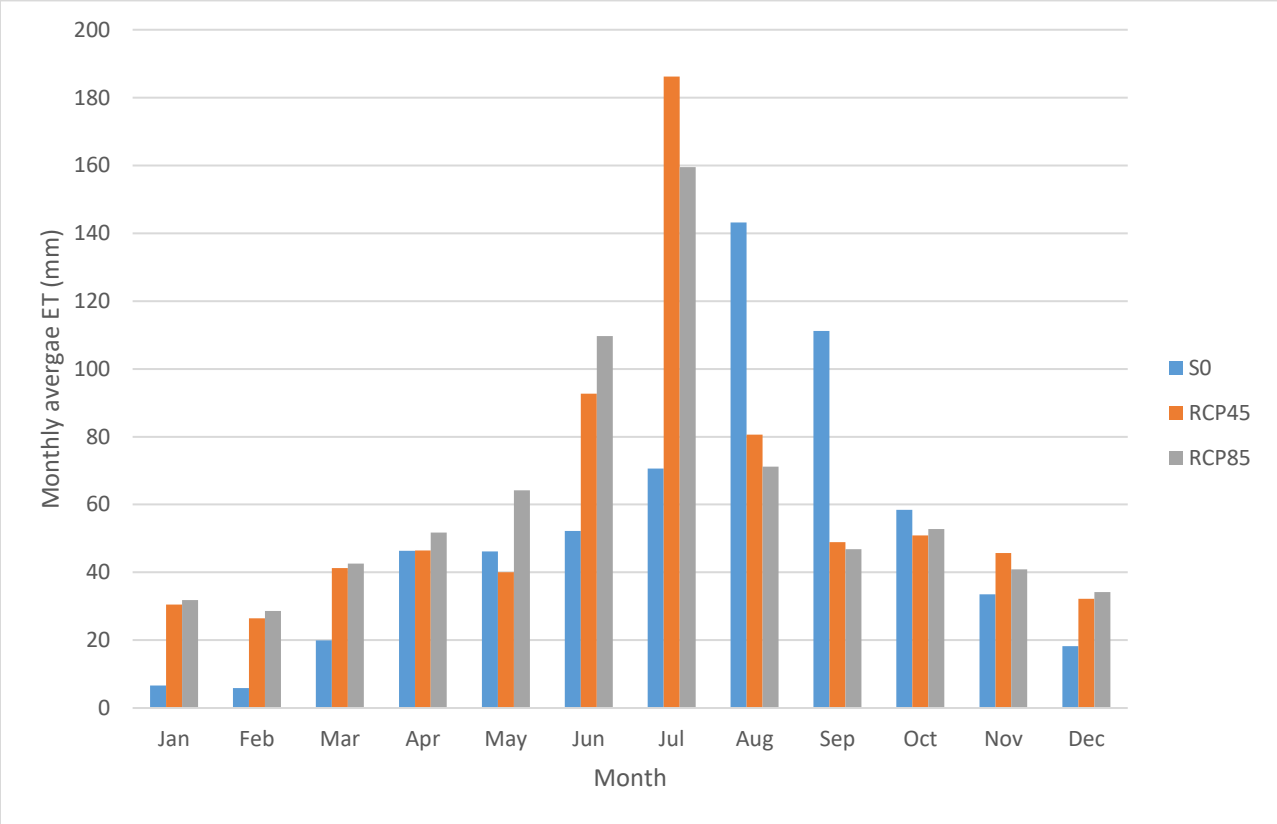

C. Future climate conditions

This sections presents the projections of future climate conditions (pcp) for the next 30 years of simulation. The values represent the average outputs from all the RCMs in terms of annual and monthly time scale.

C.1. Projection of monthly average precipitations (mm) from the RCMs

MONTH	RCP 4.5	RCP 8.5
Jan	84.69	78.07
Feb	56.57	58.81
Mar	66.06	73.23
Apr	75.98	83.48
May	67.62	84.07
Jun	103.29	98.76
Jul	94.52	97.76
Aug	91.39	101.51
Sep	97.74	95.13
Oct	84.09	97.10
Nov	78.85	76.64
Dec	82.56	89.31
Annual=	983.37	1033.86

C.2. Projection of annual average precipitations (mm) from the RCMs

Year	RCP 4.5	RCP 8.5
2023	997.97	905.60
2024	879.98	1053.94
2025	1026.54	1006.18
2026	1015.60	1109.85
2027	899.62	969.52
2028	1004.90	1013.60
2029	1022.27	953.89
2030	1056.03	943.23
2031	912.88	1042.76
2032	1062.93	1002.58
2033	896.32	1071.52
2034	934.45	1080.33
2035	961.51	1064.74
2036	1141.46	1035.48
2037	1048.93	1070.99
2038	988.47	1110.57
2039	1009.84	1091.67
2040	859.49	1067.67
2041	856.02	1066.10
2042	970.88	1021.80
2043	995.04	1040.69
2044	988.21	1020.35
2045	976.21	1002.95
2046	1156.22	1067.72
2047	906.01	1080.81
2048	1023.04	993.91
2049	960.11	1025.76

Note: The first 2 years of warmup period are not included

C.3. Projection of monthly average evapo-transpiration (mm) from the RCMs

MONTH	RCP 4.5	RCP 8.5
Jan	28.89	31.76
Feb	26.02	28.65
Mar	41.09	42.62
Apr	46.02	51.67
May	41.81	64.14
Jun	89.57	109.70
Jul	184.47	159.36
Aug	83.98	71.07
Sep	47.37	46.95
Oct	50.78	52.70
Nov	45.56	40.82
Dec	31.01	34.17
Annual=	716.57	733.62

C.4. Projection of annual average evapo-transpiration (mm) from the RCMs

Year	RCP 4.5	RCP 8.5
2023	714.25	668.68
2024	690.69	737.41
2025	701.48	716.67
2026	737.42	740.83
2027	689.74	709.32
2028	730.65	725.76
2029	713.57	713.18
2030	739.59	696.43
2031	692.31	721.94
2032	714.56	724.97
2033	699.28	740.32
2034	681.96	743.09
2035	690.60	753.40
2036	748.41	746.35
2037	747.76	738.87
2038	733.96	753.27
2039	764.01	737.09
2040	685.12	739.26
2041	668.08	759.07
2042	701.46	715.11
2043	755.90	739.74
2044	719.08	734.70
2045	703.12	739.34
2046	771.11	755.81
2047	705.69	757.31
2048	727.18	745.33
2049	720.33	754.59